Monte Carlo Studies for Parameterization of B-Mixing with Dilepton Events

by

Zhongzhi Song

B.Sc., Anhui University, 1999

M.Sc., Peking University, 2002

A THESIS SUBMITTED IN PARTIAL FULFILMENT OF
THE REQUIREMENTS FOR THE DEGREE OF

MASTER OF SCIENCE

in

The Faculty of Graduate Studies

(Physics)

THE UNIVERSITY OF BRITISH COLUMBIA

July 19, 2005

Abstract

In this thesis, we report on a Monte Carlo (MC) study of the parameterization of probability distribution functions (PDFs) for neutral B mixing using dilepton events. $\Upsilon(4S)$ decays are generated and those with at least 2 leptons in final state are used in this study. By choosing appropriate functions, a parameterization of the B meson decay time difference Δt is obtained by studying the B lifetime and the neutral B mixing frequency dependence of the dilepton events using an event re-weighting technique. Our results, combined with Monte Carlo studies of detector resolutions, can be used to obtain more precise measurements of the B mixing frequency and B lifetimes from experimental data.

Contents

List of Tables

List of Figures

Acknowledgements

I would like to thank my supervisor, Dr. Janis McKenna, whose guidance, support, and encouragement make this thesis possible. Special thanks to Dr. Tom Mattison, whose valuable comments and help make this thesis easier.

My special thanks also go to Dave Asgeirsson, whose kind help make my study at UBC very enjoyable. Thanks Dave also for proof reading the first draft of this thesis.

I would also like to thank all of the other members of the *BABAR* group at UBC, Chris, Doug, Neil, Nasim, Bryan, and Patrick. Thanks to all of you for your comments and help during the past two years at UBC.

Thank Doug Maas for computing support.

Chapter 1

Introduction

It is well established in particle physics that there are three generations of quarks and leptons. They are the up-type quarks (u, c, t), down-type quarks (d, s, b), charged leptons (e, μ, τ), and neutrinos (ν_e, ν_μ, ν_τ). They interact through the exchange of gauge bosons: the weak bosons $W^\pm$ and Z^0, the photon, and the gluons. The Standard Model (SM) of particle physics with $SU(3)\times SU(2)\times U(1)$ local gauge invariance provides an elegant theoretical framework and represents our current understanding of these fundamental particles and their interactions.

In the strong and electromagnetic interactions, the neutral current only couples with a vector current as described by Quantum Electrodynamics (QED) and Quantum Chromodynamics (QCD). One of the most striking features of the charged-current *weak* interactions, however, is that they do not couple solely to a vector current but to a linear combination of vector and axial vector currents V-A. As a consequence, the electroweak theory is a chiral gauge theory, which means that left- and right-handed fermions transform differently under the electroweak gauge group $SU(2) \times U(1)$[1].

The right-handed fermions cannot couple to $W^\pm$ via V-A current, and they are singlets under $SU(2)$:

$$E_R = (e_R, \mu_R, \tau_R)\,; \quad U_R = (u_R, c_R, t_R)\,; \quad D_R = (d_R, s_R, b_R)\,. \tag{1.1}$$

On the other hand, the left-handed fermions (quarks Q and leptons L) do couple to $W^\pm$, so they are doublets under $SU(2)$:

$$L_L \;=\; \left(\begin{pmatrix} \nu_e \\ e \end{pmatrix}_L , \begin{pmatrix} \nu_\mu \\ \mu \end{pmatrix}_L , \begin{pmatrix} \nu_\tau \\ \tau \end{pmatrix}_L \right);$$

$$Q_L = \left(\begin{pmatrix} u \\ d \end{pmatrix}_L, \begin{pmatrix} c \\ s \end{pmatrix}_L, \begin{pmatrix} t \\ b \end{pmatrix}_L \right). \tag{1.2}$$

With only gauge fields and fermions, the model is incomplete. In particular, it does not accommodate the observed non-zero masses for the quarks, charged leptons, and weak gauge bosons. To construct gauge invariant interactions coupling left- and right-handed fermions, at least one additional scalar field is necessary. It turns out that the massive weak bosons can acquire mass through the spontaneous symmetry breaking of the $SU(2) \times U(1)$ symmetry. This process, called the Higgs mechanism, requires a single Higgs doublet to acquire a vacuum expectation value. The quarks and leptons get mass from the Yukawa couplings to the Higgs doublet. Furthermore, the couplings to the Higgs doublet can also generate flavour mixing and *CP* violation[2].

The quark sector in the SM of particle physics is characterized by the Cabibbo-Kobayashi-Maskawa (CKM) matrix which relates weak eigenstates (d') to mass eigenstates (d) of down-type quarks[3]:

$$\begin{pmatrix} d' \\ s' \\ b' \end{pmatrix} = \begin{pmatrix} V_{ud} & V_{us} & V_{ub} \\ V_{cd} & V_{cs} & V_{cb} \\ V_{td} & V_{ts} & V_{tb} \end{pmatrix} \begin{pmatrix} d \\ s \\ b \end{pmatrix} \equiv \hat{V}_{\mathrm{CKM}} \begin{pmatrix} d \\ s \\ b \end{pmatrix}. \tag{1.3}$$

The matrix $\hat{V}_{\mathrm{CKM}}$ is the mixing matrix for three generations of quarks, and it is a 3×3 unitary matrix. These elements will show up in the interaction of the flavour-changing charged current between a down-quark of family i and an up-quark of family j as pictured in Fig. 1.1. The amplitude $\mathcal{M}$ can be written as

$$\mathcal{M} = -i \left(\frac{G_F M_W^2}{\sqrt{2}} \right)^{1/2} \bar{u}_j \gamma_\mu (1 - \gamma_5) d_i \cdot V_{ij}, \tag{1.4}$$

where G_F is Fermi constant, M_W is W mass, $\bar{u}_j$ and d_i are Dirac spinors representing the quarks, the γ's are Dirac matrices. This means that the coupling strength is proportional to the CKM matrix element V_{ij}. This is an example of charged-current coupling with a V-A current.

In the SM, quark flavour mixing arises from the nonzero off-diagonal elements of the CKM matrix and *CP* violation arises from the single non-zero

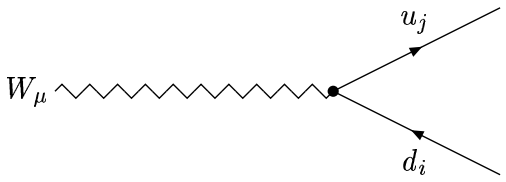

Figure 1.1: Feynman diagrams for flavour changing charged current: the W boson couples to the up-type and down-type quarks.

phase which appears in this matrix. Several parameterizations of the CKM matrix have been proposed in the literature. The two widely used ones are the standard parameterization recommended by the Particle Data Group[4] and a generalization of the Wolfenstein parameterization[5, 6].

The absolute values of the elements of the CKM matrix show a hierarchical pattern with the diagonal elements close to unity, the magnitudes $|V_{us}|$ and $|V_{cd}|$ of order 0.2 (sine of the Cabibbo angle, $\sin\theta_c$), the elements $|V_{cb}|$ and $|V_{ts}|$ of order 4×10^{-2}, and the elements $|V_{ub}|$ and $|V_{td}|$ are of order 5×10^{-3}. The Wolfenstein parameterization exhibits this hierarchy in a transparent manner. It is an approximate parameterization of the CKM matrix in which each element is expanded as a power series in the sine of the Cabibbo angle θ_c:

$$\hat{V}_{\rm CKM} = \begin{pmatrix} 1-\frac{\lambda^2}{2} & \lambda & A\lambda^3(\rho-i\eta) \\ -\lambda & 1-\frac{\lambda^2}{2} & A\lambda^2 \\ A\lambda^3(1-\rho-i\eta) & -A\lambda^2 & 1 \end{pmatrix} + \mathcal{O}(\lambda^4)\,, \qquad (1.5)$$

where the parameters for $\hat{V}_{\rm CKM}$ are chosen as λ, A, ρ, and η. Here $\lambda = \sin\theta_c \approx 0.22$, A is of order one, ρ and η are constrained by CP violation measurements.

Because of the smallness of λ and the fact that for each element the expansion parameter is actually λ^2, it is sufficient to keep only the first few terms in this expansion. In the case that higher accuracy is needed, the terms of higher order correction have to be included in phenomenological applications. A generalization of the Wolfenstein parameterization including $\mathcal{O}(\lambda^4)$ and $\mathcal{O}(\lambda^5)$ terms, which satisfies unitarity, can be found in Ref.[6].

The unitarity of the CKM matrix implies various relations between its ele-

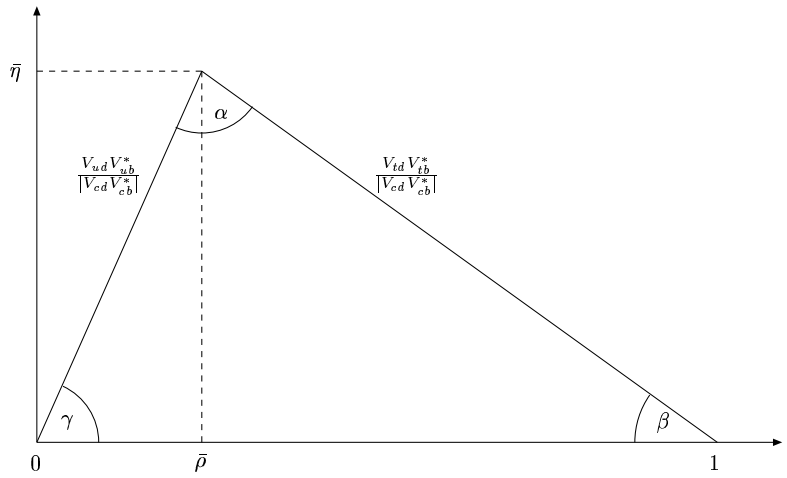

Figure 1.2: Unitarity triangle in the complex plane.

ments. In particular, we have the relation

$$V_{ud}V_{ub}^* + V_{cd}V_{cb}^* + V_{td}V_{tb}^* = 0. \tag{1.6}$$

Phenomenologically this relation is very interesting as it constrains simultaneously the elements V_{ub}, V_{cb} and V_{td} which are currently the subject of extensive study. The unitarity relation in Eq. (1.6) can be represented as a unitarity triangle in the complex $(\overline{\rho}, \overline{\eta})$ plane, where $\overline{\rho} = \rho(1-\lambda^2/2)$ and $\overline{\eta} = \eta(1-\lambda^2/2)$. Noting that to an excellent accuracy, $V_{cd}V_{cb}^*$ in the parameterization formula (1.5) is real with $|V_{cd}V_{cb}^*| = A\lambda^3 + \mathcal{O}(\lambda^7)$ and rescaling all terms in Eq. (1.6) by $A\lambda^3$ we indeed find that the relation in Eq. (1.6) can be represented as a triangle in the complex $(\overline{\rho}, \overline{\eta})$ plane as shown in Fig. 1.2. Since the angles and the sides in this triangle are given by the modulus of the elements of the mixing matrix, they are phase-convention independent and physically observable. Consequently they can be measured directly in suitable experiments, such as B meson decays. For example, the quantity $\sin(2\beta)$, where the β is one of the angles in unitarity triangle as shown in Fig. 1.2, has been measured extensively by both *BABAR* [8] and Belle[9] experiments. One can construct five additional constraints corresponding to other orthogonality relations[7], like the one in Eq. (1.6). The areas of all unitarity triangles are equal and are related to the

measure of CP violation[10].

It was long thought that CP symmetry was exact in nature and only theories that had this exact symmetry property were viable descriptions of the real observed world. The observation of CP violation in the decay $K_L^0 \to \pi^+\pi^-$ by Christenson et al. in 1964[11], however, changed that view dramatically. Interest was heightened by Sakharov's observation in 1967[12] that CP violation is a crucial feature of any theory that attempts to explain the observed asymmetry between matter and anti-matter in a universe which starts from initially symmetric conditions.

The principal interest in the studies of B meson decays in the context of the SM lies in that they provide valuable information on the weak mixing matrix–the CKM matrix. In fact, B decays can be used to determine five of the nine CKM matrix elements: V_{cb}, V_{ub}, V_{td}, V_{ts}, and V_{tb}. For example, $|V_{cb}|$ can be extracted from exclusive $B \to D^{(*)}\ell\nu$ decay processes with the help of Heavy Quark Effective Theory (HQET)[13] or from inclusive semileptonic decays $B \to X\ell\overline{\nu}$ with the help of Operator Product Expansion theory (OPE)[14].

Like the neutral K mesons, the neutral B mesons are complicated by the fact that different neutral states are relevant to the discussion of different physical processes: there are two flavour eigenstates, which have definite quark content and are most useful to understand particle production and particle decay processes; and there are eigenstates of the Hamiltonian, namely states of definite mass and lifetime, which propagate through space in a definite fashion. Since the mass eigenstates are not flavour eigenstates, the flavour eigenstates are mixed with one another as they propagate through space. This is why there is the phenomenon of particle-anti-particle mixing in neutral K, D, and B systems.

An excellent testing ground for CP violation is also provided by the B meson system through particle–antiparticle mixing. A particle that is purely B^0 at time $t = 0$ will oscillate between B^0 and $\overline{B}^0$ with a frequency[1] Δm, where Δm is the mass difference between the two neutral B mass eigenstates. If decays to

[1] We will follow the convention $c = 1$ and $\hbar = 1$, so that the mass, energy, and momentum are all measured in units of GeV. And we can also convert GeV into ps^{-1}, which means that the mass difference Δm will have the same unit as frequency.

a CP eigenstate f are observed, any difference between the rates when starting with a B^0 or with a $\overline{B}^0$ is a manifestation of CP violation. For example, a state initially produced as a B^0 ($\overline{B}^0$) can decay to $J/\psi K^0_S$ directly or can oscillate into a $\overline{B}^0$ (B^0) and then decay to $J/\psi K^0_S$. With little theoretical uncertainty in the SM, the phase difference between these amplitudes is equal to twice the angle $\beta = \arg[-V_{cd}V^*_{cb}/V_{td}V^*_{tb}]$ of the unitarity triangle as shown in Fig. 1.2. The CP-violating asymmetry measured in such kind of modes can thus provide a crucial test of the SM[15]. Any deviation from unitarity in the CKM matrix would be a clear indication of new physics.

The two B mesons produced from $\Upsilon(4S)$ decays evolve coherently, until one decays. The proper decay time difference Δt between two B mesons is governed by the following probabilities to observe an unmixed ("+") or a mixed ("−") event:

$$P(\Delta t) = \frac{1}{4\tau} e^{-|\Delta t|/\tau}(1 \pm \cos(\Delta m \Delta t)), \tag{1.7}$$

where τ is the neutral B lifetime. Therefore, we can measure the oscillation frequency as well as the neutral B meson lifetime from these probabilities.

In reality, there are three major experimental complications that affect the Δt distributions.

- The tagging algorithms that determine the b-flavour of a B meson at its time of decay have a finite probability of making a mistake, called the mistag probability. As a result, some mixed events will be tagged as unmixed events, and vice versa.

- The resolution for Δt is comparable to the lifetime and must be well understood.

- Various background levels and their time evolution properties must be understood in order to extract the lifetime and mixing frequency.

Currently, experimental studies of B meson decay are performed at the $\Upsilon(4S)$ resonance near production threshold, as well as at higher energies in proton-anti-proton collisions. By far the largest samples of B mesons have been

collected by the e^+e^- collider detectors running at $\Upsilon(4S)$ resonance, which are called "B-Factories". Both *BABAR* and Belle have accumulated approximately 150 fb^{-1} of data, which make precise measurements possible.

The PEP-II B Factory is an asymmetric e^+e^- collider designed to operate at a luminosity of 3×10^{33} $\text{cm}^{-2}\text{s}^{-1}$ and above, at a center-of-mass energy of 10.58 GeV, the mass of the $\Upsilon(4S)$ resonance[16]. The $\Upsilon(4S)$ decays almost entirely to $B^0\overline{B}^0$ or B^+B^- pairs with an upper limit on non-$B\overline{B}$ decays ratio less than 4% of the time[17], and thus provides an ideal laboratory for the study of B mesons. In PEP-II, the electron beam of 9.0 GeV collides head-on with the positron beam of 3.1 GeV , resulting in a Lorentz boost to the $\Upsilon(4S)$ of $\beta\gamma = 0.55$. This boost makes it possible to reconstruct the decay vertices of the two B mesons, to determine their relative decay times, and thus to measure the time dependence of neutral B mixing[18].

In this thesis, we study the parameterization of Δt distributions by using Monte Carlo (MC) generated events at generator level (without full detector simulation) within the *BABAR* framework. Since in real data we do not have exact B momentum (direction), the boost approximation (with an average boost for $\Upsilon(4S)$) is used to derive the difference in proper decay times from the distance between two decay vertices along the boost direction. The motivation for this Monte Carlo study is that a more precise probability distribution of experimentally measured Δt values, rather than the distribution of real Δt (which is not measurable), will help to make more precise measurements of the B meson lifetimes and the neutral B mixing frequency.

A brief review of the physics background of B semileptonic decays and the neutral B mixing is given in Chapter 2 of this thesis. In Chapter 3, we provide a brief introduction to the *BABAR* experiment, the *BABAR* detector, the simulation tool, and the event generator. In Chapter 4, we will briefly review existing neutral B mixing measurements and explain the two main approximations used in the experimental analysis, namely, the boost approximation and the point of closest approach (POCA) approximation. Strategies for data analysis are given in Chapter 5, where we will describe how the MC events were generated and

explain the method of event re-weighting and parameterization model selection. The analysis results and independent crosschecks are given in Chapter 6. Finally, we present our conclusions in Chapter 7.

Chapter 2

Physics Background

$B^0\overline{B}^0$ mixing is a result of the oscillations between B^0 and $\overline{B}^0$. An initially produced B^0 or $\overline{B}^0$ evolves in time into a superposition of B^0 and $\overline{B}^0$. The $B\overline{B}$ state produced from $\Upsilon(4S)$ decays will evolve coherently with time until one of them decays. Semileptonic B meson decays provide a simple way to determine the b quark flavour of the decaying B meson, which is essential for flavour mixing studies.

In this chapter, we first review B meson semileptonic decays in Section 2.1 as they are the basic processes for studying the neutral B mixing using dilepton events. Then we provide the quantum mechanical treatment of the two-state system of neutral B mesons in Section 2.2. Finally, in Section 2.3, we apply the knowledge of neutral B mixing from Section 2.2 to the coherent $B\overline{B}$ states produced from $\Upsilon(4S)$ decays, which represents the case studied in this thesis.

2.1 Semileptonic B meson decays

There are strong motivations for studying semileptonic B decays. First of all, these processes are related to some of the fundamental parameters of the SM. Semileptonic B decays, $B \to X_c \ell\nu$ and $B \to X_u \ell\nu$ provide an excellent laboratory to measure moduli of CKM elements, namely $|V_{cb}|$ and $|V_{ub}|$ respectively, because the strong interaction effects are greatly simplified due to the leptons in the final state. Secondly, the semileptonic B decay branching fractions have large effects on other measurements and thus need to be measured precisely. Indeed, the semileptonic decays are an important source of background for many measurements. Finally, the semileptonic B decays are useful to test various QCD effective theories.

B^+B^- and $B^0\overline{B}^0$ mesons are the lightest of the b-flavoured hadrons, hence they decay via weak interactions. Since the mass of a b-quark is much larger than its partner quark (d or u), B meson decays are mostly described by the b quark decays within the naive spectator model[19]. In the SM, other non-spectator decay processes including both tree level processes such as W-exchange and annihilation decays and higher-order loop-induced flavour-changing neutral current (FCNC)[1] decay processes are all suppressed in comparison to the spectator decays.

The dominant decay mode of a b-quark is $b \to cW^*$ where the virtual W^* eventually materializes either into a pair of leptons, $\ell\overline{\nu}$, or into a pair of quarks, $q\bar{q}'$, which will then hadronize into final states. It is called semileptonic decay if the virtual W^* converts into an $\ell\overline{\nu}$ pair, which is of primary interest for our study. If the virtual W^* converts into a quark pair, it is then called hadronic decay, which is more complicated than the semileptonic decay because of strong interactions. All other decays that do not occur through the usual $b \to c$ transition are known as rare B decays, which include both semileptonic and hadronic $b \to u$ decays that are suppressed at leading order by the small CKM matrix element V_{ub}, as well as higher order processes such as electromagnetic and gluonic penguin decays (for details, see review in Ref.[21]).

The Cabibbo favoured inclusive decay $b \to c\ell^-\overline{\nu}$ is shown in Fig. 2.1(a). We can see that the b quark can only decay directly to an ℓ^-. For comparison, a $\bar{b}$ can only decay directly to an ℓ^+ as shown in Fig. 2.1(d). Therefore, the sign of the charge of the direct lepton is the same as the sign of the charge of the b quark in the decaying B meson. That is, a B^0 or B^+ decays directly to a positively charged lepton and a $\overline{B}^0$ or B^- decays directly to a negatively charged lepton.

There are also "cascade" background processes, such as $b \to c \to s\ell^+\nu$. The decay at quark level is shown in Fig. 2.1(b,e). The virtual W^* originating from the b quark will hadronize into an $\ell^-\overline{\nu}$ pair or a quark pair (dominated by $\bar{c}s$). The leptons produced from c quark decays have the opposite charge compared with the direct leptons (comparing part(a) with part(b); and part(d)

[1]The suppression is known as the Glashow-Iliopoulus-Maiani (GIM) effect[20].

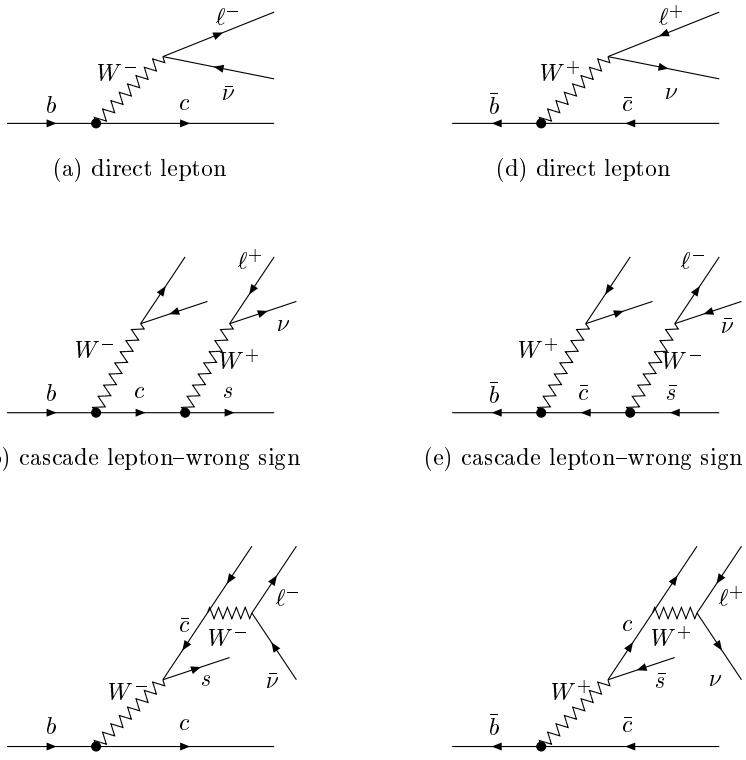

(a) direct lepton

(d) direct lepton

(b) cascade lepton–wrong sign

(e) cascade lepton–wrong sign

(c) cascade lepton–right sign

(f) cascade lepton–right sign

Figure 2.1: Feynman diagrams for semileptonic b quark decays.

with part(e) in Fig. 2.1). In B meson decays, c will mostly hadronize into D mesons and D mesons may then decay and produce the cascade lepton with the opposite charge of a direct lepton. This is called a cascade lepton with wrong sign.

Similar cascade processes occur via $b \to c\bar{c}s$ and then $\bar{c} \to \bar{s}\ell^-\overline{\nu}$ as shown in Fig. 2.1(c, f). In these cases the charge of the leptons has the same sign as that of the direct lepton. Therefore these are called cascade leptons with right sign. It should be noted that these cascade leptons with right sign are suppressed because of the smaller fraction for B to two D mesons.

These processes are very well described by the OPE, in which the decay rate is expanded in inverse powers of the heavy quark mass m_b. For the exclusive

decay channels with charmed final states such as $B \to D^* \ell\nu$ and $B \to D\ell\nu$, these channels will provide information about $|V_{cb}|$ and can be studied with HQET. For the inclusive charmless semileptonic decays $B \to X_u \ell\overline{\nu}$, these channels only constitute about 1% of the total semileptonic width. For the exclusive B charmless semileptonic decays such as $B \to \pi\ell\overline{\nu}$, these channels are well studied within the naive factorization approach[2].

In summary, the charges of the final state leptons provide information which can be used to identify the B as a B^0 (B^+) or $\overline{B}^0$ (B^-). If a final state can only originate from a B^0 or $\overline{B}^0$, then the lepton sign can be used to "tag" the flavour of the B. In a typical experiment, because of the extremely low efficiency in reconstructing both B decays, only one of them is fully reconstructed, and the other B meson is used to tag the pair by determining its b-flavour content.

2.2 B^0-$\overline{B}^0$ mixing

There are two neutral B^0-$\overline{B}^0$ meson systems, B_d^0-$\overline{B}_d^0$ and B_s^0-$\overline{B}_s^0$, which exhibit particle-antiparticle mixing[23]. The quark content for B_d is $B_d^0 = \overline{b}d$, $\overline{B}_d^0 = \overline{d}b$. Unless explicitly stated in the rest of this thesis, the B_d system is the only neutral B system that we are interested in, even though the following general discussion in this section might be still applicable to the B_s system with a small modification[3].

In the SM, transitions $B^0 \to \overline{B}^0$ and $\overline{B}^0 \to B^0$ are described at lowest order by the weak interaction box diagrams in Fig. 2.2. Such transitions are called $|\Delta B| = 2$ transitions, because they change the bottom quantum number by two units. In the SM, $|\Delta B| = 2$ amplitudes are small, so measurements of B_d mixing could easily be sensitive to new physics, which can appear in the box diagram in place of the top quark. The amplitudes of box diagrams with internal up or charm quarks are negligible compared to the diagram with two

[2]Recently, there has been new progress in the generalization of the naive factorization to exclusive nonleptonic B meson decays, using the so-called "QCD factorization approach" [22].

[3]Note that $\Upsilon(4S)$ is just at the resonance to produce $B_d^0\overline{B}_d^0$ and at an energy below the $B_s^0\overline{B}_s^0$ production threshold.

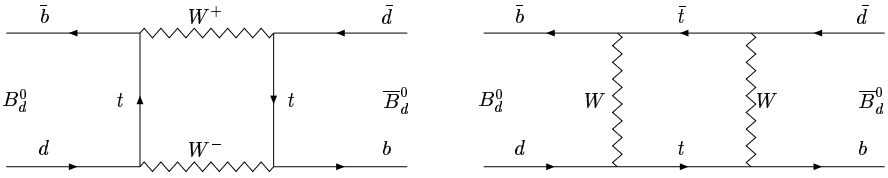

Figure 2.2: Standard Model Box diagrams inducing B_d^0-$\overline{B}_d^0$ mixing. Similar diagrams exist in which t quarks are replaced with c or u quarks.

internal top quark lines, because the amplitudes of these transitions are roughly proportional to the masses of the internal quarks.

We now consider mixing for the neutral meson B^0 and its antiparticle $\overline{B}^0$ [15]. The two mass eigenstates are B_H and B_L, where H and L stand for Heavy and Light, respectively[4]. These mass eigenstates are a linear combination of the neutral B-meson flavour eigenstates B^0 and $\overline{B}^0$,

$$|B_L\rangle = p|B^0\rangle + q|\overline{B}^0\rangle, \tag{2.1}$$

$$|B_H\rangle = p|B^0\rangle - q|\overline{B}^0\rangle. \tag{2.2}$$

The complex coefficients p and q obey the normalization condition:

$$|p|^2 + |q|^2 = 1. \tag{2.3}$$

The eigenvalue equation is

$$\mathcal{H}\begin{pmatrix} p \\ \pm q \end{pmatrix} = \left(\hat{M} - \frac{i}{2}\hat{\Gamma}\right)\begin{pmatrix} p \\ \pm q \end{pmatrix} = \left(\hat{M}_{L,H} - \frac{i}{2}\hat{\Gamma}_{L,H}\right)\begin{pmatrix} p \\ \pm q \end{pmatrix}. \tag{2.4}$$

Here $\hat{M}$ is the mass matrix and $\hat{\Gamma}$ describes the exponential decay of the system. They are both 2×2 Hermitian matrices. Since $\Gamma_{12} \ll M_{12}$, this equation gives $|q/p| \simeq 1$, which means that the CP violation in mixing is negligible in this study[23].

[4]In the neutral K meson system, mixing also has contributions from real intermediate states accessible to both K^0 and $\overline{K}^0$. As a result, the two mass eigenstates of the neutral K system have a large decay rate difference $\Delta\Gamma$ but almost identical masses. So it is more convenient to use the long-lived state K_L^0 and short-lived state K_S^0 for the K^0 system. For the B^0 system, $\Delta\Gamma$ is much smaller than Δm_d, therefore, B_H and B_L are more convenient.

Any neutral B state can be written as an admixture of the states B_H and B_L:

$$|B(t)\rangle = A_L(t)|B_L\rangle + A_H(t)|B_H\rangle, \tag{2.5}$$

where the amplitudes of this admixture evolve in time as

$$A_L(t) = A_L(0)e^{-(\frac{\Gamma_L}{2}+iM_L)t}, \tag{2.6}$$

$$A_H(t) = A_H(0)e^{-(\frac{\Gamma_H}{2}+iM_H)t}. \tag{2.7}$$

The proper time evolution of states which at time $t = 0$ were either a pure B^0 with $A_H(0) = A_L(0) = 1/(2p)$ or a pure $\overline{B}^0$ with $-A_H(0) = A_L(0) = 1/(2q)$ is given by

$$|B^0(t)\rangle = g_+(t)|B^0\rangle + \frac{q}{p}g_-(t)|\overline{B}^0\rangle, \tag{2.8}$$

$$|\overline{B}^0(t)\rangle = \frac{p}{q}g_-(t)|B^0\rangle + g_+(t)|\overline{B}^0\rangle, \tag{2.9}$$

where

$$g_+(t) = e^{-\frac{\Gamma t}{2}-iMt}\cos\left[(\frac{\Delta m}{2} - i\frac{\Delta\Gamma}{4})t\right], \tag{2.10}$$

$$g_-(t) = ie^{-\frac{\Gamma t}{2}-iMt}\sin\left[(\frac{\Delta m}{2} - i\frac{\Delta\Gamma}{4})t\right], \tag{2.11}$$

with

$$\Gamma \equiv \frac{\Gamma_H + \Gamma_L}{2};\ M \equiv \frac{M_H + M_L}{2};\ \Delta m \equiv (M_H - M_L);\ \Delta\Gamma \equiv \Gamma_H - \Gamma_L. \tag{2.12}$$

The time-dependent probabilities for the flavour states remain unchanged $(+)$ or oscillate into the other $(-)$ in the following way:

$$|g_\pm(t)|^2 = \frac{e^{-\Gamma t}}{2}\left[\cosh(\frac{\Delta\Gamma}{2}t) \pm \cos(\Delta m t)\right], \tag{2.13}$$

In the absence of CP violation, the time-integrated mixing probability for B_d system is given by[4]

$$\chi_d = \frac{\int |g_-(t)|^2 dt}{\int |g_-(t)|^2 dt + \int |g_+(t)|^2 dt} = \frac{x_d^2 + y_d^2}{2(1 + x_d^2)}, \tag{2.14}$$

where $x_d = \Delta m_d/\Gamma$, and $y_d = \Delta\Gamma/2\Gamma$.

In the SM, Δm_d can be calculated by using a low-energy Hamiltonian and the OPE. It can be shown that[24]

$$\Delta m_d \propto |V_{tb}V_{td}^*|^2. \tag{2.15}$$

Therefore, Δm_d is sensitive to both V_{tb} and V_{td}, and its measurement can provide a constraint on the side of the unitary triangle which has length of $|V_{tb}^*V_{td}|/|V_{cb}^*V_{cd}|$ as shown in Fig. 1.2.

2.3 Coherent $B\overline{B}$ states

At a B factory, the $B\overline{B}$ pair produced from the $\Upsilon(4S)$ decay is in a coherent state. From Eq. (2.8) and Eq. (2.9), we can easily verify that at any time until one particle decays, there is always exactly one B^0 and one $\overline{B}^0$ present (for reasons, see below). Once one of the particles decays, however, the other continues to evolve, and thus there are possible events with two B^0 or two $\overline{B}^0$ decays, whose probabilities are governed by the time difference between the two decays.

The two B mesons from an $\Upsilon(4S)$ decay are identified by the angle θ that they make with the electron beam (higher energy beam) direction in the $\Upsilon(4S)$ rest frame. The two-B state[5] can be written as[15],

$$\begin{aligned} S(t_f,t_b) = \frac{1}{\sqrt{2}}\Big[&B^0_{\rm phys}(t_f,\theta,\phi)\overline{B}^0_{\rm phys}(t_b,\pi-\theta,\phi+\pi) \\ &- \overline{B}^0_{\rm phys}(t_f,\theta,\phi)B^0_{\rm phys}(t_b,\pi-\theta,\phi+\pi)\Big]\sin(\theta), \end{aligned} \tag{2.16}$$

where the subscript f refers to the B meson in the forward half-space ($\theta < \pi/2$) and the subscript b refers to the backward-moving B meson ($\theta > \pi/2$); t_f and t_b are the proper times for the two B mesons.

With the help of Eq. (2.8) and Eq. (2.9), we can rewrite Eq. (2.16) as

$$\begin{aligned} S(t_f,t_b) = \frac{1}{\sqrt{2}}e^{-(\Gamma/2+iM)(t_f+t_b)}\Big\{&\cos[\Delta m_d(t_f-t_b)/2](B^0_f\overline{B}^0_b - \overline{B}^0_f B^0_b) \\ &-i\sin[\Delta m_d(t_f-t_b)/2](\frac{p}{q}B^0_f B^0_b - \frac{q}{p}\overline{B}^0_f\overline{B}^0_b)\Big\}\sin(\theta_f). \end{aligned} \tag{2.17}$$

[5]Note that $\Upsilon(4S)$ has total spin $J = 1$ and B mesons have spin $S = 0$. Momentum conservation tells that the B pair must be an antisymmetric $L = 1$ P-wave state.

Since the mass of the $\Upsilon(4S)$ state is just above the threshold of $B\overline{B}$ production, the B momentum in the $\Upsilon(4S)$ rest frame is relatively small, $\sim 335\,\mathrm{MeV}$. The two B mesons will have equal magnitude, back-to-back momenta in the $\Upsilon(4S)$ rest frame. To a first approximation, the B rest frame and the $\Upsilon(4S)$ rest frame are equivalent. Since, in general, the B flight direction in the $\Upsilon(4S)$ frame is not known, the $\Upsilon(4S)$ frame is often used in place of the B rest frame. From Eq. (2.17), one can easily find that until the time when one or the other of the two B's decays, there is always one B^0 and one $\overline{B}^0$ in the system. The decay of one of the particles stops the clock for that particle while the other continues to evolve with time. The probability of getting two B^0s or two $\overline{B}^0$s will depend on the time difference of the two B decays as shown by the $\sin[\Delta m_d(t_f - t_b)/2]$ term in Eq. (2.17).

From Eq. (2.17), one can easily derive the probabilities of getting an event without mixing (i.e., one B^0 and one $\overline{B}^0$) and an event with mixing (i.e., two B^0s or two $\overline{B}^0$s). First, we can determine the probability of getting an event by integrating over θ and ϕ, and assuming $|q/p| \simeq 1$:

$$P(\text{without mixing}(t_f, t_b)) \propto e^{-\Gamma(t_f+t_b)}\,[1 + \cos(\Delta m_d(t_f - t_b))] \tag{2.18}$$

$$P(\text{with mixing}(t_f, t_b)) \propto e^{-\Gamma(t_f+t_b)}\,[1 - \cos(\Delta m_d(t_f - t_b))] \tag{2.19}$$

Let t_{short} be the smaller of t_f and t_b. The probability of an event occurring with the first B decay at t_{short} is

$$P(t_{short}) \propto e^{-2\Gamma t_{short}} \tag{2.20}$$

Therefore, the probabilities of a $B\overline{B}$ event with and without mixing, which only depend on the time difference of the two B decays, can be obtained by dividing Eq. (2.18) and Eq. (2.19) by Eq. (2.20). These results can be written as:

$$P(B^0\overline{B}^0 \to B^0\overline{B}^0(\Delta t)) = \frac{e^{-|\Delta t|/\tau_{B^0}}}{4\tau_{B^0}}\,[1 + \cos(\Delta m_d \Delta t)] \tag{2.21}$$

$$P(B^0\overline{B}^0 \to B^0B^0(\Delta t) \text{ or } \overline{B}^0\overline{B}^0(\Delta t)) = \frac{e^{-|\Delta t|/\tau_{B^0}}}{4\tau_{B^0}}\,[1 - \cos(\Delta m_d \Delta t)] \tag{2.22}$$

where $\Delta t = t_b - t_f$, the B lifetime $\tau = 1/\Gamma$. If Δt is measured and the b-quark flavour of both B mesons at their time of decay is determined, one can extract

the B^0 lifetime τ_{B^0} and the mixing frequency Δm_d. Note that Eq. (2.21) is also valid for B^+B^- by taking $\Delta m_d = 0$ and substituting $\tau_{B^0} \to \tau_{B^+}$. Therefore, we can extract the charged B lifetime τ_{B^+} from experimental data by using Eq. (2.21) as well.

The mass difference Δm_d between the two mass eigenstates of the $(B^0\overline{B}^0)$ system can be measured by constructing the following time-dependent asymmetry:

$$\begin{aligned} \mathcal{A}(\Delta t, \Delta m_d) &= \frac{N(B^0\overline{B}^0)(\Delta t) - \left[N(B^0B^0)(\Delta t) + N(\overline{B}^0\overline{B}^0)(\Delta t)\right]}{N(B^0\overline{B}^0)(\Delta t) + \left[N(B^0B^0)(\Delta t) + N(\overline{B}^0\overline{B}^0)(\Delta t)\right]} \\ &= \cos(\Delta m_d \Delta t), \end{aligned} \tag{2.23}$$

where Δt is the time difference of the two B mesons decays.

The simplest way to determine the b flavour of the decaying neutral B is to use the charge of the leptons produced from B decays as tagging particles, as described in Section 2.1. By counting the number of "same-sign" events ($\ell^+\ell^+$ or $\ell^-\ell^-$) and "opposite-sign" events ($\ell^+\ell^-$), which correspond to "mixed" and "un-mixed" events, respectively, a measurement of Δm_d can be extracted from the asymmetry:

$$\mathcal{A}(\Delta t, \Delta m_d) = \frac{N(\ell^+\ell^-) - [N(\ell^+\ell^+) + N(\ell^-\ell^-)]}{N(\ell^+\ell^-) - [N(\ell^+\ell^+) + N(\ell^-\ell^-)]} \tag{2.24}$$

The fraction of B decays producing direct leptons is around 10 to 15%. Therefore, the direct dilepton events represent 1 to 2% of the $\Upsilon(4S) \to B^0\overline{B}^0$ decays[6], which will ensure relatively large statistics for a B mixing analysis. By measuring the asymmetry in Eq. (2.24), we can extract Δm_d from experimental data.

[6]Here, each lepton is from a direct B decay, so the fraction of dilepton events is square of the fraction of direct leptons from single B decays. If we also include the cascade leptons, we obtain a higher fraction of dilepton events.

Chapter 3

BABAR Experiment

The primary goal of the *BABAR* experiment is the systematic study of CP asymmetries in the decays of neutral B mesons. In addition to this, a sensitive measurement of the CKM matrix elements and measurements of a number of rare B meson decays are possible at *BABAR*. Studies indicate that the best source of B mesons for such a physics program is an e^+e^- collider, operating at the $\Upsilon(4S)$ resonance, but in an asymmetric mode, *i.e.*, with beams of unequal energy. The $B\overline{B}$ pair from the $\Upsilon(4S)$ decay is almost at rest in the center-of-mass (CM) frame, resulting in the B mesons having significant momenta in the laboratory frame. The PEP-II B Factory is such an asymmetric e^+e^- collider with the electron beam of 9.0 GeV colliding head-on with the positron beam of 3.1 GeV [16] . This configuration results in a Lorentz boost to the $\Upsilon(4S)$ resonance of $<\beta\gamma>= 0.55$ in the lab frame, which enables the proper time of B decays to be inferred from their measurable decay lengths, thus enabling the measurement of the time dependence of their decay rates and neutral B mixing[18].

In this chapter, we first give a brief description of the *BABAR* detector in Section 3.1. In Section 3.2, we provide some details of running the event generator software program, `EvtGen` [27], within the *BABAR* framework, which is used to simulate dilepton events from $\Upsilon(4S)$ decays for our neutral B mixing study.

3.1 The *BABAR* detector

As we stated in Chapter 1, the crucial test of CP invariance is a comparison of the time-dependent decay rates for B^0 and $\overline{B}^0$ to a self-conjugate state. For the clean experimental test, in order to maintain acceptable efficiency, we

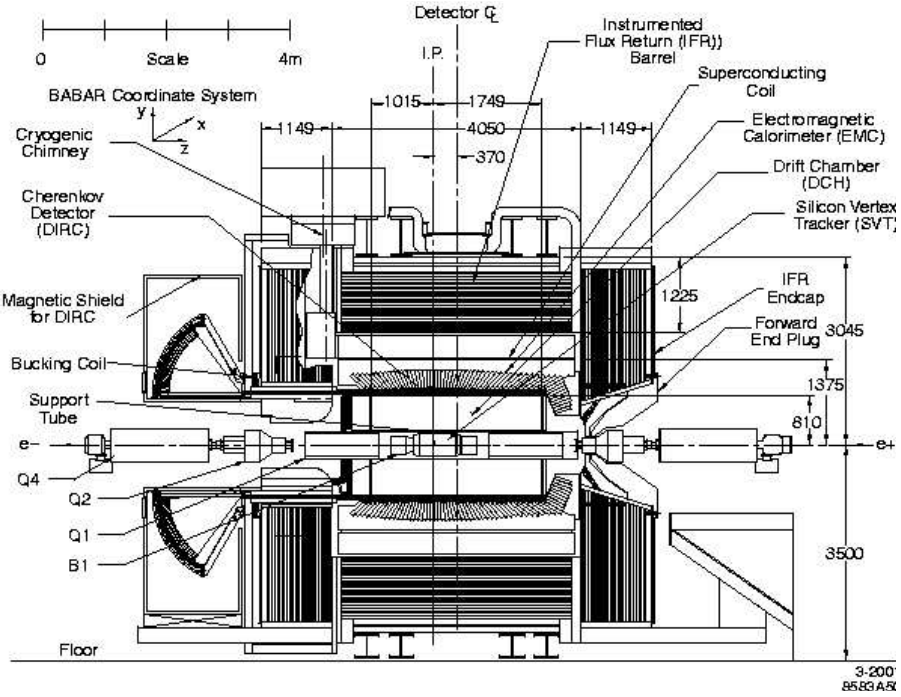

Figure 3.1: *BABAR* detector longitudinal section.

can require events in which one B meson decays to a CP eigenstate that is *fully reconstructed* and the other B meson is *tagged* as a B^0 or a $\overline{B}^0$ by its decay products: a charged lepton, a charged kaon, or other flavour sensitive features such as a low momentum charged pion from a D^* decay. The very small branching fractions of B mesons to CP eigenstates, typically of the order 10^{-4}, the need for full reconstruction of final states with two or more charged particles and several π^0s, plus the need to tag the second neutral B, place stringent requirements on the detector.

The *BABAR* detector is a charged and neutral spectrometer with large solid-angle coverage[18]. Fig. 3.1 shows a longitudinal section through the center of the detector. The inner detector consists of a silicon vertex tracker and a drift chamber for charged particle tracking and vertexing, a ring-imaging Cherenkov detector for particle identification, and a CsI calorimeter for measuring particle energies. These detector systems are surrounded by a super-conducting solenoid

that is designed for a field of 1.5 T. Outside of the solenoid is the instrumented flux return which is used for muon and neutral hadron detection. The polar angle coverage extends to 350 mrad in the forward direction and 400 mrad in the backward direction, defined relative to the high energy beam (electron beam). An overview of the coverage, the segmentation, and performance of the *BABAR* detector system is presented in Table I of Ref.[18]. Here we only provide a very brief description of each component of the detector (For more details of the detector, see Refs.[15] and [18].)

The innermost part of *BABAR* detector is the silicon vertex tracker (SVT). It has been designed to measure angles and positions of charged particles just outside the beam pipe. It is critical for the separation of the decay vertices of the B mesons and proper reconstruction of short lived particles. The SVT is composed of five layers of double-sided silicon micro-strip detectors. The inner three layers primarily provide position and angle information for the measurement of the vertex position. The outer two layers are needed for low p_T tracking and providing the coordinate and angle measurements to the drift chamber. The geometrical acceptance of the SVT is 90% of the solid angle in the CM system.

Surrounding the SVT is the the drift chamber (DCH), whose principal purpose is the momentum measurement for charged particles. The DCH has been designed to measure not only the transverse momenta and positions, but also longitudinal positions of tracks. Longitudinal information is derived from wires placed at small angles to the principal axis. The drift chamber also provides information for lower momentum particles by measuring the ionization energy loss, $\mathrm{d}E/\mathrm{d}x$, for particle identification. The DCH is of compact design, with 40 layers of small, approximately hexagonal cells. By choosing low-mass wires and a helium-based gas mixture, multiple scattering inside the DCH is minimized.

Outside of the drift chamber is the DIRC, the detector of internally reflected Cherenkov light. It is a novel ring-imaging Cherenkov detector, providing separation of pions and kaons from about 0.7 GeV to the kinematic limit of 4.5 GeV. The Cherenkov photons are emitted by a particle traveling faster than the speed of light in the surrounding medium. The mass of a charged particle can by deter-

mined by measuring the angle of the Cherenkov radiation and the momentum of the particle track. Cherenkov light is produced in the 4.9 m long bars of synthetic fused silica of rectangular cross section, 1.7 cm $\times$ 3.5 cm, and transported by total internal reflection, preserving the angle of emission, to an array of photo-multiplier tubes (PMTs). This array forms the backward wall of a toroidal water tank that is located beyond the backward end of the magnet. Images of the Cherenkov rings are reconstructed from the position and time of arrival of the signals in the PMTs. In order to identify the type of particle (e, μ, π, K, p), an unbinned maximum likelihood method is used to incorporate all the space and time information from the DIRC.

The electromagnetic calorimeter (EMC) is designed to detect electromagnetic showers with excellent energy and angular resolution over the energy range from 20 MeV to 4 GeV. This coverage allows the detection of low energy π^0s and η^0s from B decays as well as from electromagnetic and radiative processes. The EMC is composed of 6,580 thallium-doped cesium iodide crystals. It's divided into two sections, a barrel and a forward end-cap as shown in Fig. 3.1. The crystals absorb electromagnetic showers and produce scintillation light which is read out by two silicon positive-intrinsic-negative (PIN) diodes. To optimize resolution, the amount of material in front of and in-between the crystals is held to a minimum. Low-noise analog circuits and frequent, precise calibration of the electronics and energy response over the full dynamic range are crucial for maintaining the desired performance of the EMC.

The instrumented flux return (IFR) for the main magnet also serves to identify muons and to detect neutral hadrons. It was designed to have a high efficiency and good purity over a wide range of momentum down to less than 1 GeV and a high solid angle coverage. The IFR originally consisted of 19 layers of steel and resistive plate chambers (RPCs). It uses the steel of the flux return as a muon filter and hadron absorber. Muons can be identified by measuring how many layers of steel the particle traverses, and comparing that to the expected radiation length for muons. Two additional cylindrical layers of RPCs with four readout planes were placed at a radius just inside the magnet cryostat

to detect particles exiting the EMC. In 2004, some of the RPCs were replaced with LSTs (Limited Streamer Tubes).

For a neutral B mixing analysis, the most important detector capabilities include charged particle tracking, vertex reconstruction, and particle identification. All these requirements can be met by combining the different sub-detectors described above[25].

3.2 Event generator software

A piece of software called "Generators-Framework Interface" (`GenFwkInt`) is the package used to control event generators in the *BABAR* framework. One of the `GenFwkInt` interface modules is `GfiEvtGen` which interfaces to the generator called `EvtGen` [26]. `EvtGen` is a package for simulating physics processes in decays of B-mesons and other resonances at generator level, i.e., it does not include any material interactions or detector simulation. One of the novel ideas in the design of `EvtGen` is that decay amplitudes, instead of probabilities, are used for the simulation of decays. The framework uses the amplitude for each node in the decay tree to simulate the entire decay chain, including all angular correlations. `EvtGen` provides a framework into which decay models may be added. This design is efficient and leads to reusable decay models. The *BABAR* experiment uses the `EvtGen` package to simulate generic B decays in its Monte Carlo production.

`EvtGen` implements many detailed models that are important for the physics of B mesons. In particular, it has detailed models for semileptonic decays and CP-violating decays and it uses full angular distributions in sequential decays. `EvtGen` introduces mixing by generating decays of the $\Upsilon(4S)$ to the proper mixture of $B^0\overline{B}^0$, B^0B^0, and $\overline{B}^0\overline{B}^0$ final states, with the correct distributions of proper decay time difference Δt. CP asymmetries are generated in modules that modify the generated lifetime distributions of the two B's produced in the decay of the $\Upsilon(4S)$. One of the particular strengths of `EvtGen` is for semileptonic decays, in which a large number of different models are available. This is

important for the neutral B mixing study using dilepton events of this thesis.

`EvtGen` provides decay tables for generic B-meson decays. These tables contain detailed models and branching fractions for each B meson decay mode. It provides the default simulation of B-decays in the *BABAR* simulation. The generator handles only exclusive final states, *i.e.*, it does not perform any fragmentation. In order to provide a complete table of decays, it also has an interface to the `Jetset` software package[28] for generation of continuum events at the $\Upsilon(4S)$ and for generic hadronic decays of B mesons that are not implemented in the generator. For the decays of B mesons, about 60% are accounted for by exclusive states, while the other 40% are produced by `Jetset7.4`.

There are 4 basic options that control `EvtGen` [26]:

```
GEN             mode
DECAY           decay table
UDECAY          ''user'' decay table
PDT              particle data table
```

- `GEN` specifies which decay mode `EvtGen` will call. There are two options: $\Upsilon(4S)$ and *continuum*.
- `DECAY` specifies which decay table to use. The default decay table is called `DECAY.DEC`, which contains all decay models implemented by `EvtGen`.
- `UDECAY` specifies the user defined decay table, which will be read after the `DECAY.DEC` table. This allows a user to redefine the decays of certain particles after having read the generic decay table.
- `PDT` specifies the particle property table to read by `EvtGen`. The default particle data table is `pdt.table`. By modifying this file, one can change the properties of particles, such as lifetimes.

It's simplest to run the `EvtGen` within the `GeneratorsQA` package[29]. This package is setup to run the event generators in standalone mode, i.e., without detector simulation or reconstruction. Modification of the event generation procedure will typically involve changing the analysis module or adding a new

module. `EvtGen` is therefore very convenient for conducting a generator-level analysis, or quality assurance studies of the generators and `GenFwkInt` (for details about `GeneratorsQA`, see Ref.[29]). The standard way of running `EvtGen` begins with initializing particle properties according to the `pdt.table` and parsing the full standard decay table `DECAY.DEC`. After this, a user decay table is parsed in order to redefine the particle decays of interest. In this way, the user decay file will override the standard decay table.

The main `EvtGen` decay table is `DECAY.DEC`, which contains world average values for the generic decays of B-mesons and other lighter mesons and baryons. For details about the format and syntax of the decay table, see Ref.[27]. Here we provide some simple examples to illustrate the basic format of the decay table. The following is an example for $\Upsilon(4S) \to B\overline{B}$ decay:

```
Decay Upsilon(4S)
0.50000 B+  B-                  VSS;
0.49913 B0  anti-B0             VSS_BMIX dm;
Enddecay
```

A decay entry begins with the key word "`Decay`" and ends with "`Enddecay`". Each entry in the table starts with the branching fraction for the decay channel and is followed by a list of the decay products. After each decay product a model name is listed. This model name specifies how to model the decay of the particle. In the example above, "`VSS_BMIX`" is a model for the decay of a vector meson (the $\Upsilon(4S)$) into a pair of scalar particles ($B^0\overline{B}^0$) with mixing. "`VSS`" is the same model for $\Upsilon(4S) \to B^+B^-$, without mixing. Note that 0.087% of $\Upsilon(4S)$ decays will be non B $\overline{B}$ final states. These models make proper use of the polarization of the $\Upsilon(4S)$ such that the B and $\overline{B}$ are produced with the appropriate decay angles. The variable "dm" is the mixing frequency (Δm_d) of the neutral B mesons as defined in `DECAY.DEC`.

Final state radiation using the `PHOTOS` [30] package may be included in each decay mode. This option is invoked by the key word `PHOTOS`, which is placed after the list of decay daughters, but before the model name. In the following example for $B^0 \to D^{*-}\ell^+\nu$, the `EvtGen` will call the `PHOTOS` package and use

a HQET inspired parameterization of the decay spectrum with parameters for ρ^2, R_1, and R_2 respectively:

```
Decay B0
0.5000  D*- e+  nu_e          PHOTOS HQET3S1 0.92 1.18 0.72;
0.5000  D*- mu+ nu_mu                HQET3S1 0.92 1.18 0.72;
Enddecay
```

In `EvtGen`, all particle property information is contained within the particle data table. Here is an example of part of the `pdt.table`:

```
name     id  mass    width max_Dm 3*Q 2*S lifetime*c Lund-KC
e-       11  0.00051  0     0     -3  1     0          11
e+      -11  0.00051  0     0      3  1     0           0
B0       511 5.2794   0     0      0  0     0.462     107
anti-B0 -511 5.2794   0     0      0  0     0.462       0
B+       521 5.2791   0     0      3  0     0.502     108
B-      -521 5.2791   0     0     -3  0     0.502       0
```

The "`id`" is the particle number according to the standard high energy physics numbering scheme. In columns 3 to 5, the "`mass`", the "`width`", the "maximum allowed deviation from the mean mass in the downward direction" all have units of GeV. The sixth column contains 3 times the charge of the particle and the seventh column contains twice the spin. The $c\tau$ is the lifetime times the speed of light and it is quoted in units of mm. The last column is the Lund-KC particle identity number[27], which is used for the interface to `Jetset`.

To set the particle data and decay table, and to specify $\Upsilon(4S)$ decays, the following code is placed in the decay Tcl script file:

```
module talk GfiEvtGen
  PDT          set ~/mypdt.table
  DECAY        set ~/myDECAY.DEC
  GENERATE     set "Upsilon(4S)"
exit
```

Here "`mypdt.table`" and "`myDECAY.DEC`" are the user modified versions of the default `pdt.table` and `DECAY.DEC`, respectively.

We can direct the generator to produce only events which satisfy some specific conditions by using a generator-level filter to make the selection. This saves

a lot of computer time which would otherwise be spent simulating events that are of no interest. For example, the following Tcl commands will only allow events with e^+e^- or $\mu^+\mu^-$ in the final states of $\Upsilon(4S)$ decays.

```
module talk GefSelectFilter
  BooNew        Pdt1 = GefPdtList
  BooNew        Pdt2 = GefPdtList
  BooObjects    Pdt1   and e+ e-
  BooObjects    Pdt2   and mu+ mu-
  BooCompose    myfilter = or Pdt1 Pdt2
  beforeFilter  set    myfilter
exit
```

The filter that we used for our dilepton events generation is very much the same as the example above but included all combinations of dileptons.

To generate multiple runs with non-overlapping random numbers, we can change the run number for each run by:

```
module talk RacTestInput
  run  set  1
exit
```

where the run number 1 is specified, and it can be changed for the following runs to be 2, 3, 4, etc.

After compiling and linking (for details, see Ref.[29]), we are ready to run the executable called "`GeneratorsQAApp`" from our working directory. We instruct it to generate one million events and then exit as follows:

```
ev begin -nev 1000000
exit
```

The output of `EvtGen` is a set of 4-vector momenta and vertex positions for the decay products. The following is part of an example output for an event generated with `EvtGen`:

```
Id          Px       Py       Pz       E        Vx       Vy       Vz
e-       -0.1881 -0.0074  8.9953  8.9973 -0.0906  0.2750  0.6745
e+        0.0664  0.0031 -3.1103  3.1110 -0.0906  0.2750  0.6745
Upsilon -0.1218 -0.0043  5.8850 12.1083 -0.0906  0.2750  0.6745
anti-B0 -0.3649 -0.1597  2.9009  6.0371 -0.0906  0.2750  0.6745
B0       0.2431  0.1555  2.9840  6.0712 -0.0906  0.2750  0.6745
D*+      0.7218 -1.6926  1.8923  3.3176 -0.0934  0.2737  0.6965
mu-      0.0781  1.2371  0.8515  1.5075 -0.0934  0.2737  0.6965
```

The momenta are in units of GeV and vertex coordinates (`Vx`, `Vy`, `Vz`) are in units of centimeters. These four-vectors are normally used as the input to the down stream detector response simulation, which is outside of the scope of this thesis.

All of the information of the generated decays will be stored in an NTuple contained within an HBOOK file, which can be converted into a `Root` file for subsequent analysis. All of our data analysis will be based on this `Root` file, which contains all of the information needed for our Monte Carlo study.

Chapter 4

Neutral B Mixing Frequency Measurement

Since the neutral B mixing frequency Δm_d is sensitive to both of the CKM matrix elements $|V_{tb}|$ and $|V_{td}|$, its measurement is of fundamental importance in particle physics. The value of Δm_d has been measured by many experiments around the world since the late 1980's. Recently, more precise measurements of Δm_d are possible with the help of high luminosities and clean backgrounds at asymmetric B factories.

In this chapter we first briefly review the existing neutral B mixing measurements in Section 4.1. We will focus on more precise measurements from B factories, for which a neutral B mixing parameterization is studied in this thesis. The boost approximation and the point of closest approach (POCA) method are introduced and explained in Sections 4.2 and 4.3, respectively. These are the two major approximations used in these measurements and in our Monte Carlo analysis as well.

4.1 Brief review of B^0-$\overline{B}^0$ mixing measurements

Time-integrated measurements of neutral B mixing were published for the first time in 1987 by UA1[31] and ARGUS [32], and since then by many other experiments, such as CLEO[33] and LEP experiments. These measurements are typically based on counting same-sign and opposite-sign lepton pairs from semileptonic decays of the produced $b\bar{b}$ pairs. Assuming $\Delta\Gamma_d = 0$, the time-integrated

mixing probability for B_d system in Eq. (2.14) becomes

$$\chi_d = \frac{x_d^2}{2(1+x_d^2)} \quad \text{with} \quad x_d = \frac{\Delta m_d}{\Gamma_d}. \tag{4.1}$$

By using this relation, the measured average $\chi_d = 0.182 \pm 0.015$ from ARGUS and CLEO converts to[34]

$$\Delta m_d = 0.493 \pm 0.032\,\text{ps}^{-1}. \tag{4.2}$$

These time-integrated analyses, however, cannot easily separate the contributions from the different b-hadron species produced from the $b\overline{b}$ pair. Furthermore, Δm_d has to be inferred from the time-integrated probability as shown in Eq. (4.1) (for details, see the review of B^0-$\overline{B}^0$ mixing in Ref.[4]).

Better sensitivity can be obtained from time-dependent analyses aimed at the direct measurement of the oscillation frequency Δm_d. This frequency can be measured from the proper time distributions of B_d^0 candidates identified through their decays in flavor-specific modes, and suitably tagged as mixed or unmixed (see Section 2.1 for details).

At high-energy colliders (LEP and Tevatron), the proper decay time is measured from the distance L between the B production and decay vertices, and from an estimate of the B momentum p, given by

$$t = \frac{L}{\beta\gamma} = \frac{m_B}{p} L, \tag{4.3}$$

where m_B is the B meson mass. We will also use this relation to calculate the proper B decay time for event re-weighting in our Monte Carlo study.

At asymmetric B factories (KEKB, PEP-II) with $e^+e^- \to \Upsilon(4S) \to B^0\overline{B}^0$, the proper decay time for a B meson can be measured from its traveled distance z along the beam direction (ignoring the small transverse distance) by using:

$$t \simeq \frac{z}{\beta\gamma}. \tag{4.4}$$

Since the boosts for the two B mesons are unknown and unequal (due to unequal momenta) in the lab frame, the proper decay time difference between

the two B candidates is estimated by an average boost[1] as

$$\Delta t \simeq \frac{\Delta z}{<\beta\gamma>}, \tag{4.5}$$

where Δz is the spatial separation between the two B decay vertices along the boost direction.

Many time-dependent neutral B_d oscillation analyses have been published by experiments around the world. A variety of techniques have been used: ALEPH[35], DELPHI[36], L3[37], and OPAL[38] used hadronic Z decays from $e^+e^- \to Z \to b\bar{b}$; CDF[39] used the Fermilab Tevatron $p\bar{p}$ Collider operating at $\sqrt{s} = 1.8\,\text{TeV}$; *BABAR* [40, 41, 42] and Belle[44, 45] used $e^+e^- \to \Upsilon(4S) \to B^0\overline{B}^0$. All individual experiment averages are listed in Fig. 4.1, which are obtained by the B oscillations working group within the Heavy Flavour Averaging Group (HFAG)[34]. Combining all published time-dependent measurements and accounting for all identified correlations, yields[2]:

$$\Delta m_d = 0.510 \pm 0.003 \pm 0.004\,\text{ps}^{-1}. \tag{4.6}$$

Assuming $\Delta\Gamma_d = 0$ and no CP violation in mixing, and using the measured B_d^0 lifetime, the time-integrated and time-dependent Δm_d measurements in Eq. (4.2) and Eq. (4.6) are combined to yield the world average value[34]

$$\Delta m_d = 0.509 \pm 0.005\,\text{ps}^{-1}. \tag{4.7}$$

It's worth noting that the most recent and precise analyses at the asymmetric B factories measure simultaneously Δm_d and the neutral B meson lifetime $\tau(B^0)$. The simultaneous measurements of neutral B lifetime and mixing frequency by *BABAR* are based on fully[41] or partially[42] reconstructed $B^0 \to D^*\ell\nu$ decays. On the other hand, the latest Belle analysis[45], based on fully reconstructed hadronic B^0 decays and $B^0 \to D^*\ell\nu$ decays, extracts simultaneously Δm_d, $\tau(B^0)$, and $\tau(B^+)$. The results of these three simultaneous measurements of Δm_d and $\tau(B^0)$ are displayed in a two-dimensional plot in

[1] *BABAR* and Belle have average boost $<\beta\gamma>$ of 0.55 and 0.425, respectively.

[2] The first quoted error is statistical and the second one is systematic. This applies to all the quoted measurement errors through this thesis.

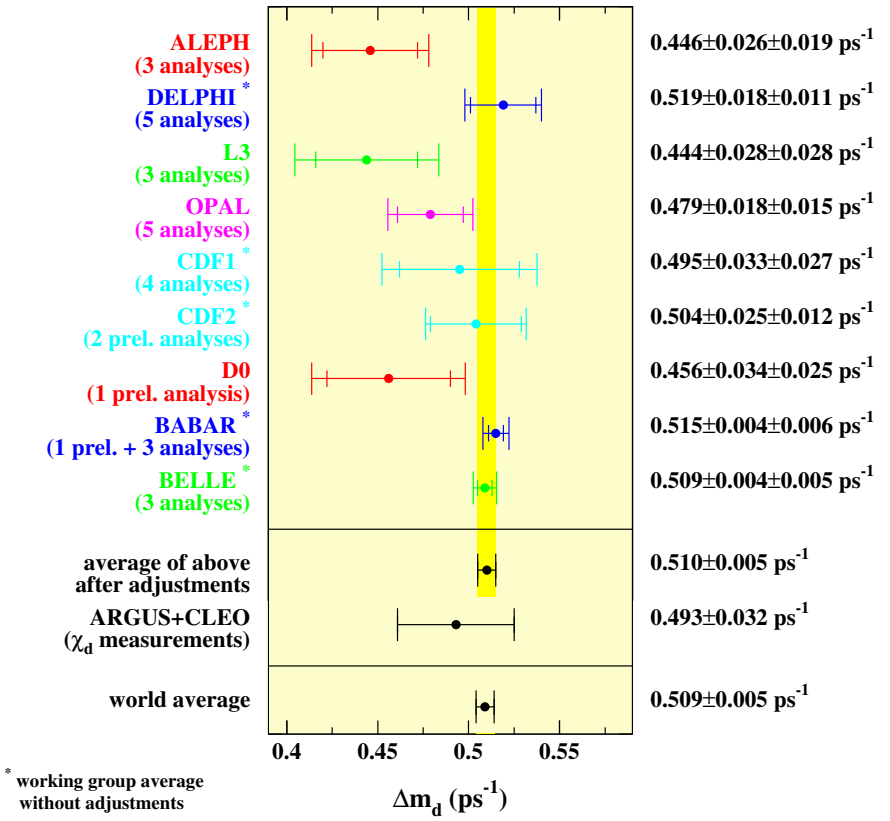

Figure 4.1: Average of Δm_d measurements from different experiments. This plot is taken from Ref.[34].

Fig. 4.2. Taking into account all statistical and systematic correlations, evaluating at the measured charged B lifetime $\tau(B^+)$, the three measurements are combined to yield the average values:

$$\Delta m_d = 0.514 \pm 0.005\ \mathrm{ps}^{-1}, \tag{4.8}$$

$$\tau(B^0) = 1.532 \pm 0.011\ \mathrm{ps}, \tag{4.9}$$

with a total correlation of -0.31[34].

One can see from Fig. 4.1 that measurements from B factories are more precise than others. Since the *BABAR* and Belle experiments are using almost the same technique to measure Δm_d, we will only provide more details of the measurement analyses made by *BABAR*, the experiment on which this thesis is

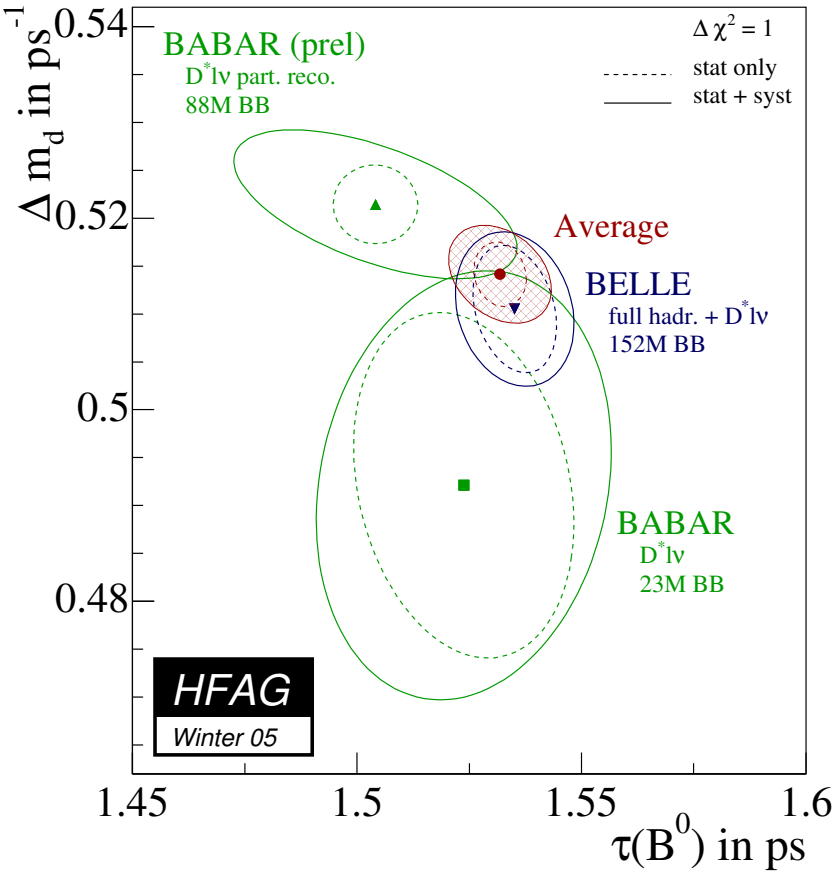

Figure 4.2: Simultaneous measurements of Δm_d and τ_{B^0}. The average of the three measurements is indicated by the shaded ellipse. This plot is taken from Ref.[34].

based.

BABAR had previously performed several precision measurements of the $B^0\overline{B}^0$ oscillation frequency Δm_d [40, 41, 42]. In those analyses, the total decay-rate difference between B^0 and $\overline{B}^0$, CP violation in mixing and CPT violation were assumed to be negligible. Recently, a generalized $B^0\overline{B}^0$ mixing analysis was performed which didn't make these assumptions[43]. In all of these analyses, the experimental technique consisted of first fully reconstructing a B meson

and measuring the vertex position of this "B_{reco}". The vertex of the second B, which is called "B_{tag}", was determined using the remaining charged tracks of the event. The flavour of "B_{tag}" was determined from the charge of leptons and/or other tracks among the remaining tracks, such as kaon(s) and soft pion(s). The distance along the beam direction between the "B_{reco}" and "B_{tag}" vertices was then used to estimate the lifetime difference Δt between the two B mesons, using the boost approximation. The reconstructed B pairs were classified in categories which depended on the flavours of "B_{reco}" and "B_{tag}". A fit to the measured Δt distributions in the different categories was performed to extract the $B^0\overline{B}^0$ mixing parameters.

In previous measurements, the $B^0\overline{B}^0$ pairs are classified as "mixed" or "unmixed". The parameter Δm_d is extracted from the asymmetry in Eq. (2.24).

In the generalized analysis, the B pairs are classified in 6 different categories: B^0B^0, $B^0\overline{B}^0$, $\overline{B}^0B^0$, $\overline{B}^0\overline{B}^0$, B^0B_{CP}, $\overline{B}^0B_{CP}$, where the two B mesons are B_{tag} and B_{reco}, respectively. Unlike the previous mixing analysis, the inclusion of CP eigenstates for B_{reco} in this analysis leads to a more complex fit formula (for details, see Ref.[43]).

4.2 Boost approximation

One of the advantages of an asymmetric B factory is that the proper B decay time can be inferred from the corresponding measurable decay length by using the boost approximation. In the following, we will briefly explain how the boost approximation works.

Let the 4-momenta of the e^-, e^+, and $\Upsilon(4S)$ be (using convention P=(E, P_x, P_y, P_z)):

$$\begin{aligned} P_{e^-} &= (p_1,\ 0,\ 0,\ p_1); \\ P_{e^+} &= (p_2,\ 0,\ 0, -p_2); \\ P_{\Upsilon(4S)} &= (p_1 + p_2,\ 0,\ 0,\ p_1 - p_2). \end{aligned} \tag{4.10}$$

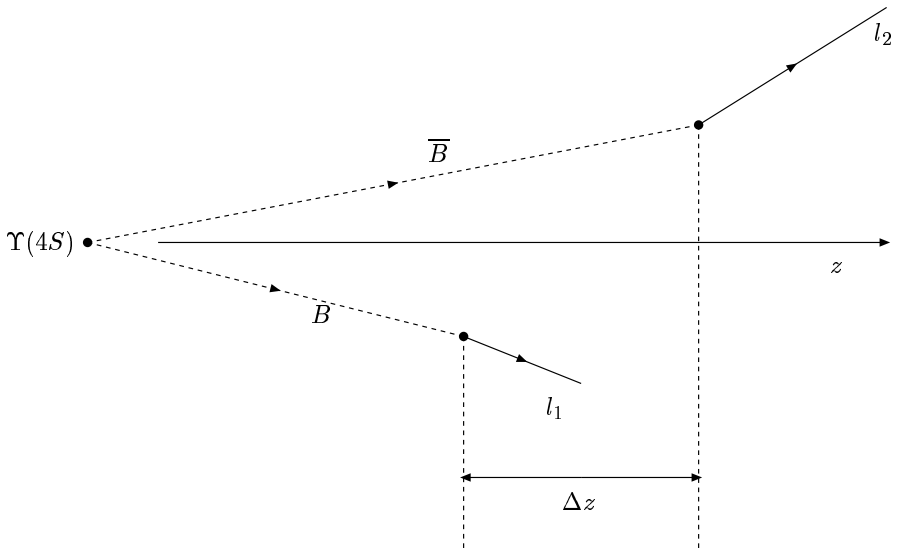

Figure 4.3: Two B decay vertices, showing displacement along the boost axis, Δz.

It follows that the boost factor of $\Upsilon(4S)$ is given by

$$\beta\gamma = \frac{|\vec{P}_{\Upsilon(4S)}|}{m_{\Upsilon(4S)}} = \frac{p_1 - p_2}{m_{\Upsilon(4S)}} = \frac{9.0 - 3.1}{10.58} = 0.558. \tag{4.11}$$

where the nominal momenta of the e^- (9.0 GeV) and the e^+ (3.1 GeV), and the $\Upsilon(4S)$ mass (10.58 GeV) were used.

In the real experiment, there are small transverse momenta and small fluctuations in the e^+e^- 4-momenta. We can randomly select a Monte Carlo event as an example with the following 4-momenta in units of GeV:

$$\begin{aligned} P_{e^-} &= (\ 8.9844, -0.1902, -0.0085,\ \ 8.9824); \\ P_{e^+} &= (\ 3.1099,\ \ 0.0666,\ \ 0.0025, -3.1092); \\ P_{\Upsilon(4S)} &= (12.094\ , -0.1236, -0.0060,\ \ 5.8733). \end{aligned} \tag{4.12}$$

which results in a boost of

$$\beta\gamma = \frac{|\vec{P}_{\Upsilon(4S)}|}{m_{\Upsilon(4S)}} = \frac{5.8746}{10.58} = 0.553. \tag{4.13}$$

In the data analysis, the average boost $< \beta\gamma >= 0.55$ was used for the *BABAR* experiment. We will choose this same value in our Monte Carlo analysis as well.

Since the two B mesons are almost at rest in the $\Upsilon(4S)$ frame, the proper time difference between their decays is estimated with the help of this boost by,

$$\Delta t \simeq \frac{\Delta z}{< \beta\gamma >}, \tag{4.14}$$

where Δz is the z coordinate difference between the two B decay vertices as shown in Fig. 4.3.

This approximation neglects the B meson's motion in the $\Upsilon(4S)$ rest frame (i.e. a momentum of 335 MeV), and could in principle introduce a systematic Δm_d shift which is not negligible at the level of accuracy expected (better than 2% on Δm_d). Since it is not possible to determine the exact boost, the effect of this bias was studied with a toy Monte Carlo by comparing the fitted value of Δm_d with the true Δt and with $\Delta z / < \beta\gamma >$. The relative systematic error related to the correction of the shift is about 0.3%[46].

4.3 Point of closest approach–POCA

The problem of estimating the z coordinate of the B decay vertex with the use of only the lepton track can be solved to a first approximation by taking the z coordinate of the point of closest approach between the track and the beam spot in the x-y plane. This estimator is a fairly good way to determine the z position of the B decay vertices, since the selected direct leptons have rather high momenta, which result in relatively small errors on the track positions.

The point of closest approach (POCA) with respect to the decay vertex of the $\Upsilon(4S)$ (also the e^+e^- collision point) in the x-y plane is calculated for each leptonic track. The corresponding z coordinates represent the best approximation of the z coordinates of the decay vertices of the two B mesons. More details can be found in Ref.[46].

The topology of the dilepton event in the transverse plane is shown in Fig. 4.4. In experimental analysis, the point on the lepton track closest to

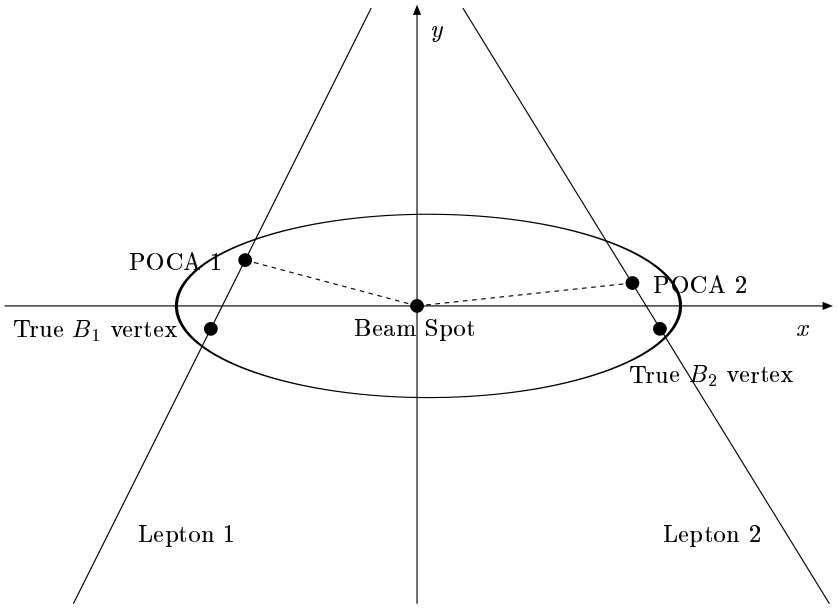

Figure 4.4: Dilepton event topology in the transverse plane.

the beam spot (average of collision points) is taken as an estimation of the true vertex. That is, in Fig. 4.4, "POCA 1" and "POCA 2" are chosen as estimations of "True B_1 vertex" and "True B_2 vertex", respectively. Then use x and y coordinates of these POCA points to find the corresponding z coordinates on the lepton tracks. Therefore, the estimated vertex difference Δz is obtained by using this "POCA" approximation.

To simulate real data analysis, we follow this same POCA approach even though we know the exact B decay vertices in our Monte Carlo simulated events. For example, let the real B decay vertex, the lepton momentum, and the e^+e^- collision point for one dilepton event be, respectively,

$$\begin{aligned} \vec{X} &= (x,\ y,\ z); \\ \vec{P} &= (p_x,\ p_y,\ p_z); \\ \vec{X^0} &= (x^0,\ y^0,\ z^0). \end{aligned} \tag{4.15}$$

The estimated vertex $\vec{X}'$ should be on the lepton track. It can be written as,

$$\vec{X}' = \vec{X} + s \cdot \vec{P}, \tag{4.16}$$

where s is a constant.

Therefore, the estimated z coordinate of the B decay vertex is

$$z' = z + s \cdot p_z. \tag{4.17}$$

The constant s is determined by finding the POCA within the x-y plane. That is, s is determined by the minimization condition:

$$\frac{\partial (X'_\perp - X^0_\perp) \cdot (X'_\perp - X^0_\perp)}{\partial s} = 0, \tag{4.18}$$

where the subscript "$\perp$" represents the transverse components of a vector. Solving this equation gives the following value for s:

$$s = \frac{P_\perp \cdot (X^0_\perp - X_\perp)}{P_\perp \cdot P_\perp}. \tag{4.19}$$

Plugging Eq. (4.19) into Eq. (4.17) gives our estimate of the z coordinate for the B decay vertex

$$z' = z + \frac{P_\perp \cdot (X^0_\perp - X_\perp)}{P_\perp \cdot P_\perp} \cdot p_z, \tag{4.20}$$

which we will call "POCA z". The z coordinate difference of the two B vertices, therefore, will be called "POCA Δz". From Eq. (4.20), we see that different values of real Δz can end up with the same value of POCA Δz. By using the boost approximation as discussed in Section 4.2, it means that different "real" Δt will contribute to the same POCA estimated Δt. This is usually called the smearing effect of the POCA approximation.

In the real experiment, we cannot know exactly the collision point for each event. Therefore, the nominal beam spot for each run will be used as an estimation of the average collision point. Even though we know the exact collision point for each Monte Carlo event, we will follow the same method as that of real experiment data by using the beam spot for each run. The beam spot is fixed for each run in our Monte Carlo generation and is equivalent to the average e^+e^- collision point in that run.

Chapter 5

Analysis Strategy

To get exact distributions of the measured proper decay time difference Δt for the two B meson decays, we need to study how these distributions depend on lifetime and mixing frequency. This is achieved by studying Δt distributions with different values of lifetime and mixing frequency and parameterizing the changes. As a result, the parameterized Δt distributions can be used to extract values for the B lifetime τ_B and the neutral B mixing frequency Δm_d from experimental data.

In this chapter, we first explain how our events were generated and classified in Sections 5.1 and 5.2, respectively. The details of event re-weighting are given in Section 5.3. Finally, we explain our choice of parameterization model and fitting strategy in Section 5.4.

5.1 Event generation

The two key physics parameters of interest in generating Monte Carlo events are the B meson lifetime and the neutral B mixing frequency. As explained in Section 3.2, they are defined in the files `pdt.table` and `DECAY.DEC`, respectively. We can change the values of the B lifetime and the neutral B mixing frequency in these two files for event generation.

The default values[1] and the ones we used in our Monte Carlo simulation are listed in Table 5.1. We chose the B lifetimes to be 4 times longer than the default values and generated all events without mixing. The reason for using longer lifetimes is that we want to get more statistics for events with larger time difference Δt, which makes our later event re-weighting more reliable in

[1] We quote these default values in the rest of this thesis by using a superscript "0" for each of the symbols: $\tau^0_{B^0}$, $\tau^0_{B^+}$, and Δm^0_d.

	Default Value	Our Choice	World Average (PDG[4])
τ_{B^0} (ps)	1.541	4×1.541	1.536
τ_{B^+} (ps)	1.674	4×1.674	1.671
Δm_d (ps^{-1})	0.489	0	0.502

Table 5.1: B lifetimes and the neutral B mixing frequency: Default values versus our choice. The default values are very close to the 2004 world average values with fractional difference less than 3%.

that region. Similarly, the reason for choosing zero mixing is to make our event re-weighting reliable along all values of Δt (more details will follow in Section 5.3.).

As explained in Section 3.2, we use a generator-level filter to require *at least* 2 leptons in the final state of $\Upsilon(4S)$ decays, where either of the leptons could be an electron or a muon[2]. The two highest-momenta leptons of the final state will be selected as our dilepton signal. The lepton pairs are ordered in their momenta in the lab frame: *lepton 1* is always the lepton with the highest momentum and *lepton 2* is the lepton with the second highest momentum. Therefore, Δt (or Δz) is a signed quantity, with the value of lepton 1 minus that of lepton 2, i.e., $\Delta t = t_1 - t_2$ and $\Delta z = z_1 - z_2$.

80 million events passing our filter were generated by the generator package `EvtGen` within the *BABAR* framework. All of these events were generated with the parameter values specified in Table 5.1. The Δt distributions for any value of neutral B mixing frequency can be obtained by re-weighting these generated events.

An additional 35 million dilepton events with default lifetimes and mixing frequency were also independently generated as test events. This second set of 35 million events are used to obtain Δt distributions without any event re-weighting. We then use these distributions and our parameterization results (from the first 80 million events) to extract the B meson lifetimes and the neutral B mixing frequency. By comparing the fitted values with the expected values

[2] We do not include tau as our signal lepton because it has a very short lifetime ($\tau \simeq 0.29\,\text{ps}$), and is not detected directly.

MC Information	Particle	Used in Part of Analysis
ID	Leptons, B mesons	Event classification
Vertex	Leptons and $\Upsilon(4S)$	POCA and boost
Momentum	Leptons	POCA approximation
Proper Decay Time	B mesons	Event re-weighting

Table 5.2: Monte Carlo event information used in our analysis.

for B lifetimes and mixing frequency, we can cross check our parameterization method.

All of the necessary information that we need for each event in our analysis is listed in Table 5.2. This information is extracted for the generated events from the generator by using a Monte Carlo truth analysis module as described in Section 3.2. It is stored in an NTuple and is ready to be read out by later analysis modules.

Here particle identities (ID) for leptons and their B parents are essential for event classification. The vertices of selected leptons and the e^+e^- collision point, which is the same as the $\Upsilon(4S)$ production vertex, are used in the POCA and boost approximations as shown in Sections 4.2 and 4.3. Momenta of leptons are needed in the POCA approximation as well. The proper decay times of the lepton B parents are used to re-weight the generated events (details of event re-weighting will be given in Section 5.3.).

All the information listed in Table 5.2 is available directly from the MC-truth information for each generated event, except for the proper time of B decays, which are calculated by

$$t_{proper} = \frac{m_B}{p} L, \tag{5.1}$$

where L is the distance between the B production and decay vertices, and p is the B meson momentum in the Lab frame [3].

[3] As mentioned in Section 4.1, this technique is also used by other B mixing studies at high-energy colliders, such as Tevatron, where the boost approximation doesn't hold.

5.2 Event classification

Dilepton events are classified by three combined criteria as shown in Table 5.3. In the following, we explain each of them in detail.

Criterion	Category
Lepton Sign	Same Sign (SS) Opposite Sign (OS)
Lepton Momentum	High-High (HH) High-Low (HL) Low-Low (LL)
Lepton B Parent	Same B (SB) Opposite Charged B (OCB) Opposite Neutral B (ONB)

Table 5.3: Dilepton event categories. All events are classified by combining these three criteria.

- Lepton Sign of Charge

  Firstly, the two selected leptons are classified by their sign of charge. An event is called *Same Sign* (SS) event if the two leptons have same sign of charge; Otherwise, it is called an *Opposite Sign* (OS) event.

- Lepton Momentum

  Secondly, the two selected leptons are classified by their momenta with the definition of High (H) and Low (L) momenta as follows,

$$\begin{aligned} \text{Low:} \quad & 0.5\,\text{GeV} \leq p < 1.2\,\text{GeV}; \\ \text{High:} \quad & 1.2\,\text{GeV} \leq p < 5.0\,\text{GeV}. \end{aligned} \tag{5.2}$$

  To simulate real data analysis, leptons with momenta lower than 0.5 GeV are removed because of their poor resolution and low efficiency in detector, even though there is no detector simulation in our analysis. Momentum of the first and the second leptons are classified into *High-High* (HH), *High-Low* (HL), and *Low-Low* (LL) combinations. Since the two leptons are

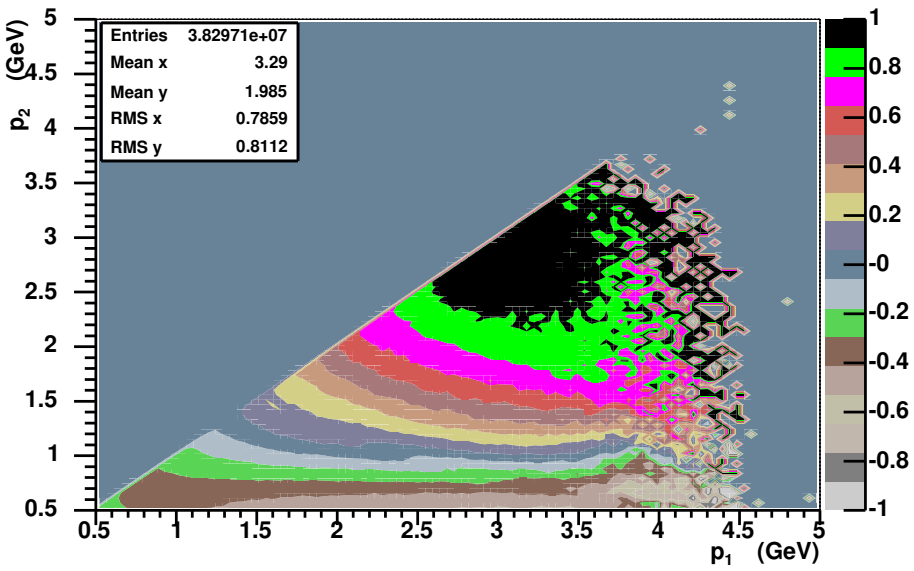

Figure 5.1: Re-scaled 2-D momentum contour plot of dilepton events.

sorted by their momenta, there is no Low-High category in our selected events.

The division of Low and High momentum is obtained with the help of a 2-D contour plot of lepton momentum as shown in Fig. 5.1, where the x-axis is the momentum of lepton 1 and the y-axis is the momentum of lepton 2. The contour plot was obtained by using opposite neutral B events with weight 1 for the correct sign dileptons and with weight -1 for the wrong sign dileptons[4]. The contours are rescaled by the sum of correct and wrong dilepton events so that they have moduli no larger than 1. In case of equal number of correct and wrong sign dilepton events, we get the zero contour in the plot, which has the same colour as the region without any events (the upper-left part of the plot). We choose 1.2 GeV as our event division as it is very close to the zero contour shown in Fig. 5.1.

[4]If two leptons have right-right or wrong-wrong signs, they keep the correct sign of their B parents (OS or SS). Therefore, they are called "correct sign" dileptons. On the other hand, if one lepton has the correct sign and the other has the wrong sign, they are called "wrong sign" dileptons. The division of the lepton momentum was chosen as the region with roughly equal right and wrong dilepton events.

In this way, the High-High events are mostly correct sign dilepton events, High-Low events are a mixture of correct and wrong sign dileptons, and Low-Low events are mostly wrong sign dileptons as shown by the negative contours.

- Lepton B Parent

  Thirdly, the two selected leptons are also classified by their B parents. If the two leptons of an event come from the same B parent, then it is called a *Same B* (SB) event. If they come from different B parents, it is then called an *Opposite Charged B* (OCB) event or an *Opposite Neutral B* (ONB) event, depending on the charge of the B parents.

The sample distributions of the "POCA Δt"[5] are shown in Fig. 5.2 (SB), Fig. 5.3 (OCB), and Fig. 5.4 (ONB). All of these distributions are obtained from the test events with the default values of B lifetimes and mixing frequency as specified in Table 5.1. In each of the figures, the first column is for the opposite sign events and the second column is for the same sign events. Similarly, the three rows correspond to High-High, High-Low, and Low-Low events, respectively.

For the same B events shown in Fig. 5.2, most of the dilepton events have opposite sign. This is because the first leptons with highest momentum are mostly direct leptons with the correct sign. The secondary leptons are mostly produced from cascade D decays. As explained in Section 2.1, these cascade leptons mostly have the wrong sign of charge compared to a direct lepton. Therefore, the two leptons produced from the same B decay mostly have opposite signs. The reason for having very a small number of same sign events with High-High momenta is that both of the leptons come from B cascade decays, which are very unlikely to both have momentum larger than 1.2 GeV. We get more same sign events in the Low-Low category because the two leptons are more likely to be both cascade leptons with the same sign of charge. Since both

[5]The Δt converted from the POCA Δz by using the boost approximation is called the "POCA Δt" in the rest of this thesis.

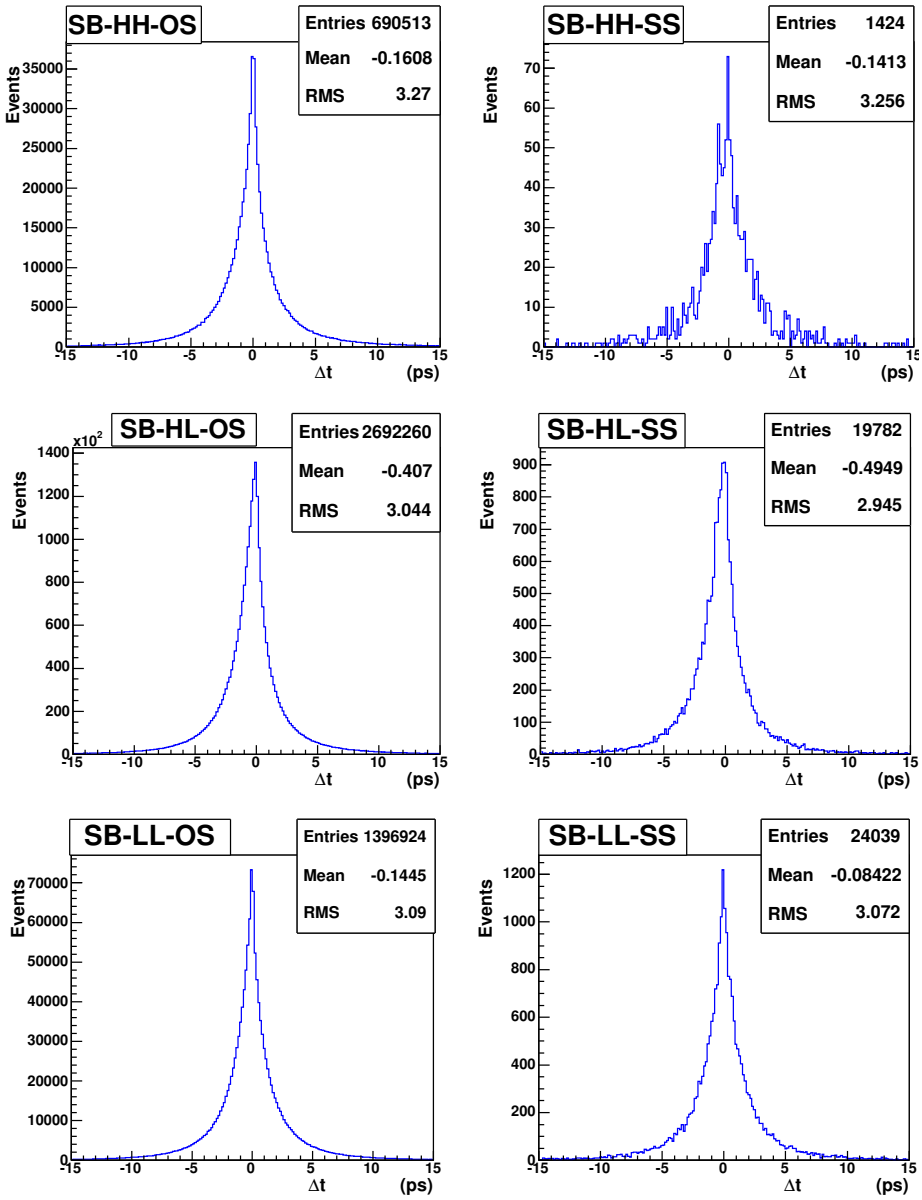

Figure 5.2: POCA Δt distributions for the same B (SB) events. In this category, both of the two leptons come from the same B parent. The two columns correspond to opposite sign (OS) and same sign (SS), respectively. The three rows are High-High (HH), High-Low (HL), and Low-Low (LL) momenta categories.

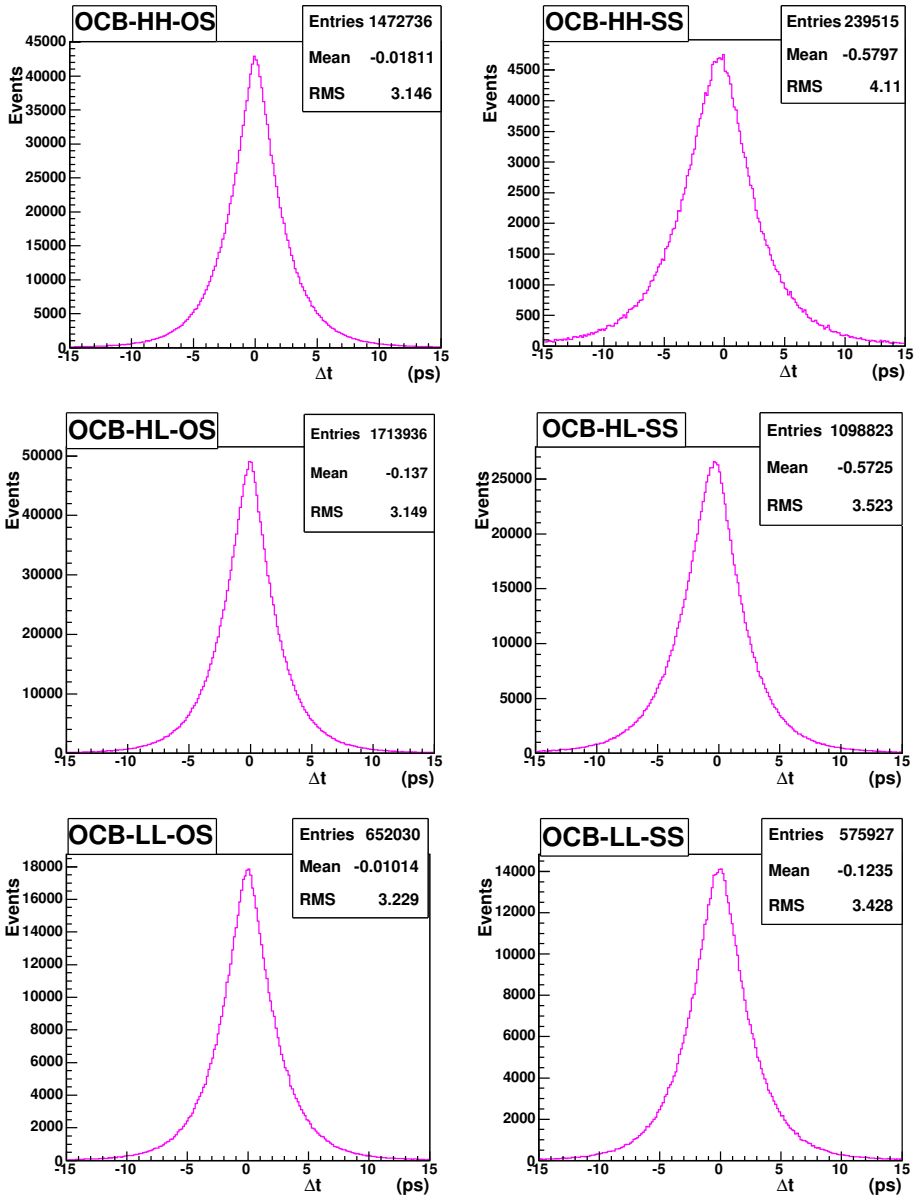

Figure 5.3: POCA Δt distributions for the opposite charged B (OCB) events. In this category, the two leptons come from opposite charged B mesons. That is, one lepton comes from B^+ and the other lepton comes from B^-. The two columns correspond to opposite sign (OS) and same sign (SS), respectively. The three rows are High-High (HH), High-Low (HL), and Low-Low (LL) momenta categories.

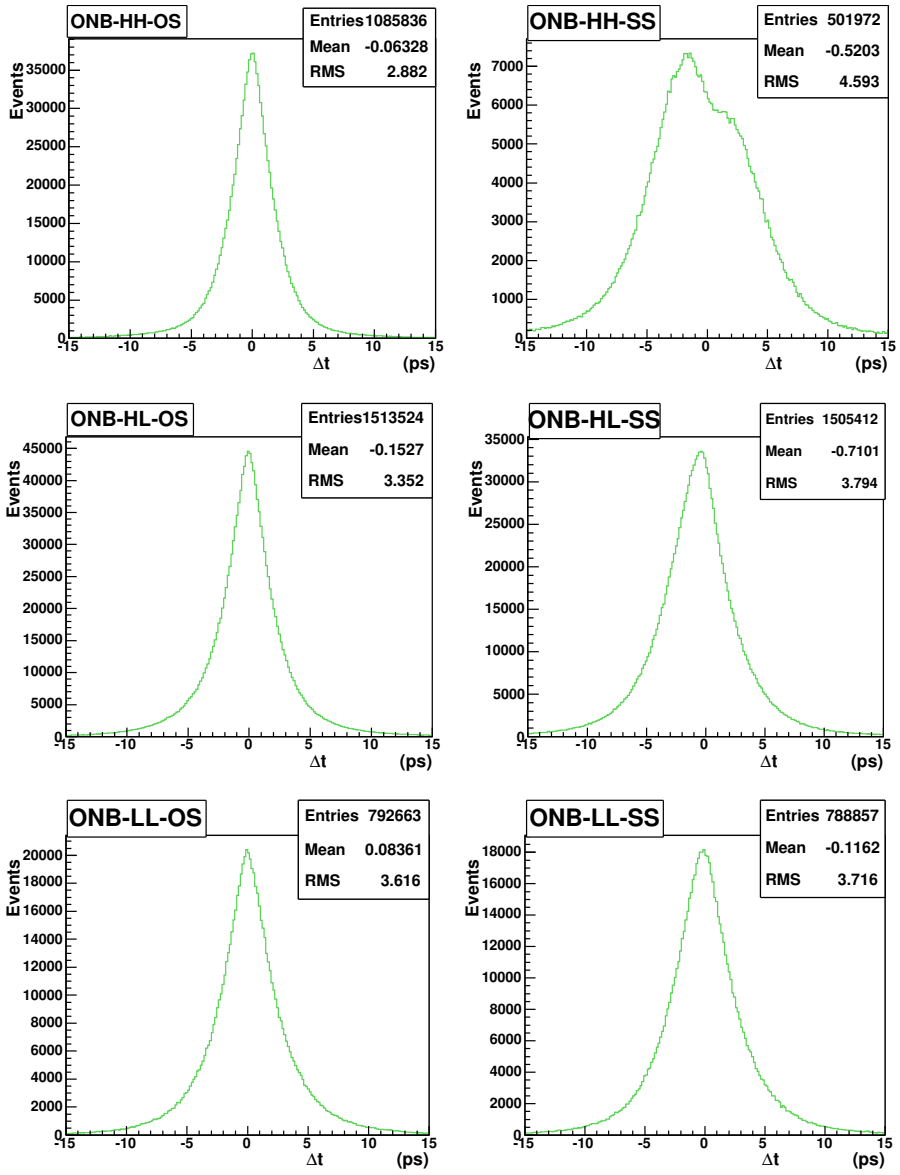

Figure 5.4: POCA Δt distributions for the opposite neutral B (ONB) events. In this category, the two leptons come from opposite neutral B mesons. Because of neutral B mixing, the two leptons can come from either of B^0B^0, $\overline{B}^0\overline{B}^0$, or $B^0\overline{B}^0$. But they must come from different B parents. The two columns correspond to opposite sign (OS) and same sign (SS), respectively. The three rows are High-High (HH), High-Low (HL), and Low-Low (LL) momenta categories.

of the two leptons are coming from the same B parent, the Δt distributions are independent of the B lifetime and the neutral B mixing frequency. Therefore, no parameterization is needed for these categories.

Similar reasoning also holds for the opposite charged B events in Fig. 5.3. Since charge is conserved, we will always have one B^+ and one B^-. In cases where both leptons keep the correct sign of their B parents or both are wrong, we get opposite sign events. In case one of the leptons keeps the correct sign and the other keeps the wrong sign of their B parents, we get same sign events. We still have a greater number of opposite sign events than same sign events. Since the two leptons come from opposite charged B mesons, the distributions depend only on the charged B lifetime, but not on the neutral B mixing frequency at all because charged mesons cannot mix. One of the goals of this thesis is to find a parameterization function for these opposite charged B Δt distributions.

When it comes to the opposite neutral B events in Fig. 5.4, there is one additional complexity compared to the opposite charged B events. Due to neutral B mixing, we can have same sign neutral B pairs (i.e., B^0B^0 or $\overline{B}^0\overline{B}^0$), therefore we still have a chance to get same sign events even when both leptons are direct leptons with correct signs. In this case, the distributions will depend on both the neutral B lifetime and the mixing frequency. The primary goal of this thesis is to find a parameterization function for these distributions, which can be used in precise measurements of the neutral B mixing frequency Δm_d.

For each of the distributions, we fill the events into a histogram with a range of ± 15 ps. Each of the histograms is divided into 200 Δt bins. For each of the 200 Δt bins, the bin content will change with varying lifetimes and/or mixing frequency. The primary task of the following two sections is to explain how to get distributions with different lifetimes and mixing frequency through event re-weighting, and how this behaviour can be parameterized for each bin of all categories.

5.3 Event re-weighting

As described in Section 2.3, the probability of getting an event with a neutral B pair produced from $\Upsilon(4S)$ decays can be written as

$$P_{nomix}(t_1, t_2, \tau_{B^0}, \Delta m_d) \propto \frac{1}{\tau_{B^0}^2} e^{-(t_1+t_2)/\tau_{B^0}} \left[1 + \cos(\Delta m_d (t_1 - t_2))\right], \quad (5.3)$$

$$P_{mix}(t_1, t_2, \tau_{B^0}, \Delta m_d) \propto \frac{1}{\tau_{B^0}^2} e^{-(t_1+t_2)/\tau_{B^0}} \left[1 - \cos(\Delta m_d (t_1 - t_2))\right], \quad (5.4)$$

where t_1 and t_2 are the proper decay times of the two B mesons. Eq. (5.3) and Eq. (5.4) hold for neutral B pairs without mixing (nomix) and with mixing (mix), respectively.

Since there is no mixing for charged B mesons, the probability of getting a charged B pair is

$$P_c(t_1, t_2, \tau_{B^+}) \propto \frac{1}{\tau_{B^+}^2} e^{-(t_1+t_2)/\tau_{B^+}}. \quad (5.5)$$

All the weights that we used in re-weighting the generated events into events with different lifetimes and mixing frequency are listed in Table 5.4. Our choice of lifetimes ($4 \times \tau^0$) and mixing frequency ($\Delta m_d = 0$) for generation are used in

Generated Category	Re-weighted Category	Weight
OCB (OS/SS)	OCB (OS/SS)	$\frac{P_c(t_1,t_2,\tau_{B^+})}{P_c(t_1,t_2,4\times\tau^0_{B^+})}$
ONB (OS)	ONB (OS)	$\frac{P_{nomix}(t_1,t_2,\tau_{B^0},\Delta m_d)}{P_{nomix}(t_1,t_2,4\times\tau^0_{B^0},0)}$
	ONB (SS)	$\frac{P_{mix}(t_1,t_2,\tau_{B^0},\Delta m_d)}{P_{nomix}(t_1,t_2,4\times\tau^0_{B^0},0)}$
ONB (SS)	ONB (OS)	$\frac{P_{mix}(t_1,t_2,\tau_{B^0},\Delta m_d)}{P_{nomix}(t_1,t_2,4\times\tau^0_{B^0},0)}$
	ONB (SS)	$\frac{P_{nomix}(t_1,t_2,\tau_{B^0},\Delta m_d)}{P_{nomix}(t_1,t_2,4\times\tau^0_{B^0},0)}$

Table 5.4: Weights for event re-weighting. The probability functions are given in Eqs. (5.3)-(5.5). Re-weighting can change the lepton sign for opposite neutral B events (ONB), but not for opposite charged B events (OCB) nor the same B events (SB).

the denominators of the weights. The values of lifetimes and mixing frequency in the numerators of the weights can be any value of interest. In our analysis, we vary these values by $\pm 10\%$ around the default values shown in Table 5.1.

For charged B events, the weight only depends on the charged B lifetime. Event re-weighting won't change the event category. For neutral B events, the event category can change when we re-weight the generated events with mixing. In this case, event re-weighting changes the sign type of some of the leptons (OS $\longleftrightarrow$ SS). This is how we recover the neutral B mixing from the generated un-mixed events.

It is the right time now to explain the physics parameters we chose in our event generation. Firstly, we can see from Table 5.4 that all the weights are ratios of two probabilities. From the probability function in Eq. (5.3) for un-mixed events, we can see that there is zero probability for some values of Δt if Δm_d is non-zero. This would make our event re-weighting unreliable since Eq. (5.3) appears in the denominators of the weights for opposite neutral B events. Therefore, $\Delta m_d = 0$ is a very good choice and makes our event re-weighting reliable for all values of Δt. Secondly, the probability of getting an event with longer B decay times of t_1 and t_2 becomes larger with longer lifetime. Therefore longer lifetime in the generation makes our event re-weighting more reliable in the larger Δt region (the tails in the Δt distributions).

5.4 Model selection and fitting strategy

With the help of the event categories and event re-weighting described above, we are now ready to introduce our model selection for the parameterization of Δt distributions.

As mentioned in Section 2.3, the probability of getting a direct dilepton event can be written as

$$P(\Delta t, \tau_{B^0}, \Delta m_d) = \frac{e^{-|\Delta t|/\tau_{B^0}}}{4\tau_{B^0}} [1 \pm \cos(\Delta m_d \Delta t)] \quad (5.6)$$

$$P(\Delta t, \tau_{B^+}) = \frac{e^{-|\Delta t|/\tau_{B^+}}}{4\tau_{B^+}} [1 \pm 1] \quad (5.7)$$

where the "+" sign is for OS events and the "−" sign is for SS events. Eq. (5.6) and Eq. (5.7) describe opposite neutral B events and opposite charged B events, respectively.

As explained in Chapter 4, we have to use the POCA and boost approximations to estimate Δt from Δz. Therefore, we need to study the distributions for this POCA Δt even though we know the distributions for the unmeasurable "real" Δt as shown in Eqs. (5.6) and (5.7). Furthermore, the probabilities listed in the equations above only apply to direct dileptons (where both leptons come from B meson decays directly). We want to know the distributions not only for these direct dileptons but also for other events where one or both leptons comes from B cascade decays. We need to choose our own parameterization functions for the POCA Δt in our Monte Carlo analysis.

For charged B events, the distributions only depend on the charged B lifetime. As an example, the Δt distributions for the sum of same sign and the opposite sign (OS+SS) events with varying B lifetime are shown in Fig. 5.5, where the lifetime is changed by $\pm 10\%$ around the default value ($\tau^0_{B^+} = 1.674\,\mathrm{ps}$). All these distributions are obtained from event re-weighting, as explained in Section 5.3. Therefore, we need only one function of B lifetime, which can be written as

$$P(\Delta t, \tau) = f(\Delta t, \tau), \tag{5.8}$$

where $f(\Delta t, \tau)$ is a function of Δt and τ.

Similarly, distributions for neutral B events depend on both the neutral B lifetime and the mixing frequency. For example, the Δt distributions with varying B lifetime and mixing frequency are shown in Fig. 5.6 (OS+SS) and Fig. 5.7 ((OS-SS)/(OS+SS)), where the lifetime and the mixing frequency are both changed by $\pm 10\%$ around the central values ($\tau^0_{B^0} = 1.541\,\mathrm{ps}$ and $\Delta m^0_d = 0.489\,\mathrm{ps}^{-1}$). As explained in Section 5.2, the High-High category has mostly opposite sign dileptons while the High-Low and Low-Low categories have almost equal number of the same sign and opposite sign dileptons. This explains why the asymmetries change with momentum in Fig. 5.7. All of these distributions

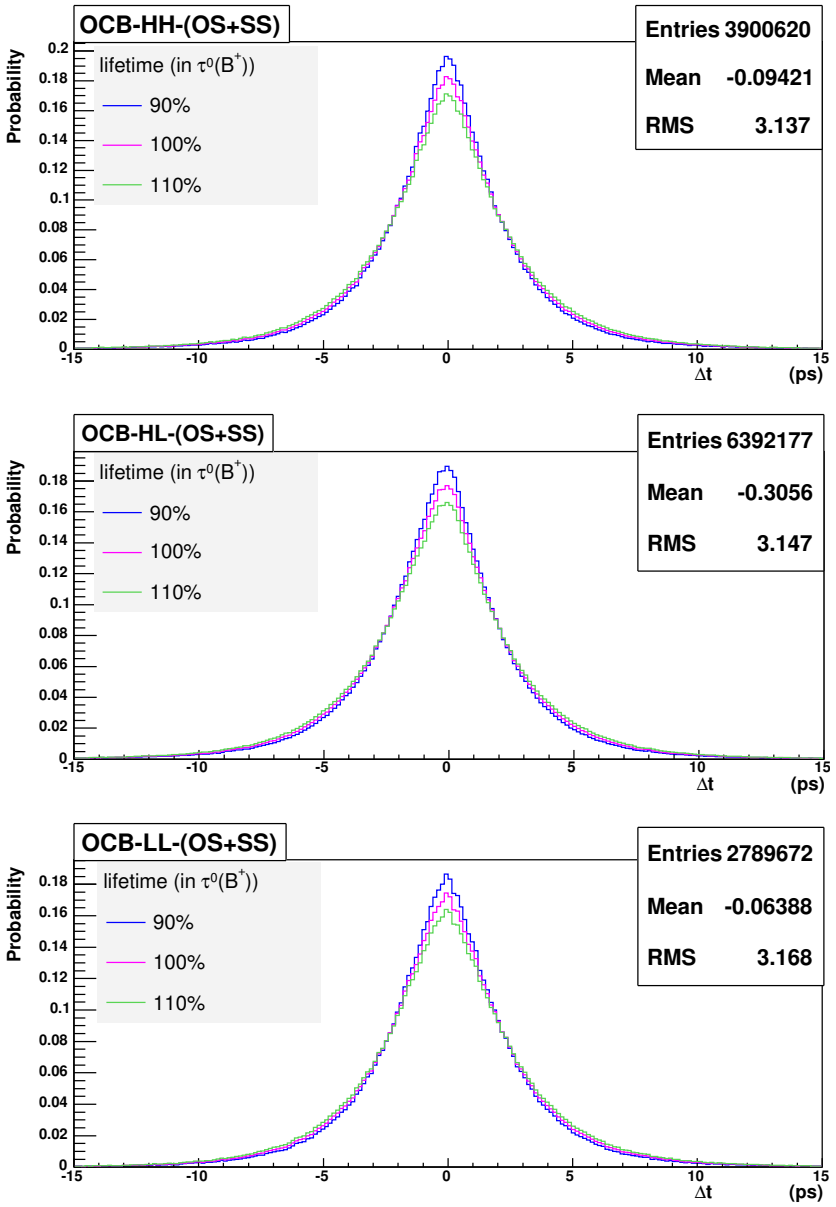

Figure 5.5: POCA Δt distributions of the sum of the same sign and opposite sign (OS+SS) for opposite charged B (OCB) events. For each category, we changed the charged B lifetime by $\pm 10\%$ around the default value ($\tau^0_{B^+}$).

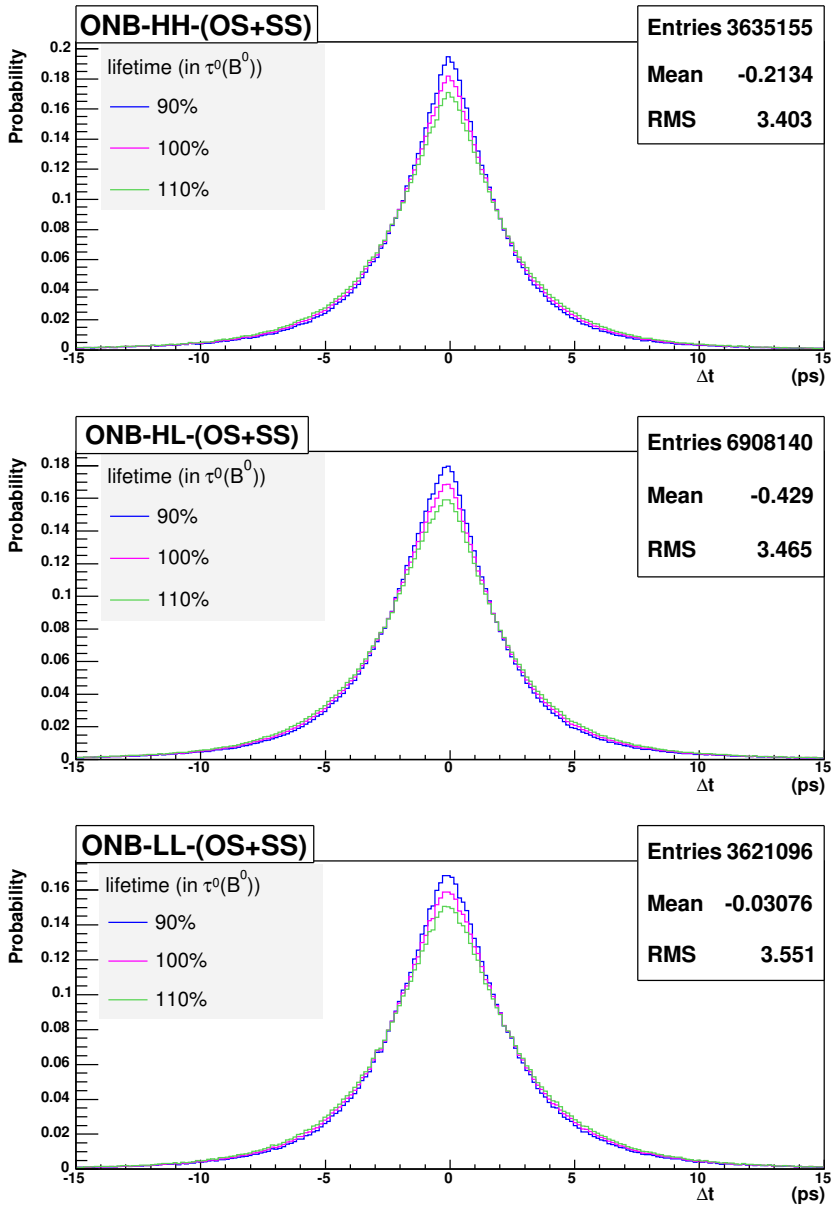

Figure 5.6: POCA Δt distributions of the sum of the same sign and opposite sign (OS+SS) for opposite neutral B (ONB) events. For each category, we changed the neutral B lifetime by $\pm 10\%$ around the default value ($\tau^0_{B^0}$).

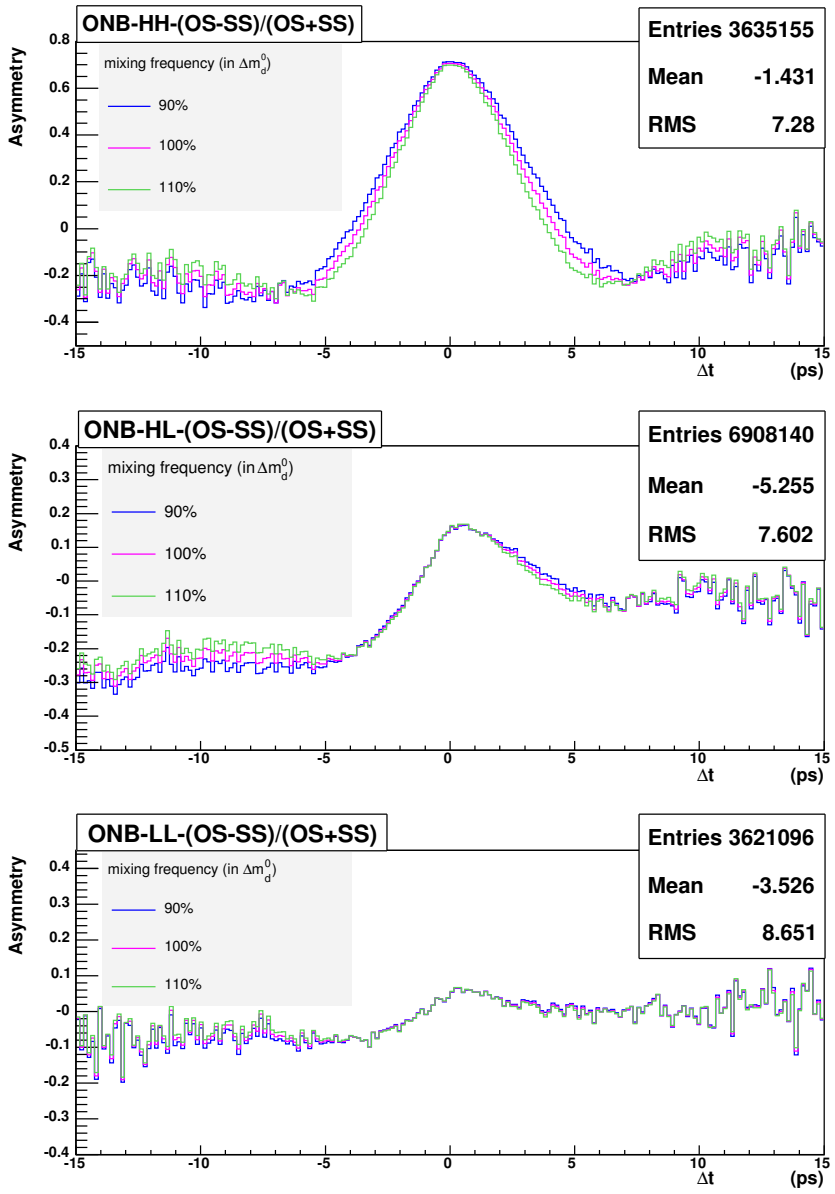

Figure 5.7: POCA Δt asymmetries between the opposite sign and the same sign events (OS-SS)/(OS+SS) for opposite neutral B (ONB) categories. For each category, the neutral B lifetime is fixed at default value ($\tau^0_{B^0}$) and the mixing frequency varied by $\pm 10\%$ around the default value (Δm^0_d).

are obtained from event re-weighting and the distributions in Fig. 5.7 are evaluated with the default lifetime. Therefore, we need one function of lifetime, similar to that for charged B events and another function of Δm_d as follows:

$$P(\Delta t, \tau, \Delta m) = f(\Delta t, \tau) \left[\frac{1}{2} \pm \frac{1}{2} g(\Delta t, \Delta m) \right], \tag{5.9}$$

where $g(\Delta t, \Delta m)$ is a function of Δt and Δm, and "$\pm$" stands for opposite sign and same sign events, respectively. The primary goal of this study is to determine this $g(\Delta t, \Delta m)$.

The lifetime part, $f(\Delta t, \tau)$, only depends on the B lifetime. The reason for the choice of the mixing part comes from the fact that the sum of OS and SS events will not depend the value of the mixing frequency Δm. Therefore the mixing parts must cancel out in the sum of the opposite sign and same sign events. With some simple algebra, one can show that the constant $1/2$ in Eq. (5.9) will not cause any problem and is chosen for convenience. If we choose any other constant, it will not change any of our results in an important way.

To make our fitting more reliable (with a smaller number of parameters[6]) and to test our choice of function forms, we fit the lifetime and mixing functions step by step. First, we fit the distributions of OS+SS to obtain $f(\tau)$ by

$$P_{OS} + P_{SS} = f(\tau) \equiv \frac{\tau^0}{\tau} e^{\beta_0 + \beta_1 \frac{\tau^0}{\tau} + \beta_2 (\frac{\tau^0}{\tau})^2 + \beta_3 (\frac{\tau^0}{\tau})^3}, \tag{5.10}$$

where τ^0 is the default B lifetime, and the β's are parameters. This functional form is motivated by the fact that it should be an exponential decay term with a normalization factor as shown in Eq. (5.7).

We then use the asymmetry between OS and SS to obtain the function $g(\Delta m)$ by

$$\frac{P_{OS} - P_{SS}}{P_{OS} + P_{SS}} = g(\Delta m) \equiv \gamma_0 + \gamma_1 (\Delta m)^2 + \gamma_2 (\Delta m)^4 + \gamma_3 (\Delta m)^6, \tag{5.11}$$

[6] If there are too many parameters to fit, the minimization and error analysis package `Minuit` [47] is very poor at parameter estimation. But with a reasonable number of parameters, it works very well for all the fits in our analysis. Our experience is that `Minuit` is not good at estimating the initial value of parameters. This can be overcome by using `Fumili` [48], another minimization package (not as good as `Minuit` in error analysis), to estimate reasonable initial values of parameters and then pass them to `Minuit`. This solved all the problems we had during our analysis.

where the γ's are parameters. Here we choose only even power of the mixing frequency by noting the fact that neutral B events only depend on mixing frequency through the $\cos(\Delta m \Delta t)$ term, which is even in Δm.

Note that there is no Δt dependence in Eqs. (5.10) and (5.11). This is because we use the same functional form in the fitting for each of the bins with a different value of Δt in the distributions. Therefore all Δt information will be kept in the parameters: $\beta(\Delta t)$'s and $\gamma(\Delta t)$'s. Therefore, the primary goal of the next step fitting is to extract all these parameters for each bin in the Δt distributions.

We also tried other functional forms which have clearer physics interpretation than that listed above but the fitted results were not as good (as determined by residuals) as the one we chose in our final analysis. For example, we also proposed,

$$P_{OS} + P_{SS} = f(\tau, \Delta t) \equiv \frac{e^{-|\Delta t+\beta|/\tau}}{4\tau}; \tag{5.12}$$

$$\frac{P_{OS} - P_{SS}}{P_{OS} + P_{SS}} = g(\Delta m, \Delta t) \equiv \cos\left[\Delta m(\Delta t + \gamma)\right]. \tag{5.13}$$

These functional forms have very nice physics interpretation. For each bin with a fixed small region of Δt, there are contributions from events with real Δt that is different from the POCA Δt [7]. Therefore, we add extra terms (β in Eq. (5.12) and γ in Eq. (5.13)) to Δt to account for the average effect of this smearing. In the special case of no smearing effect, i.e., $\beta = \gamma = 0$, Eqs. (5.12) and (5.13) are equivalent with Eqs. (5.6) and Eq. (5.7) for real Δt. It turns out that they work very well for direct dileptons but not for the cascade leptons, which have more complicated smearing that cannot be accounted for linear shift in Δt. Hence the functions in Eqs. (5.10) and (5.11) are used in the final analysis.

In our analysis, the normalized Δt distributions with different lifetime and mixing frequency for opposite sign and same sign events will be substituted into Eqs. (5.10) and (5.11) for P_{OS} and P_{SS}, respectively. We fit the parameterization function $f(\tau)$ first to extract $\beta(\Delta t)$'s for each Δt bin. This applies to

[7] This is the smearing effect from the POCA approximation as discussed in Section 4.3

both charged and neutral B events. For neutral B events, we then calculate the asymmetry in Eq. (5.11) by using the fitted $(P_{OS} + P_{SS})$ in the denominator from the first step fits, and a perform parameterization fit for $g(\Delta m)$ to extract $\gamma(\Delta t)$'s. By doing this calculation, we are actually simultaneously fitting the lifetime and mixing frequency but in two steps (see reasons explained above).

In summary, we perform parameterization fits of $f(\tau)$ for all 200 Δt bins in each distribution (charged or neutral B events of different momentum categories), and have parameterization fits of $g(\Delta m)$ for all 200 Δt bins in each of the neutral B event distributions. After all of these fits are done, we then plug all the β's and γ's back in Eqs. (5.10) and (5.11). With all these parameters known, the functions depend only on lifetimes and mixing frequency. Finally, we get $f(\tau_{B^+})$ for charged B events, $f(\tau_{B^0})$ and $g(\Delta m_d)$ for neutral B events. All of these results are presented in the next chapter.

Chapter 6

Analysis Results

We parameterize the POCA Δt distributions in terms of their dependence on B lifetime and mixing frequency. As a result, these parameterized distributions are written in the form of functions of the B lifetime and the neutral B mixing frequency. Therefore, measurements of the POCA Δt distributions can be used to extract these two physics parameters from experimental data.

In this chapter, we first present our results of parameterization fits from varying the B lifetime and the mixing frequency in Sections 6.1 and 6.2, respectively. The consistency test of these fits is given in Section 6.3. To test our parameterization method, we provide cross-checks in Section 6.4. Effects of the event re-weighting on the POCA approximation, especially the effect on using the beam spot as an estimation of the collision point, are discussed in Section 6.5.

6.1 Parameterization fits I– varying B lifetime

As mentioned in Chapter 5, the sum of the same sign and opposite sign events (OS+SS) depends only on the B lifetime. Therefore, we vary the B lifetime through event re-weighting to study this dependence. Our goal is to parameterize the (OS+SS) distributions as functions of the B lifetime.

In our analysis, we vary lifetimes for both neutral and charged B mesons by $\pm 10\%$ around the default values by choosing 11 different sets of lifetimes, i.e., changing the lifetimes by 2% for each set[1]. As a result, we get 11 sets of distributions with different B lifetimes for each of the event categories through

[1]To test the applicability of the parameterization functions for larger ranges of lifetime and mixing frequency, we vary them by $\pm 50\%$. After that test, we vary them only $\pm 10\%$ to get better interpolation results in this smaller region around the default values as shown in Table 5.1.

event re-weighting as discussed in Section 5.3. Each of the 200 Δt bins of each distribution will yield 11 probability values, corresponding to 11 different values of B lifetime. These probability values therefore can be parameterized as an analytic function of B lifetime.

As explained in Section 5.4, we choose the parameterization function as

$$P_{OS} + P_{SS} = f(\tau) \equiv \frac{\tau^0}{\tau} e^{\beta_0 + \beta_1 \frac{\tau^0}{\tau} + \beta_2 (\frac{\tau^0}{\tau})^2 + \beta_3 (\frac{\tau^0}{\tau})^3}, \tag{6.1}$$

where τ^0 is the default B lifetime ($\tau^0_{B^+}$ for charged B and $\tau^0_{B^0}$ for neutral B), and the β's are fit parameters. These parameters can be extracted from a fit for the 11 probability values with varying lifetime τ.

Examples of the parameterization fits with varying B lifetime are shown in Fig. 6.1 for the opposite charged B events. Here we only show 8 out of 200 fits from the High-High momentum event category. For examples of High-Low and Low-Low momentum event categories, see Fig. .(A.1-A.4) in Appendix A.

In each of the graphs in Fig. 6.1, the 11 points are the probabilities for that Δt bin with 11 different values of lifetime (τ). By fitting[2] these points using the function $f(\tau)$ in Eq. (6.1), we obtain the corresponding parameter values for the $\beta(\Delta t)$'s, which are shown in Fig. 6.2 for all 200 Δt bins (200 points in the graphs). We can see that $\beta_3(\Delta t)$ is very close to zero in a large range (± 10 ps) of Δt. This indicates that higher powers of (τ_0/τ) are not necessary for $f(\tau)$ in Eq. (6.1). Since we do not need the errors of these parameters in our analysis, we ignore them at this moment. We show a meaningful way to test the consistency of these fits in Section 6.3.

We then plug these fitted parameter values into Eq. (6.1), so that it is now a function of charged B lifetime only. The results of the fitted parameterization function $f(\tau)$ for opposite charged B categories are shown in Fig. 6.3. In the figure, we provide examples of $f(\tau)$ with three different values of τ: $0.9\tau^0_{B^+}$, $\tau^0_{B^+}$, $1.1\tau^0_{B^+}$ (where $\tau^0_{B^+} = 1.674$ ps). This covers the range we chose in varying the charged B lifetime in the parameterization fits.

Following the same procedure as described above for charged B categories,

[2] We use a χ^2 minimization method for all fits in this thesis.

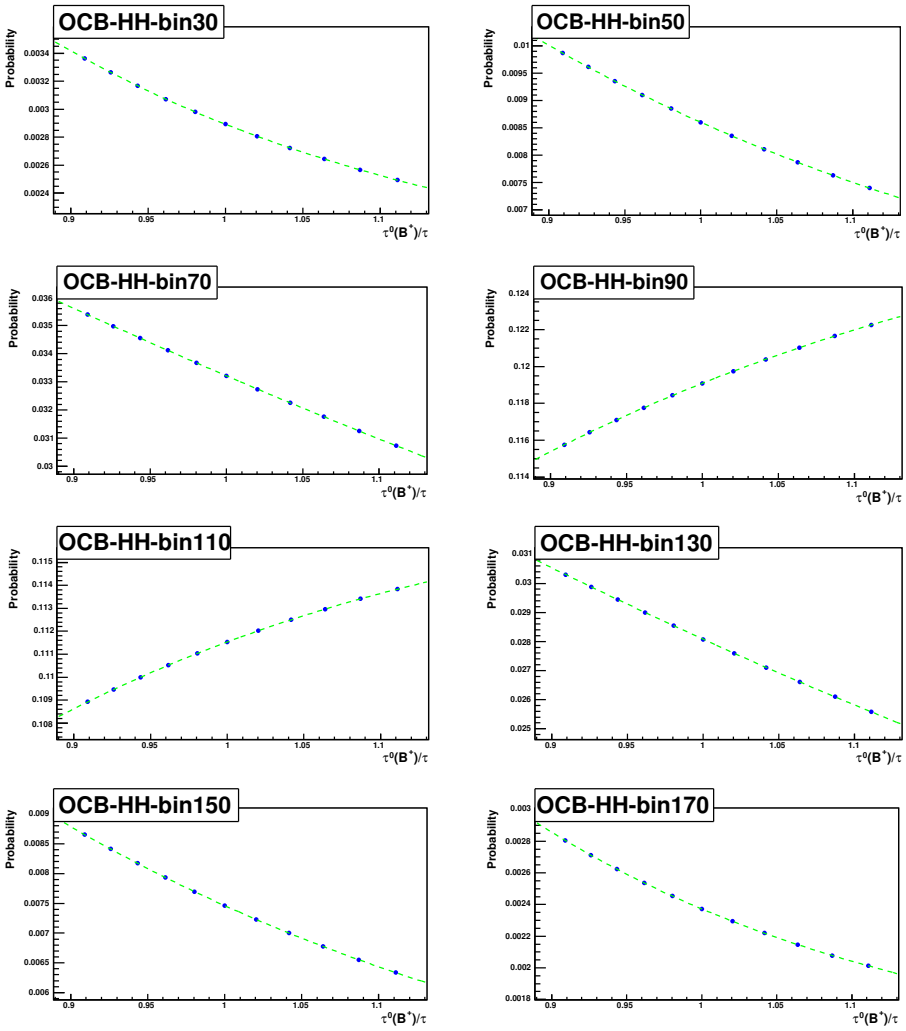

Figure 6.1: Examples of $f(\tau)$ fits for the opposite charged B High-High momentum category events (OCB-HH). Here we only show 8 out of 200 fits for the 200 Δt bins. The x axis is the ratio between the default lifetime and the varying lifetime: $\tau^0_{B^+}/\tau$. The y axis is the sum of the same sign and opposite sign (OS+SS) probabilities.

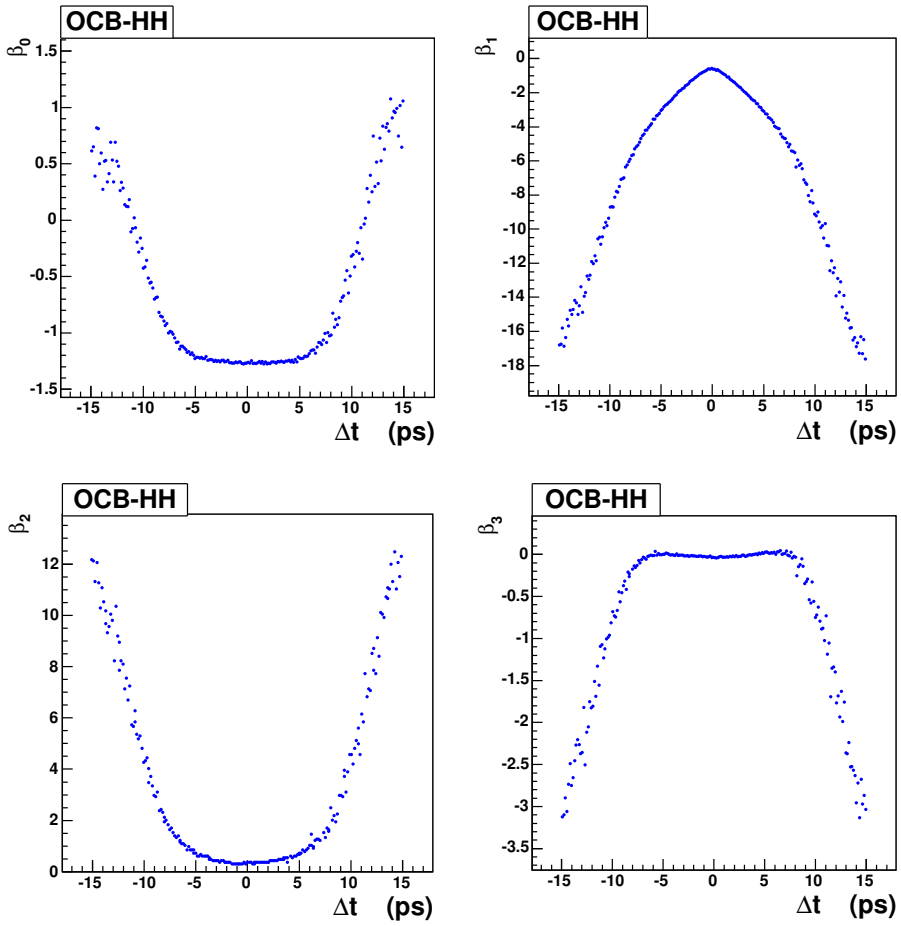

Figure 6.2: Fitted parameters ($\beta(\Delta t)$'s) of $f(\tau)$ for the opposite charged B High-High momentum category events (OCB-HH).

examples of the $f(\tau)$ fits for opposite neutral B High-High momentum category are shown in Fig. 6.4. The corresponding fitted parameter values as functions of Δt are shown in Fig. 6.5. For examples of fits and the fitted parameter values for High-Low and Low-Low categories, see Figs. (A.5-A.8) in Appendix A.

By plugging the fitted parameter values into Eq. (6.1), we obtain the fitted $f(\tau)$ for opposite neutral B categories as shown in Fig. 6.6. In the figure, we plot

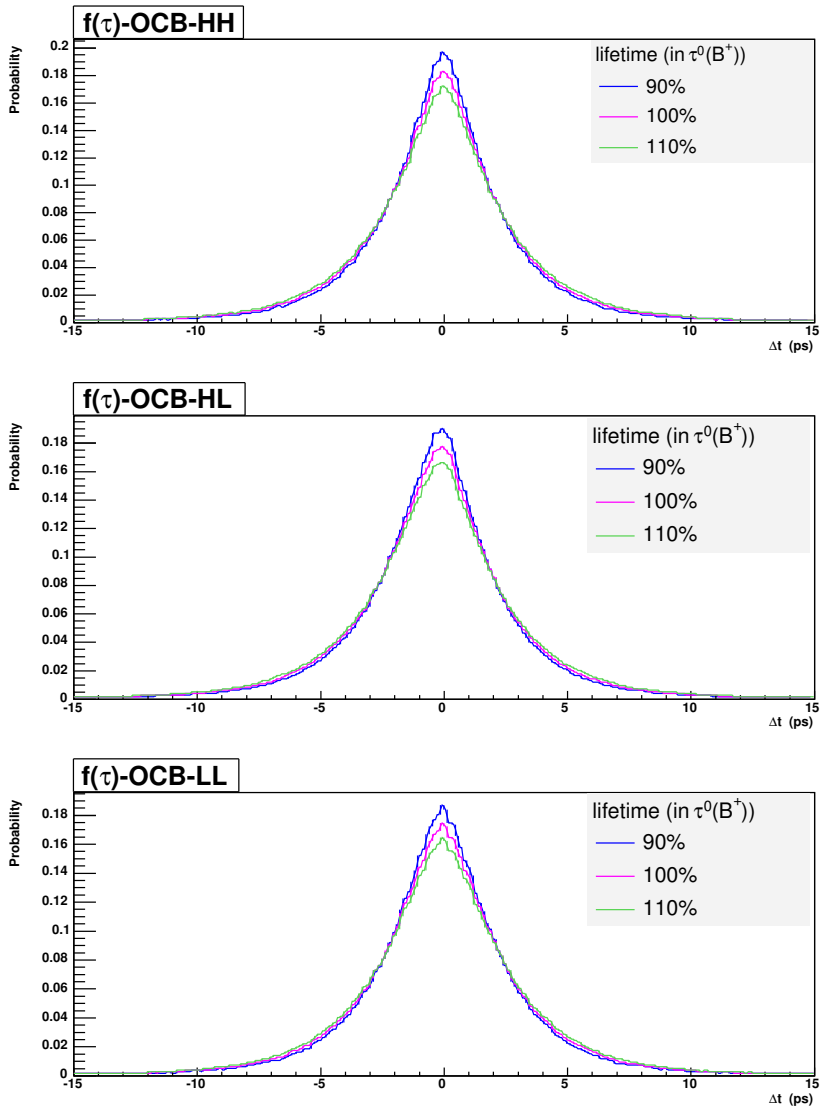

Figure 6.3: Fitted parameterization function $f(\tau)$ for the opposite charged B category events (OCB). The three rows are the High-High (HH), High-Low (HL), and Low-Low (LL) momenta categories.

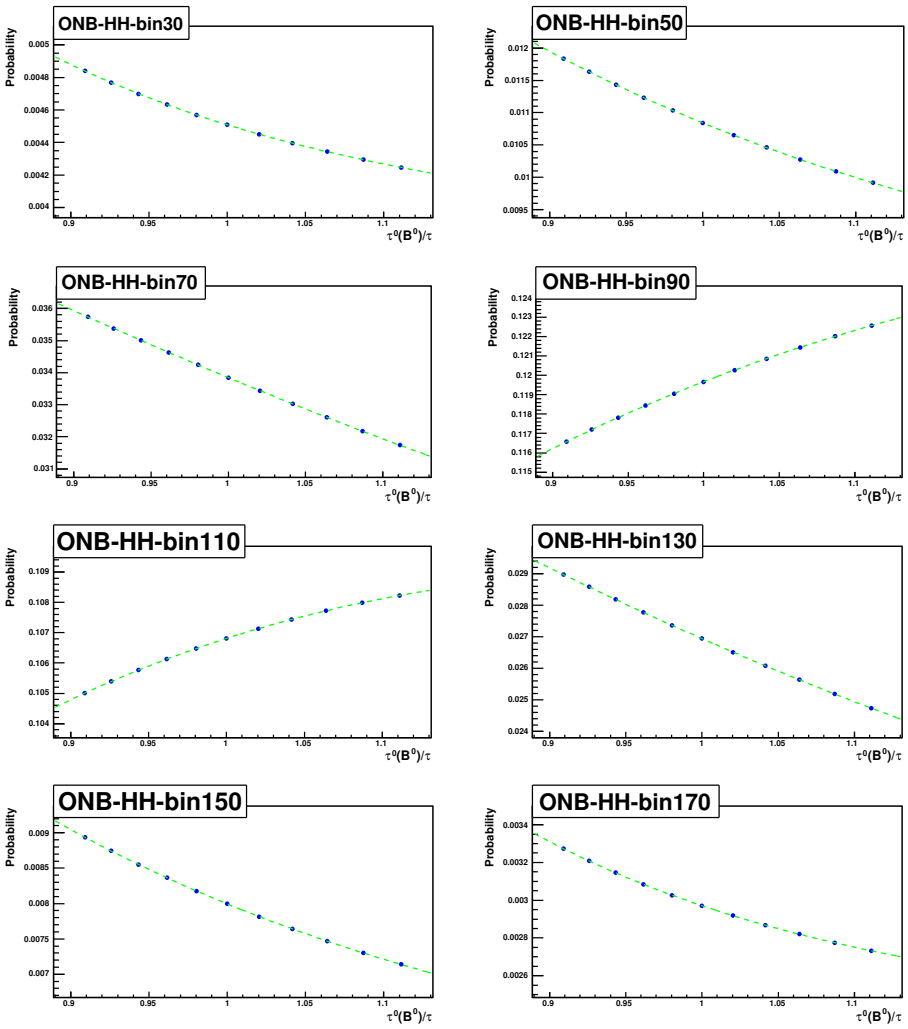

Figure 6.4: Examples of $f(\tau)$ fits for the opposite neutral B High-High momentum category events (ONB-HH). Here we only show 8 out of 200 fits for the 200 Δt bins. The x axis is the ratio between the default lifetime and the varying lifetime: $\tau^0_{B^0}/\tau$. The y axis is the sum of the same sign and opposite sign (OS+SS) probabilities.

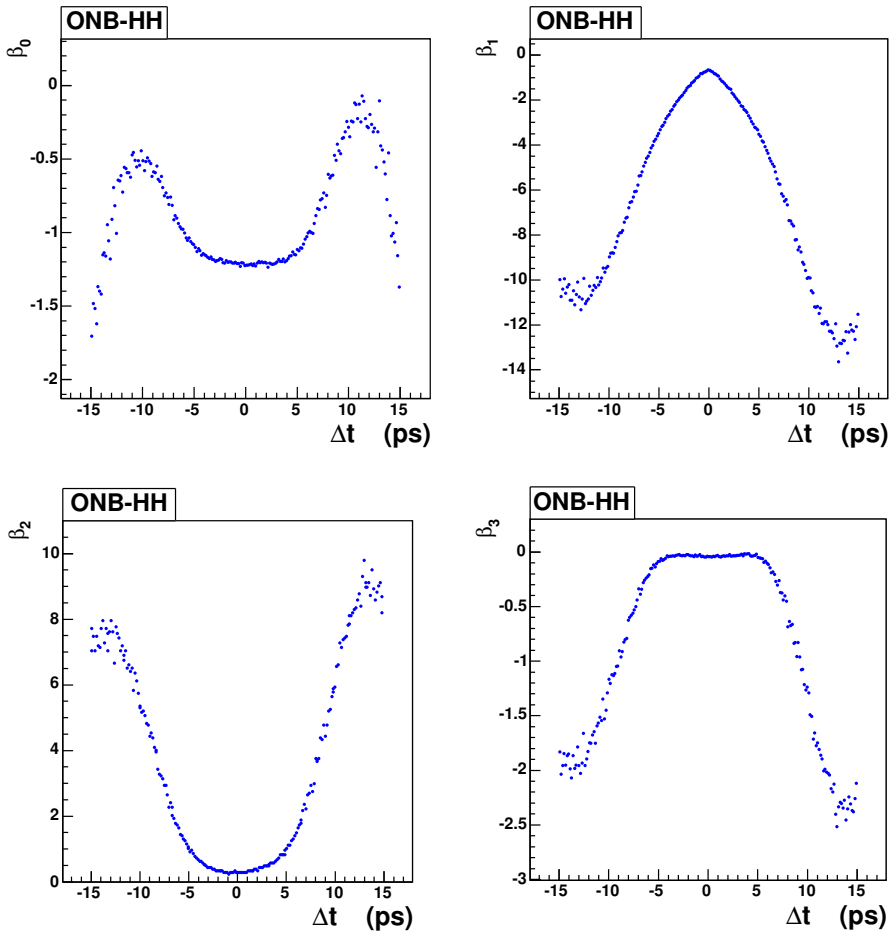

Figure 6.5: Fitted parameters ($\beta(\Delta t)$'s) of $f(\tau)$ for opposite neutral B High-High category events (ONB-HH).

fitted $f(\tau)$ for opposite neutral B category events, again, with three different values of τ: $0.9\tau^0_{B^0}$, $\tau^0_{B^0}$, $1.1\tau^0_{B^0}$ (where $\tau^0_{B^0} = 1.541$ ps). This covers the range we chose in varying the neutral B lifetime in the parameterization fits.

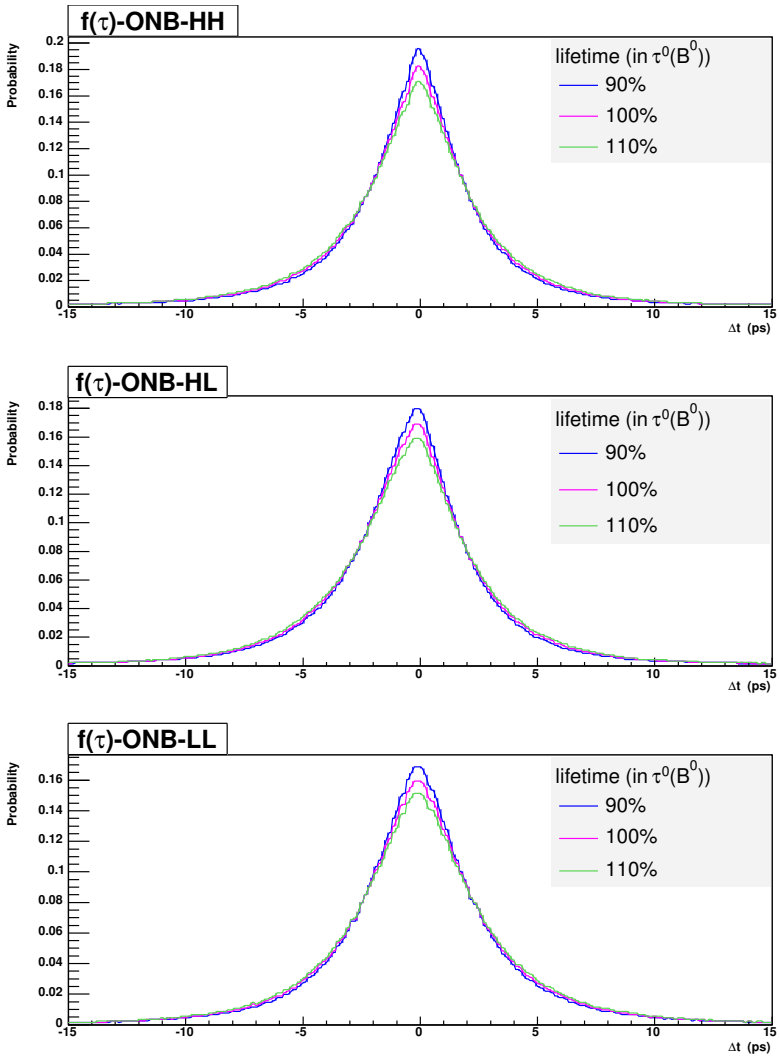

Figure 6.6: Fitted parameterization function $f(\tau)$ for opposite neutral B category events (ONB). The three rows are the High-High (HH), High-Low (HL), and Low-Low (LL) momenta categories.

6.2 Parameterization fits II–varying B mixing frequency

To examine the dependence on neutral B mixing, we use the asymmetry between the opposite sign and the same sign probabilities. The parameterization function $g(\Delta m)$ is chosen in Section 5.4 as

$$\frac{P_{OS} - P_{SS}}{P_{OS} + P_{SS}} = g(\Delta m) \equiv \gamma_0 + \gamma_1(\Delta m)^2 + \gamma_2(\Delta m)^4 + \gamma_3(\Delta m)^6, \qquad (6.2)$$

where the γ's are parameters which can be extracted from bin by bin fits.

As explained in Section 5.4, we use the fitted value for the sum of the opposite sign and the same sign probabilities (OS+SS) in the denominator of Eq. (6.2), so that the POCA Δt distributions are simultaneously parameterized in the B lifetime and the mixing frequency. In our case, the asymmetries are obtained from Eq. (6.2) by using the fitted values in Fig. 6.6.

Examples of $g(\Delta m)$ fits are shown in Fig. 6.7 for opposite neutral B High-High momentum category events. The points in the figure correspond to the asymmetry between the opposite and the same sign probabilities for that bin with 11 different values of mixing frequency Δm. These fits determine the values of the parameters in Eq. (6.2) ($\gamma(\Delta t)$'s), which are shown in Fig. 6.8. The corresponding results for High-Low and Low-Low momentum categories are shown in Fig. .(A.9-A.12) in Appendix A.

Since the parameters are estimated from these fits, we then plug them into Eq. (6.2). As a result, $g(\Delta m)$ depends only on the mixing frequency Δm. The fitted parameterization function $g(\Delta m)$ for opposite neutral B categories is shown in Fig. 6.9. Similarly, we provide in the figure results of fitted $g(\Delta m)$ with three different values of Δm: $0.9\Delta m_d^0$, Δm_d^0, $1.1\Delta m_d^0$ (where $\Delta m_d^0 = 0.489\,\mathrm{ps}^{-1}$). This covers the range we chose in varying the neutral B mixing frequency in the parameterization fits.

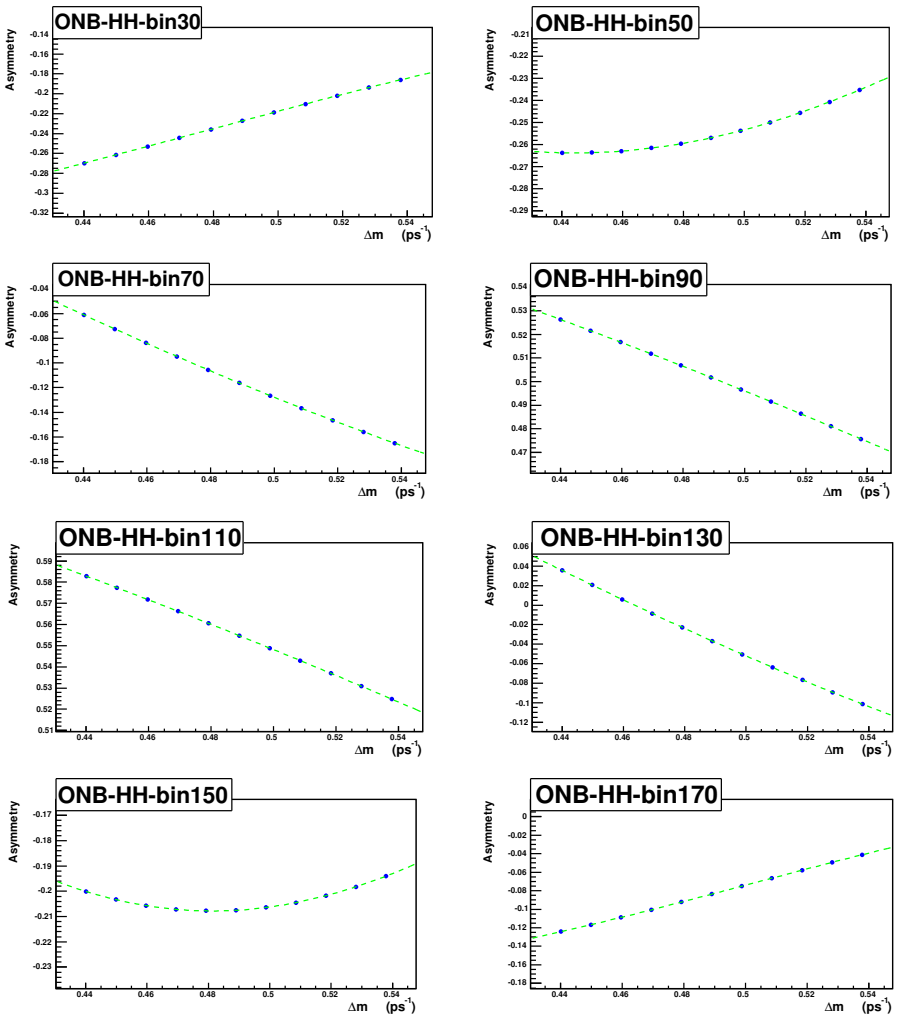

Figure 6.7: Examples of $g(\Delta m)$ fits for opposite neutral B High-High category (ONB-HH). Here we only show 8 out of 200 fits for 200 Δt bins. The x axis is the varying B mixing frequency Δm. The y axis is the asymmetry between the opposite and the same sign probabilities.

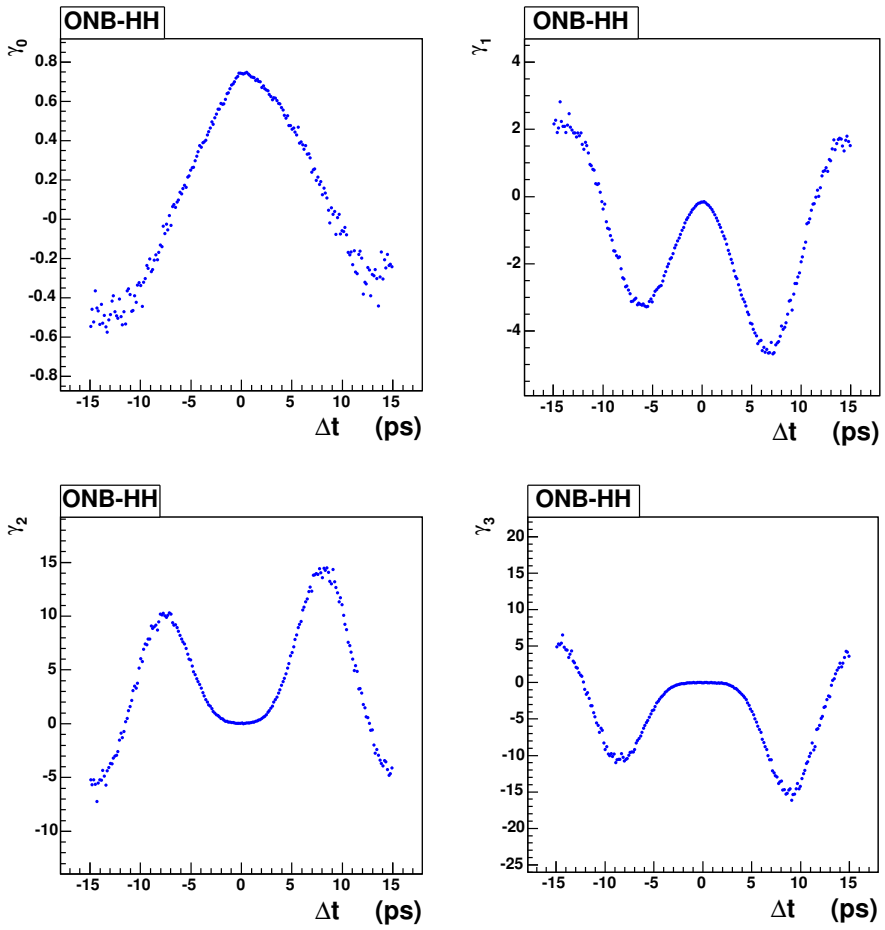

Figure 6.8: Fitted parameters ($\gamma(\Delta t)$'s) of $g(\Delta m)$ for opposite neutral B High-High momentum category events (ONB-HH).

6.3 Consistency test of parameterization

In this section, we test the consistency of our parameterization fits presented in Sections 6.1 and 6.2 in getting functions $f(\tau)$ and $g(\Delta m)$.

The idea is as follows: we fit re-weighted distributions, from which the parameterization functions ($f(\tau)$ and $g(\Delta m)$) are obtained, to extract the associ-

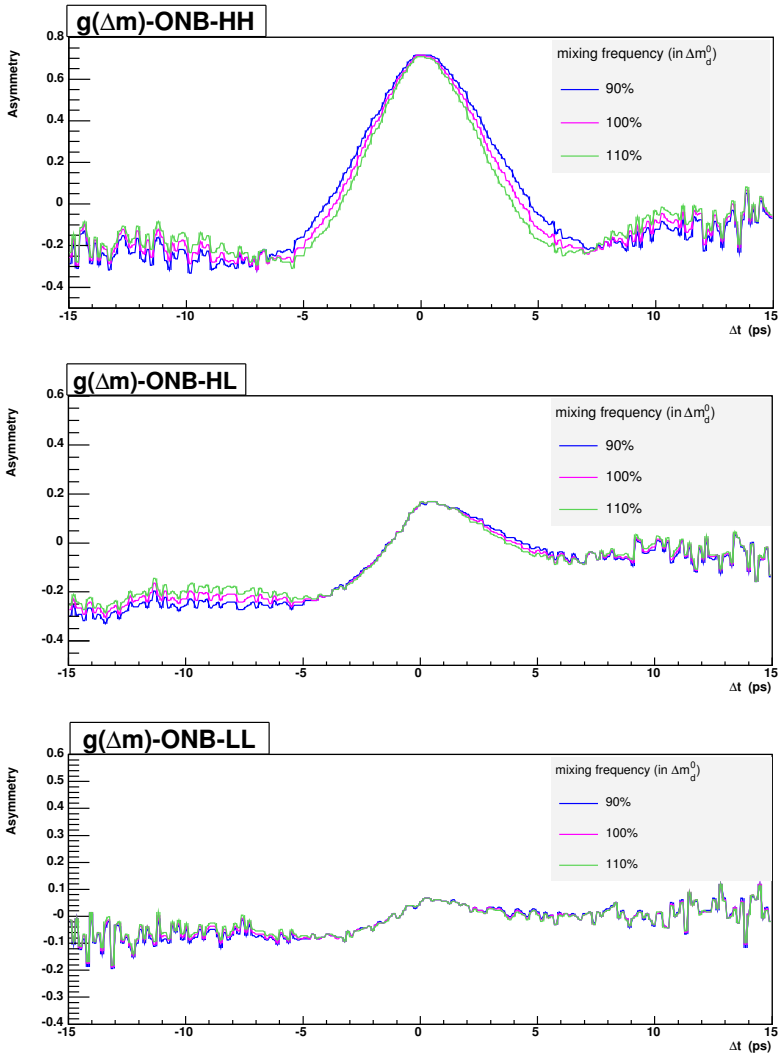

Figure 6.9: Fitted parameterization function $g(\Delta m)$ for opposite neutral B categories events (ONB). The three rows are the High-High (HH), High-Low (HL), and Low-Low (LL) momenta categories.

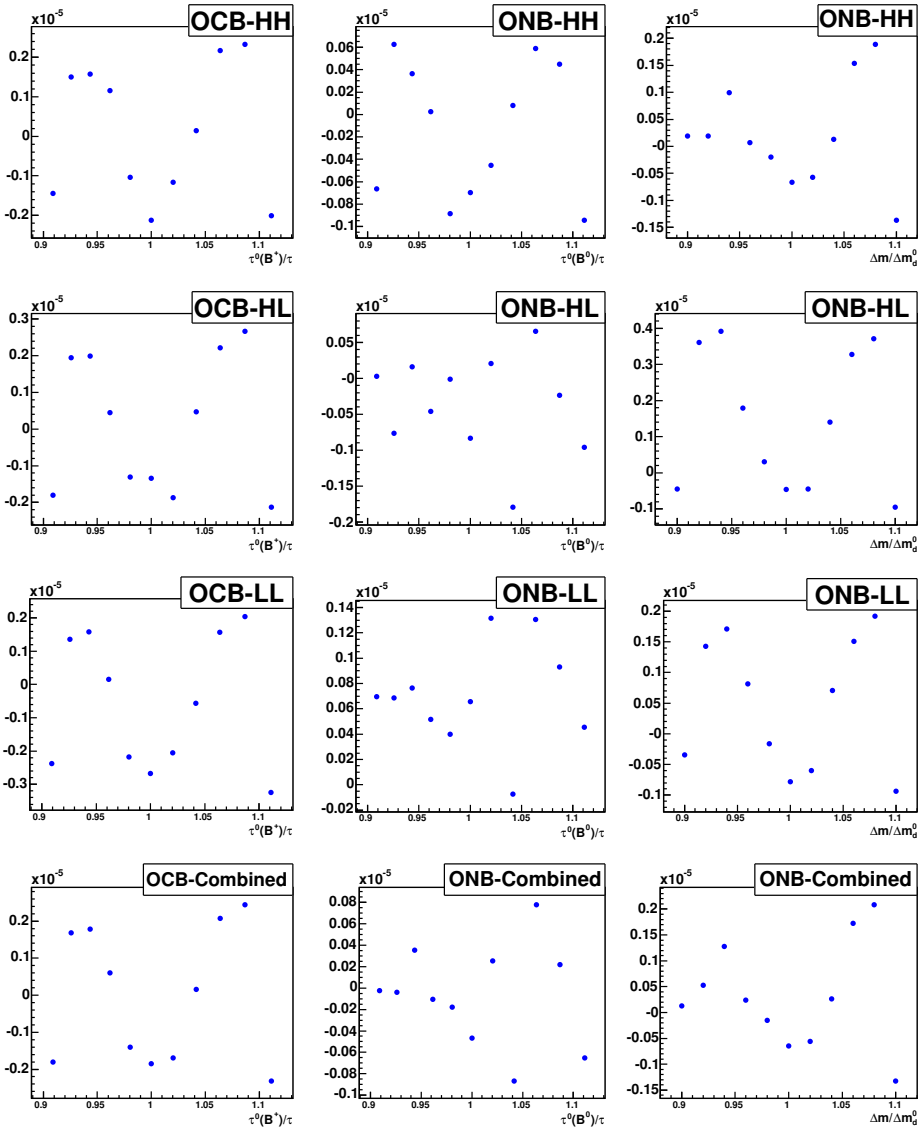

Figure 6.10: Consistency test of the parameterization fits. The points are the fractional difference between the fitted values and the "true" values of the lifetime. The first two columns are $f(\tau)$ tests for OCB and ONB categories. The last column is the $g(\Delta m)$ tests for ONB categories. The first three rows are HH, HL, and LL momenta categories. The fourth row is the simultaneous fits for the three momenta categories.

ated B lifetimes and the neutral B mixing frequency. We then compare these fitted values with the expected values as used in the event re-weighting. If our parameterization model and the fits are good enough, there should no sizable discrepancy between the original and fitted values of the B lifetimes and the neutral B mixing frequency.

In Fig. 6.10, we show the test of consistency of the parameterization fits for all categories. It is measured by the difference between the fitted values and the expected values of the B lifetimes and the neutral B mixing frequency. For easy comparison, all these values are rescaled by the default values as specified in Table 5.1. The first two columns are $f(\tau)$ tests for opposite charged B (OCB) and opposite neutral B (ONB) categories. The third column is the $g(\Delta m)$ tests for ONB categories. The first three rows are the High-High, High-Low, and Low-Low momenta categories. The fourth row is the simultaneous fits for all three momenta categories. From the figure, we can see that the fitted values (both lifetimes and mixing frequency) are very close to the expected values, with deviations of less than 5 parts per million. This shows that our functional form and the parameterization fits provide excellent results. That is, the fitted parameterization functions describe the distributions for all re-weighted events with extremely high accuracy.

6.4 Crosschecks of the parameterization approach

With the parameterization results presented in Sections 6.1 and 6.2, whose consistency is tested in Section 6.3, we are now ready to use them to extract B lifetimes and mixing frequency from independently generated Monte Carlo test events (still without any detector simulation). This serves as a cross check of our parameterization method. These test events are generated with default lifetimes ($\tau^0_{B^+}$ and $\tau^0_{B^0}$) and mixing frequency (Δm^0_d) as described in Section 5.1.

Following the same classification as discussed in Section 5.2, the same sign

and opposite sign events are summed together (OS+SS) to extract B lifetimes. We also calculate the asymmetry between the opposite sign and same sign ((OS-SS)/(OS+SS)) for opposite neutral B events to extract the B mixing frequency.

The results of fitting the (OS+SS) POCA Δt distributions with $f(\tau)$ are shown in Fig. 6.11 and Fig. 6.12 for charged and neutral B events, respectively. In the figures, the first three rows are fits for the High-High, High-Low, and Low-Low momenta events. These three momenta events are chained together in the fourth row. That is, the first peak of the fourth row is for High-High momentum events, the middle peak is for High-Low events, and the third peak is for Low-Low momentum events. Therefore, the fourth row is a simultaneous lifetime fit for these three momenta events. The ratios between the default and fitted lifetimes are also printed on the graphs. The expected value of the ratio is 1. Our fitted ratios are very close to this expected value with less than 0.2% deviation. All these fitted ratios are consistent with the expected values without biases if statistical errors are included.

For the mixing frequency fits, we first calculate the asymmetry between the opposite sign and the same sign events by using the fitted results in Fig. 6.12 for (OS+SS) (for reasons, see Section 5.4). We then fit these asymmetries by using the parameterization function $g(\Delta m)$. The fitted mixing frequencies are shown in Fig. 6.13. In the figures, the first three rows are fits for the High-High, High-Low, and Low-Low momenta events. Similar to lifetime fits, a simultaneous mixing frequency fit for these three momenta events is also shown in the figure. The ratios between Δm and Δm_d^0 are very close to the expected value of 1 with less than 1% deviation. Note the exception of the Low-Low category, which is insensitive to the mixing frequency (see the third row in Fig. 6.9) because the mixing signals are highly diluted. Taking into account statistical errors, all of these fitted ratios are consistent with the expected values without biases.

All of these tests prove that our analyses, especially the event re-weighting and the parameterization function fits, are consistent with less than 1% unbiased deviations from the expected values of the B lifetimes and the neutral B mixing frequency.

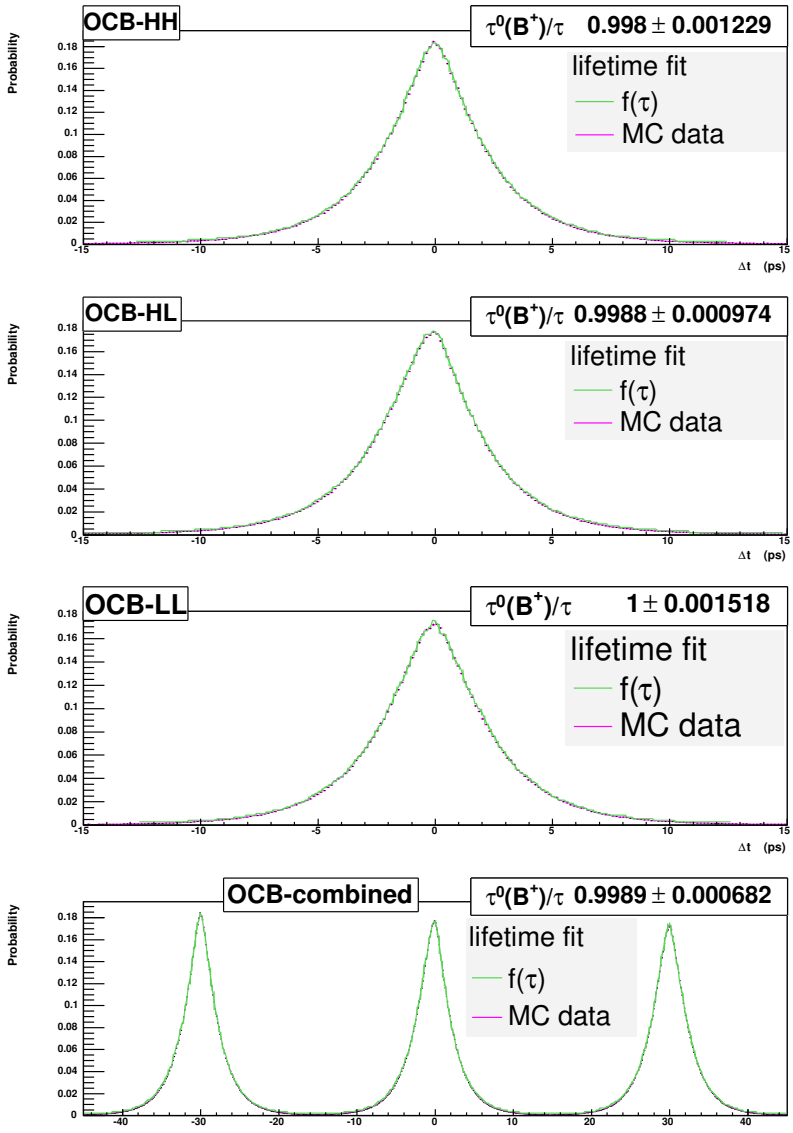

Figure 6.11: Lifetime fits for charged B samples. The fitted lifetimes are quoted as ratios to the default value, $\tau^0_{B^+}/\tau$. The first three rows are HH, HL, and LL momenta categories. The fourth row is a simultaneous fit of all three momenta categories shown in the first three rows.

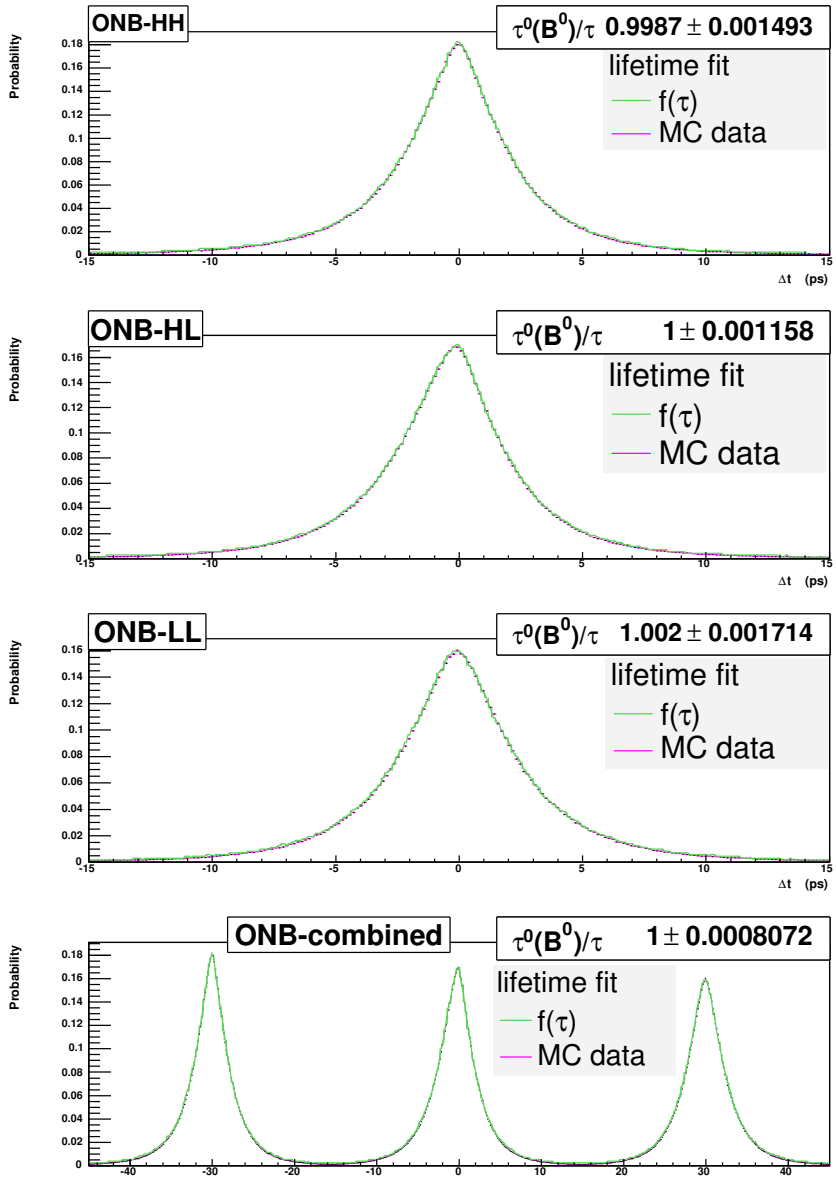

Figure 6.12: Lifetime fits for neutral B samples. The fitted lifetimes are quoted as ratios to the default value, $\tau^0_{B^0}/\tau$. The first three rows are HH, HL, and LL momenta categories. The fourth row is a simultaneous fit of all three momenta categories shown in the first three rows.

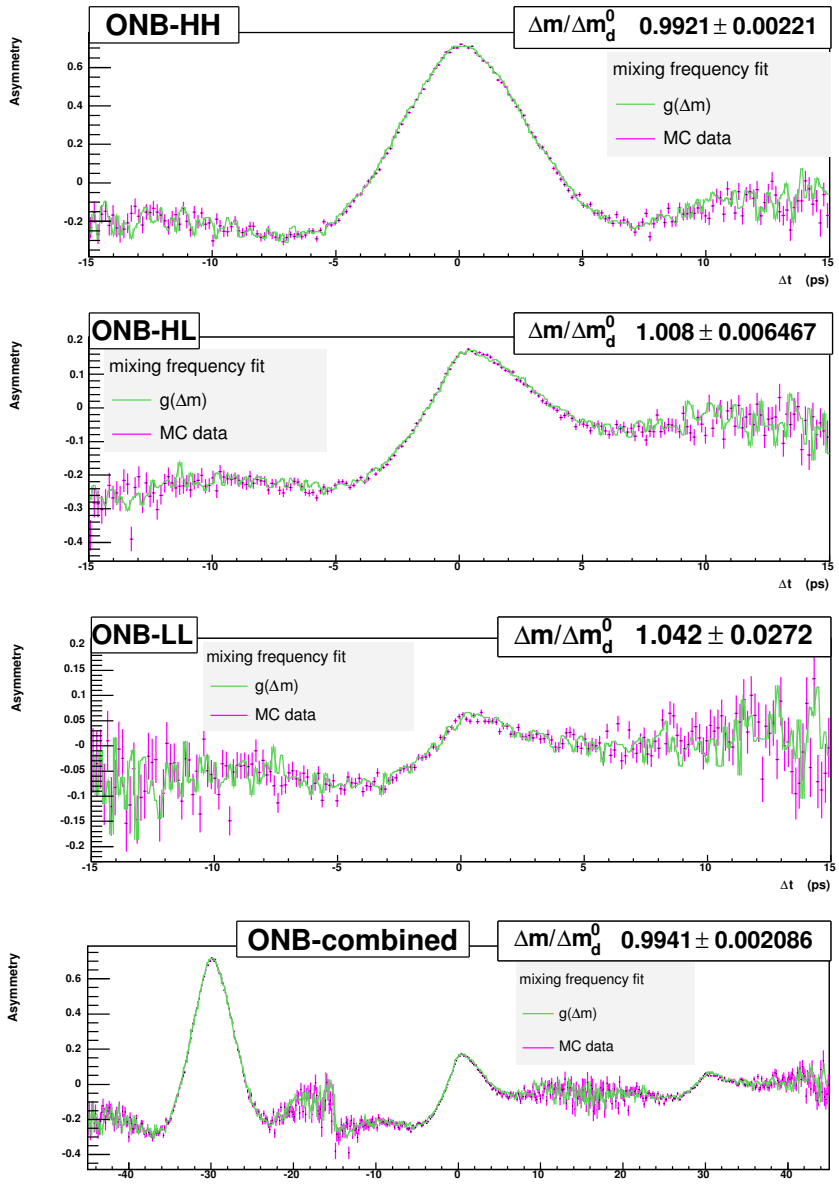

Figure 6.13: Mixing frequency fits for neutral B samples. The fitted B mixing frequencies are quoted as ratios to the default value, $\Delta m/\Delta m^0$. The first three rows are the HH, HL, and LL momenta categories. The fourth row is a simultaneous fit of all three momenta categories shown in the first three rows.

6.5 Effects of event re-weighting on the POCA approximation

In this thesis, we use the event re-weighting technique in getting the parameterization for Δt distributions of B mixing. As mentioned before, we use the beam spot rather than the precise e^+e^- collision point for each event in the POCA Δz calculation[3]. In our Monte Carlo generated events, however, we know both the real Δz and the precise collision point for each event. Therefore, we can study effects of event re-weighting on the POCA approximation, especially the effect on averaging the collision points by using the beam spot in the POCA Δz calculation.

The procedure is exactly the same as described in Sections 6.1, 6.2, and 6.4. We repeat the crosschecks in Section 6.4 by using different methods for calculating Δz for both the parameterization and the test events. The three methods to calculate Δz are:

- Using the MC-Truth Δz directly;
- Using the precise collision point for each event in the POCA Δz calculation;
- Using the beam spot for each run as an estimate of the collision point in the POCA Δz calculation. This method is the same one used in the main body of this thesis.

In the following, we present results of crosschecks for these three methods together for easier comparison. For details, see Section 6.4 as an example.

Results of the fitted charged B lifetimes with different methods of calculating Δz are listed in Table 6.1. The results are quoted in the same way as in Section 6.4. The quoted errors are obtained from χ^2 fits.

We can see that results from using real Δz and the POCA Δz with precise collision point are very close to each other. They are also very close to the results from the POCA Δz using beam spot. We conclude that our event re-weighting

[3]The boost approximation is always used to convert Δz into Δt.

Category \ Method	Real Δz	Collision point	Beam spot
High-High	1.0000 ± 0.0008	1.0000 ± 0.0009	0.9980 ± 0.0012
High-Low	0.9997 ± 0.0007	0.9993 ± 0.0008	0.9988 ± 0.0010
Low-Low	1.0030 ± 0.0011	1.0010 ± 0.0013	1.0000 ± 0.0015
Combined	1.0000 ± 0.0005	1.0000 ± 0.0005	0.9989 ± 0.0007

Table 6.1: Charged B lifetime fits with three different methods of calculating Δz: real Δz; POCA Δz with precise collision point; and POCA Δz using beam spot for each run. The quoted results are the ratio between the default lifetime and the fitted lifetime: $\tau^0_{B^+}/\tau$.

Category \ Method	Real Δz	Collision point	Beam spot
High-High	1.0020 ± 0.0010	1.0010 ± 0.0011	0.9987 ± 0.0015
High-Low	1.0010 ± 0.0008	1.0020 ± 0.0009	1.0000 ± 0.0012
Low-Low	0.9984 ± 0.0012	0.9992 ± 0.0014	1.0020 ± 0.0017
Combined	1.0010 ± 0.0005	1.0010 ± 0.0006	1.0000 ± 0.0008

Table 6.2: Neutral B lifetime fits with three different methods of calculating Δz: real Δz; POCA Δz with precise collision point; and POCA Δz using beam spot for each run. The quoted results are the ratio between the default lifetime and the fitted lifetime: $\tau^0_{B^0}/\tau$.

does not change the smearing effect of POCA approximation (including using the beam spot) in a significant way for charged B events.

In Table 6.2, we list the results for the fitted neutral B lifetime with different methods of calculating Δz. Similar to the charged B lifetime fitting, all three methods give almost identical results and all are unbiased with deviation less than 1%.

Results for the fitted neutral B mixing frequency with different methods of calculating the Δz are listed in Table 6.3. We see that results from using real Δz and the the POCA Δz with precise collision point are still very close to each other. They give better results [4] than the method of using beam spot for each

[4] As we discussed before, the Low-Low momentum events are insensitive to the B mixing frequency. Therefore, we compare only results of the simultaneous fits in the last row in Table 6.3.

Category \ Method	Real Δz	Collision point	Beam spot
High-High	0.9994 ± 0.0017	0.9984 ± 0.0018	0.9921 ± 0.0022
High-Low	1.0070 ± 0.0056	1.0010 ± 0.0052	1.0080 ± 0.0065
Low-Low	1.0700 ± 0.0235	1.0860 ± 0.0226	1.0420 ± 0.0272
Combined	1.0000 ± 0.0017	0.9992 ± 0.0017	0.9941 ± 0.0021

Table 6.3: Neutral B mixing frequency fits with three different methods of calculating Δz: real Δz; POCA Δz with precise collision point; and POCA Δz using beam spot for each run. The quoted results are the ratio between the fitted mixing frequency and the default value: $\Delta m / \Delta m_d^0$.

run as an estimation of the collision point.

In summary, the effect of the event re-weighting on the POCA approximation (comparing results from using the real Δz and the POCA Δz with collision point in the tables) is insignificant compared to the statistical uncertainties in the fitting procedures. The effect of event re-weighting on using the beam spot for each run in the POCA Δz calculation (comparing results from using the POCA Δz using collision point with the POCA Δz using the beam spot) is also very small except in the neutral B mixing frequency fitting. This might be explained by the fact that the event re-weighting does not change any smearing effect of the POCA approximation (as explained in Section 4.3) in a sizable way. Since the lifetime fitting is based on the sum of the same sign and the opposite sign events, it should be insensible to any small smearing shift. For the mixing frequency fitting, however, we use the asymmetry between the same sign and the opposite sign, which might be more sensitive to even a small smearing shift due to the event re-weighting.

Chapter 7

Conclusion

The time evolution of B mesons is governed by the overall decay rate $\Gamma_B = 1/\tau_B$ and by the mass difference Δm_d of the two neutral mass eigenstates. A precision measurement of the $B^0\overline{B}^0$ mixing frequency is of fundamental importance since it is sensitive to the CKM matrix element $|V_{tb}|$ which has not previously been measured with great precision and sensitive to new physics beyond the SM. At the same time, a precise determination of the B lifetimes reduces the systematic error on measurements of the the elements of the CKM matrix, such as $|V_{cb}|$ and $|V_{ub}|$. Therefore, simultaneous and precise measurements of the neutral B mixing frequency and B lifetimes, provide stringent constraints on the CKM matrix.

In this thesis, we studied the parameterization of the neutral B mixing probability distribution functions of the proper decay time difference Δt of the B pairs resulting from $\Upsilon(4S)$ decays. Dilepton events from $\Upsilon(4S)$ decays were generated by the `EvtGen` generator package within the *BABAR* framework.

Following the same method applied in the real experimental data analysis, the boost approximation and the point of closest approach (POCA) were used to estimate the proper decay time difference Δt in our Monte Carlo analysis. By choosing appropriate functions, the parameterization was obtained from bin by bin fits of Δt distributions with different B lifetimes and neutral B mixing frequencies. These distributions were obtained from re-weighting the Monte Carlo generated events, which have a fixed lifetime and mixing frequency.

For each of the distributions, events are divided into 200 Δt bins within $\pm$ 15 ps. For each of the Δt bins, we perform parameterization fits by varying lifetimes and mixing frequency. As the charged B events are independent of

neutral B mixing, we obtained the parameterization results as a function of only the charged B lifetime. For the neutral B events, the parameterization depends on both the neutral B lifetime and the neutral B mixing frequency. Therefore, we obtained parameterization results for neutral B events as functions of the neutral B mixing frequency and the neutral B lifetime.

The parameterization approach was tested with another independently generated set of test dilepton events. The deviations in extracting the B lifetimes and the neutral B mixing frequency are less than 1% from the expected values, without biases. We also examined the effects of event re-weighting on the POCA approximation, especially the effect on using the beam spot for each run as an estimate of precise e^+e^- collision point. All of these effects turn out to be insignificant.

Our results presented in this thesis, combined with Monte Carlo studies of detector resolutions, provide a tested technique to perform precise measurements of the neutral B mixing frequency and B lifetimes from experimental data.

Bibliography

[1] S. L. Glashow, Nucl. Phys. **22**, 579 (1961); S. Weinberg, Phys. Rev. Lett. **19**, 1264 (1967); A. Salam, "in Proceedings of the 8th Nobel symposium", ed. N. Swartholm, *et al.* (1968).

[2] K. Anikeev, *et al.*, Fermi Lab-Pub-01/197, hep-ph/0201071, (2002).

[3] N. Cabibbo, Phys. Rev. Lett. **10**, 531 (1963); M. Kobayashi and T. Maskawa, Prog. Th. Phys. **49**, 652 (1973).

[4] Particle Data Group, S. Eidelman *et al.*, Phys. Lett. B **592** 1 (2004).

[5] L. Wolfenstein, Phys. Rev. Lett. **51**, 1945 (1983).

[6] A. J. Buras, M. E. Lautenbacher and G. Ostermaier, Phys. Rev. D **50**, 3433 (1994).

[7] R. Aleksan, B. Kayser and D. London, Phys. Rev. Lett. **73**, 18 (1994); J.P. Silva and L. Wolfenstein, Phys. Rev. D **55**, 5331 (1997); I.I. Bigi and A.I. Sanda, hep-ph/9909479.

[8] *BABAR* Collaboration, B. Aubert *et al.*, Phys. Rev. Lett. **86**, 2525 (2001); Phys. Rev. Lett. **87**, 091801 (2001); Phys. Rev. Lett. **89**, 201802 (2002).

[9] Belle Collaboration, K. Abe *et al.*, Phys. Rev. Lett. **86**, 2509(2001); Phys. Rev. Lett. **87**, 091802 (2001); Phys. Rev. D **66**, 071102(R)(2002).

[10] C. Jarlskog, Phys. Rev. Lett. **55**, 1039 (1985); Z. Phys. C **29**, 491 (1985).

[11] J.H. Christenson, J.W. Cronin, V.L. Fitch, and R. Turlay, Phys. Rev. Lett. **13**, 138 (1964).

[12] A.D. Sakhorov, Pis'ma Zh. Eksp. Teor. Fiz. **5**, 32 (1967); JETP Lett. **5**, 24 (1967).

[13] M.A. Shifman, M.B. Voloshin, Sov. J. Nucl. Phys. **45**, 292 (1987); N. Isgur and M. B. Wise, Phys. Lett. B **232**, 113 (1989); **237**, 527 (1990).

[14] M. Neubert and T. Becher, Phys. Lett. B **535**, 127 (2002).

[15] *BABAR* Collaboration, (ed. P. F. Harrison and H. R. Quinn), SLAC-R-0504, Oct. 1998. 1056pp.

[16] "PEP-II: An Asymmetric B Factory", Conceptual Design Report, SLAC-418, LBL-5379 (1993).

[17] CLEO Collaboration, B. Barish *et al.*, Phys. Rev. Lett. **76**, 1570 (1996).

[18] *BABAR* Collaboration, B. Aubert *et al.*, Nucl. Instrum. Meth A **479**, 1 (2002).

[19] M. Neubert and C. T. Sachrajda, Nucl. Phys. B **483**, 339 (1997).

[20] S. L. Glashow, J. Iliopoulos and L. Maiani, Phys. Rev. D **2**, 1285 (1970).

[21] A. Ali, hep-ph/9606324, (1996).

[22] M. Beneke *et al.*, Phys. Rev. Lett. **93**, 1914 (1999); Nucl. Phys. B **591**, 313 (2000); **B606**, 245 (2001).

[23] T.D. Lee and C.S. Wu, Ann. Rev. Nucl. Sci. **16**, 511 (1966); I.I. Bigi and A.I. Sanda, "*CP* Violation", Cambridge Univ. Press, 2000.

[24] A.J. Buras, W. Slominski, and H. Steger, Nucl. Phys. B **245**, 369 (1984).

[25] *BABAR* Collaboration, B. Aubert *et al.*, Phys. Rev. D **66**, 032003 (2002).

[26] http://www.slac.stanford.edu/~lange/EvtGen

[27] D.J. Lange, Nucl. Instrum. Meth A **462**, 152 (2001); A. Ryd, *et al.*, *BABAR* Analysis Document 522, (2003); URL: http://www.lns.cornell.edu/~ryd/

[28] T. Sjöstrand, Comp. Phys. Commun. **82**, 74 (1994).

[29] http://www.slac.stanford.edu/BFROOT/www/Physics/Tools/generators

[30] E. Richter-Was, Phys. Lett. B **303**, 163 (1993).

[31] UA1 Collaboration, C. Albajar *et al.*, Phys. Lett. B **186**, 247 (1987).

[32] ARGUS Collaboration, H. Albrecht *et al.*, Phys. Lett. B **192**, 245 (1987); Z. Phys. C **55**, 357 (1992); Phys. Lett. B **324**, 249 (1994).

[33] CLEO Collaboration, B.H. Behrens *et al.*, Phys. Rev. Lett. **71**, 1680 (1993); Phys. Lett. B **490**, 36 (2000).

[34] HFAG, hep-ex/0505100; http://www.slac.stanford.edu/xorg/hfag/osc

[35] ALEPH Collaboration, D. Buskulic *et al.*, Z. Phys. C **75**, 397 (1997).

[36] DELPHI Collaboration, J. Abdallah *et al.*, Eur. Phys. Jour. C **28**, 155 (233).

[37] L3 Collaboration, M. Acciarri *et al.*, Eur. Phys. Jour. C **5**, 195 (1998).

[38] OPAL Collaboration, G. Abbiendi *et al.*, Phys. Lett. B **493**, 266 (2000).

[39] CDF Collaboration, T. Affolder *et al.*, Phys. Rev. D **60**, 112004 (1999).

[40] *BABAR* Collaboration, B. Aubert *et al.*, Phys. Rev. Lett. **88**, 221802 (2002); Phys. Rev. D **66**, 032003 (2002); Phys. Rev. Lett. **88** 221803 (2002);

[41] *BABAR* Collaboration, B. Aubert *et al.*, Phys. Rev. D **67**, 072002 (2003).

[42] *BABAR* Collaboration, B. Aubert *et al.*, hep-ex/0408039.

[43] *BABAR* Collaboration, B. Aubert *et al.*, Phys. Rev. Lett. **92**, 181801 (2004); Phys. Rev. D **70**, 012007 (2004).

[44] Belle Collaboration, K. Abe *et al.*, Phys. Rev. Lett. **86**, 3228 (2001); K. Hara *et al.*, Phys. Rev. Lett. **89**, 251803 (2002); T. Tomura *et al.*, Phys. Lett. B **542**, 207 (2002); N.C. Hastings *et al.*, Phys. Rev. D **67**, 052004 (2002); Y. Zheng *et al.*, Phys. Rev. D **67**, 092004 (2003).

[45] Belle Collaboration, K. Abe *et al.*, Phys. Rev. D **71**, 072003 (2005).

[46] *BABAR* Collaboration, C. Bozzi *et al.*, BAD Note 28 (2000).

[47] http://wwwasdoc.web.cern.ch/wwwasdoc/minuit/

[48] http://root.cern.ch/root/html/TFumili.html

Glossary

CKM	Cabibbo-Kobayashi-Maskawa
CM	Center-of-mass
DCH	Drift Chamber
DIRC	Detector of Internally Reflected Cherenkov light
EMC	Electromagnetic Calorimeter
FCNC	Flavour-changing Neutral Current
GIM	Glashow-Iliopoulus-Maiani
HH	High-High
HL	High-Low
HQET	Heavy Quark Effective Theory
IFR	Instrumented Flux Return
LL	Low-Low
MC	Monte Carlo
OCB	Opposite Charged B
ONB	Opposite Neutral B
OPE	Operator Product Expansion
OS	Opposite Sign
PDF	Probability Distribution Function
PDG	Particle Data Group
PMT	Photo-multiplier Tubes
POCA	Point of Closest Approach
QCD	Quantum Chromodynamics
QED	Quantum Electrodynamics
RPC	Resistive Plate Chamber
SB	Same B
SM	Standard Model
SS	Same Sign
SVT	Silicon Vertex Tracker
Tcl	Tool Command Language

Appendix A

More Figures

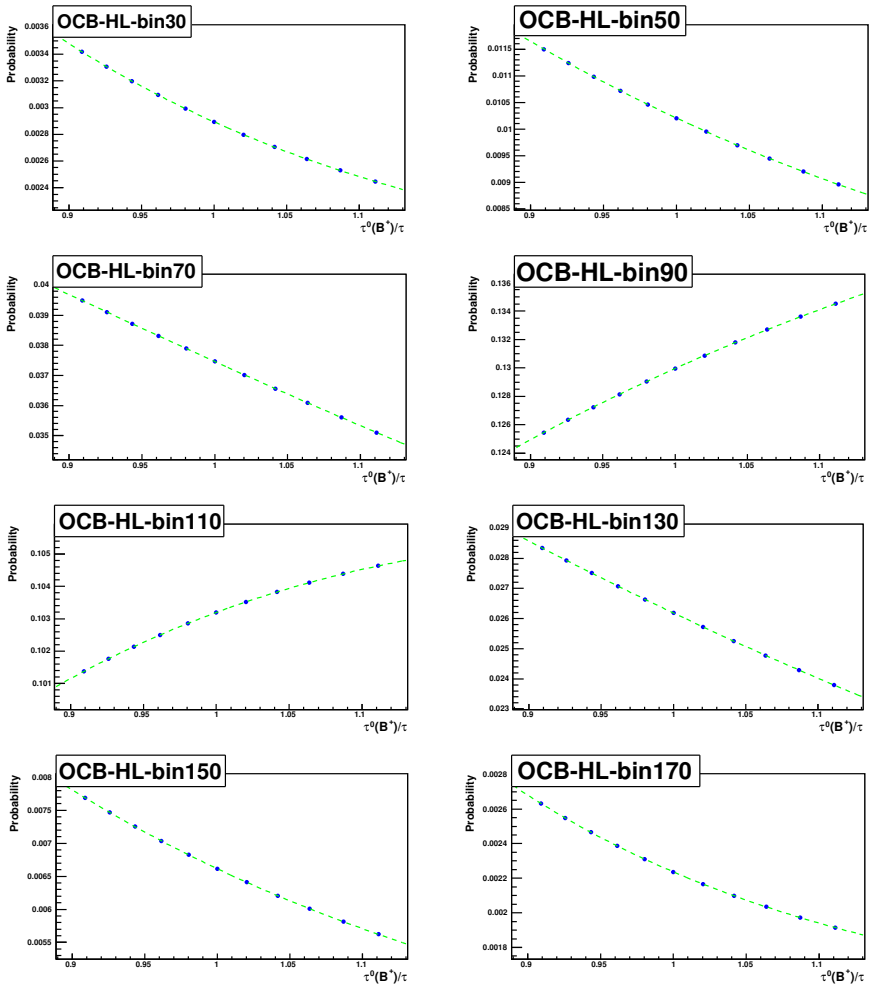

Figure A.1: Examples of $f(\tau)$ fits for the opposite charged B High-Low momentum category events (OCB-HL). Here we only show 8 out of 200 fits for the 200 Δt bins. The x axis is the ratio between the default lifetime and the varying lifetime: $\tau^0_{B^+}/\tau$. The y axis is the sum of the same sign and opposite sign (OS+SS) probabilities.

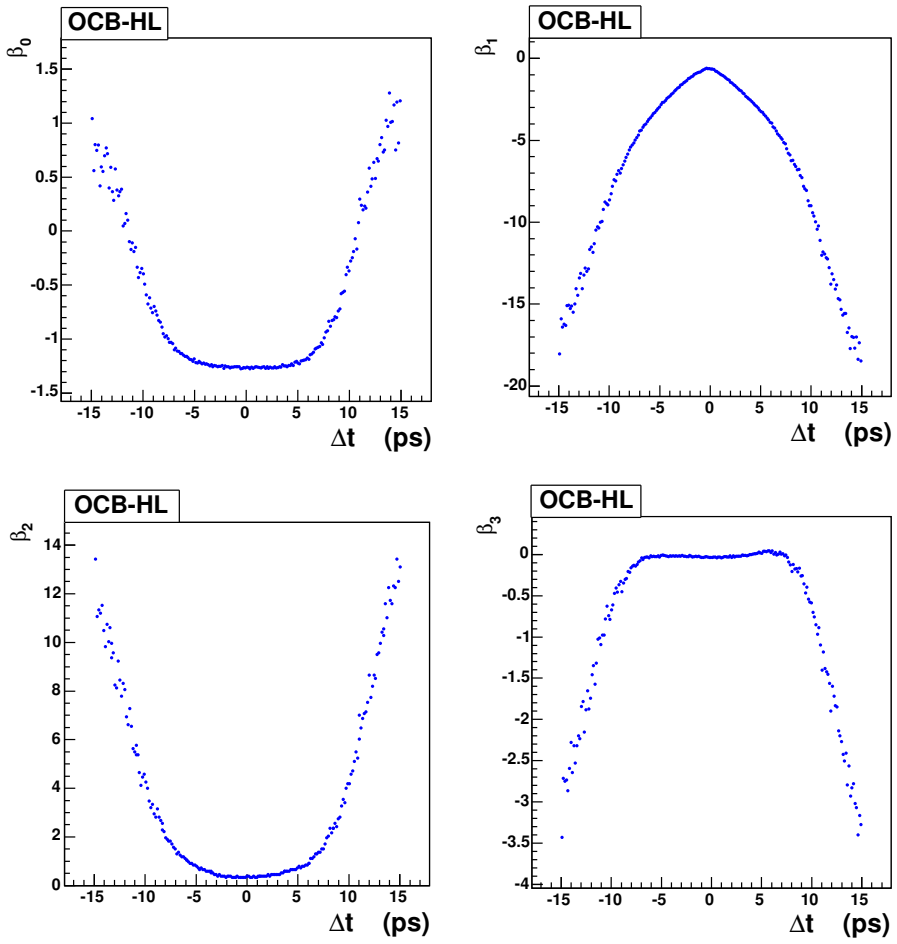

Figure A.2: Fitted parameters ($\beta(\Delta t)$'s) of $f(\tau)$ for the opposite charged B High-Low momentum category events (OCB-HL).

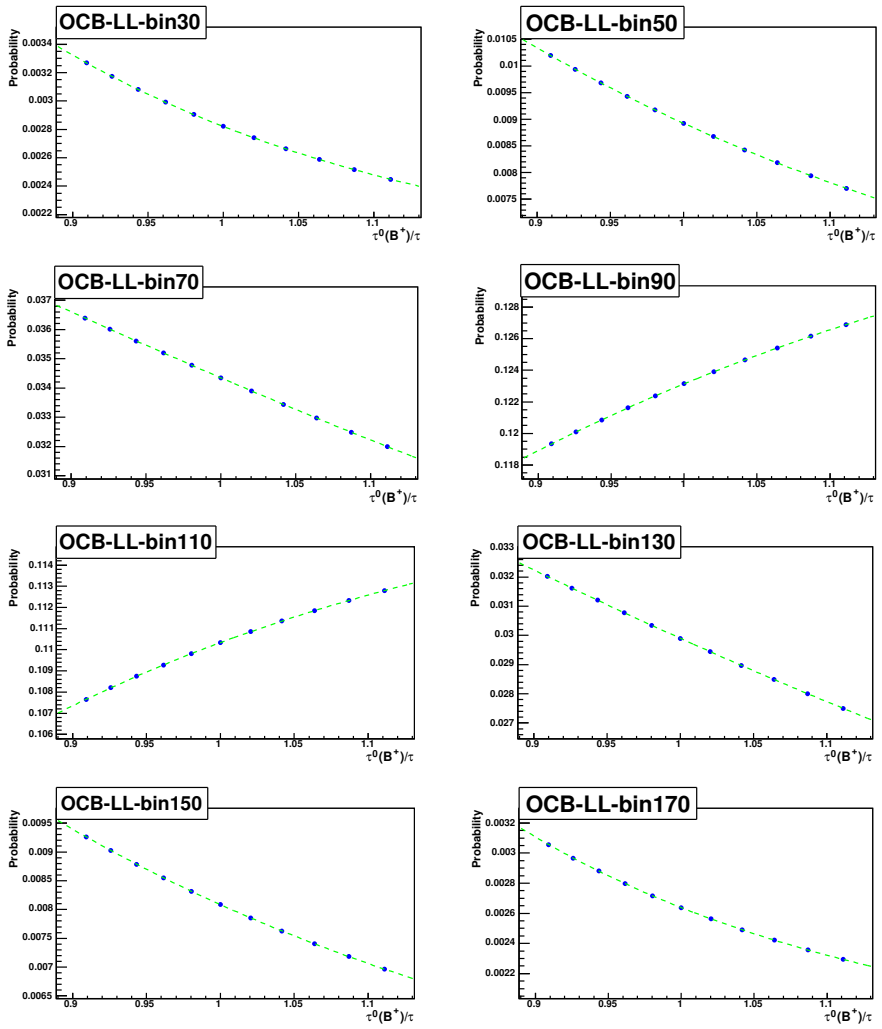

Figure A.3: Examples of $f(\tau)$ fits for the opposite charged B Low-Low category momentum events (OCB-LL). Here we only show 8 out of 200 fits for the 200 Δt bins. The x axis is the ratio between the default lifetime and the varying lifetime: $\tau^0_{B^+}/\tau$. The y axis is the sum of the same sign and opposite sign (OS+SS) probabilities.

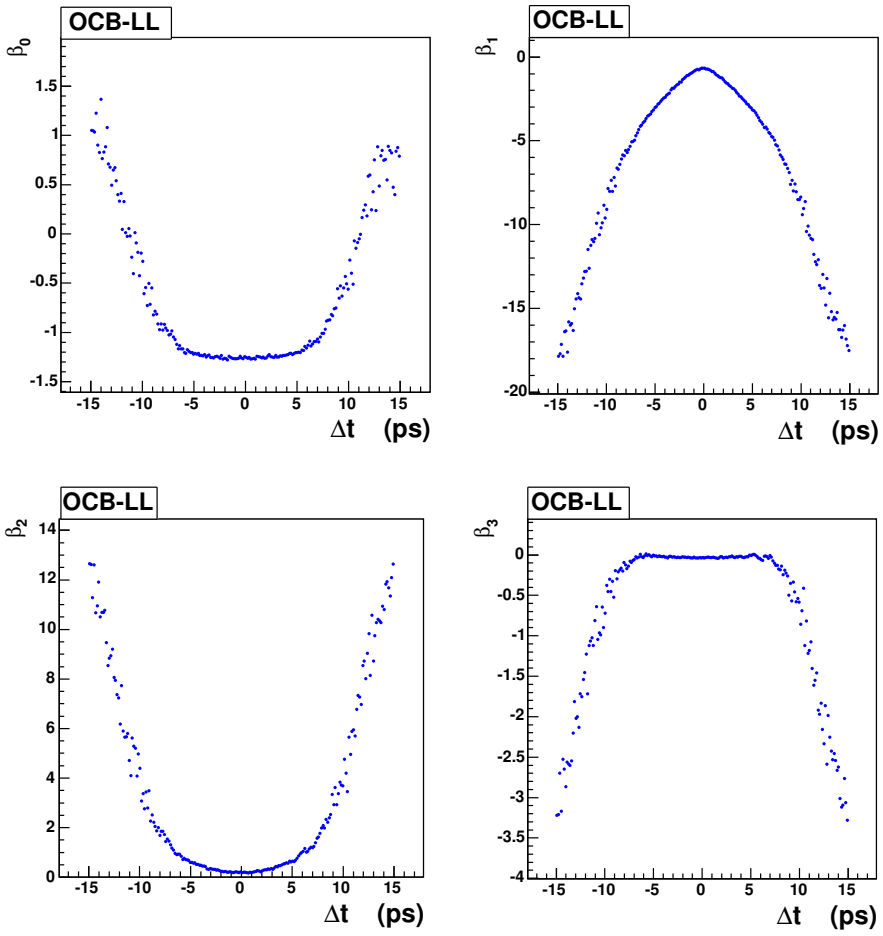

Figure A.4: Fitted parameters ($\beta(\Delta t)$'s) of $f(\tau)$ for the opposite charged B Low-Low momentum category events (OCB-LL).

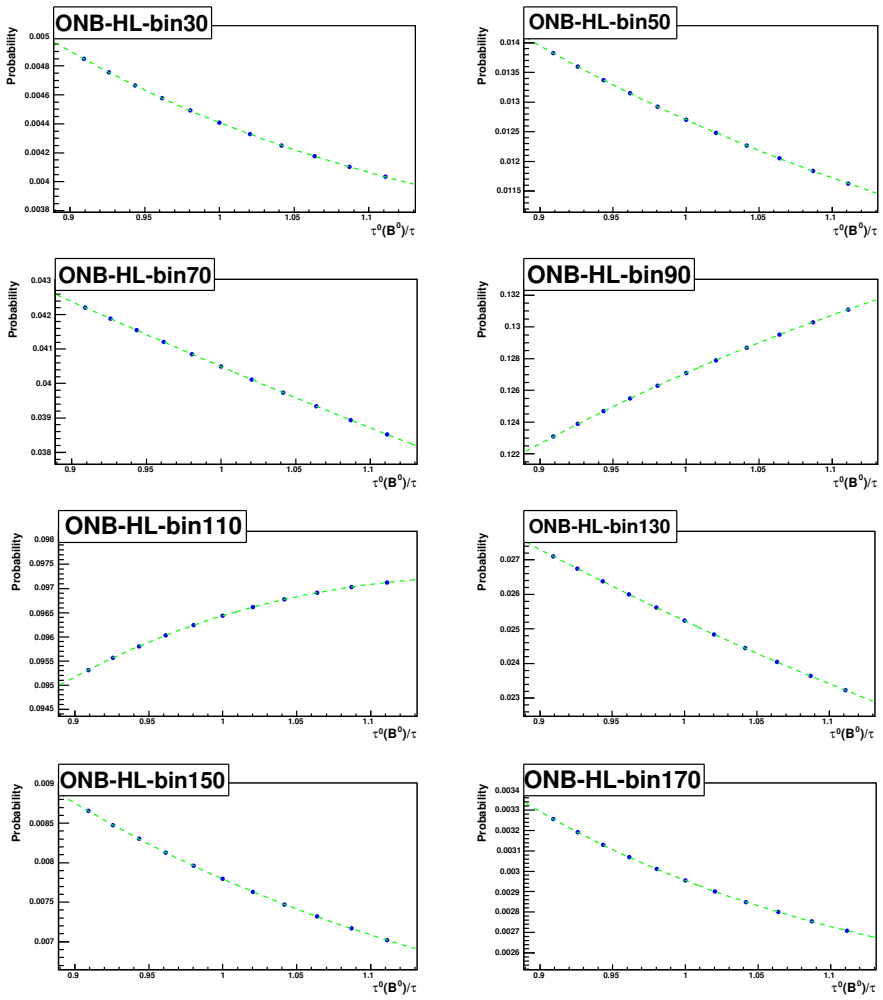

Figure A.5: Examples of $f(\tau)$ fits for the opposite neutral B High-Low momentum category events (ONB-HL). Here we only show 8 out of 200 fits for the 200 Δt bins. The x axis is the ratio between the default lifetime and the varying lifetime: $\tau^0_{B^0}/\tau$. The y axis is the sum of the same sign and opposite sign (OS+SS) probabilities.

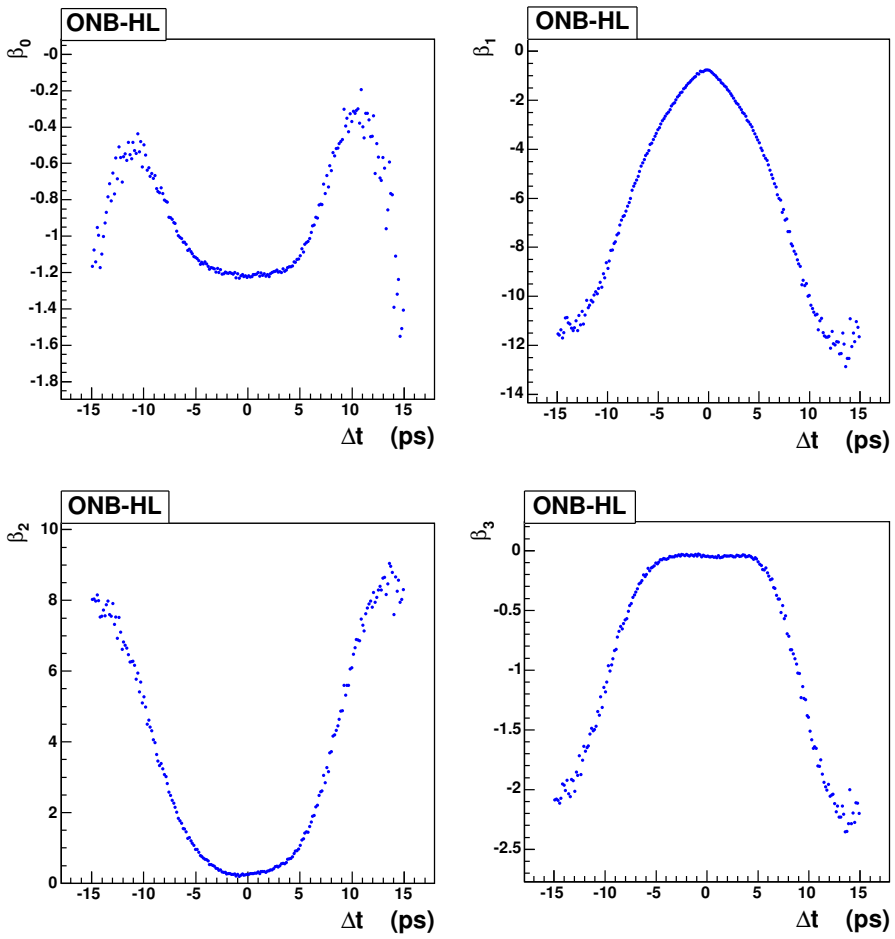

Figure A.6: Fitted parameters ($\beta(\Delta t)$'s) of $f(\tau)$ for the opposite neutral B High-Low momentum category events (ONB-HL).

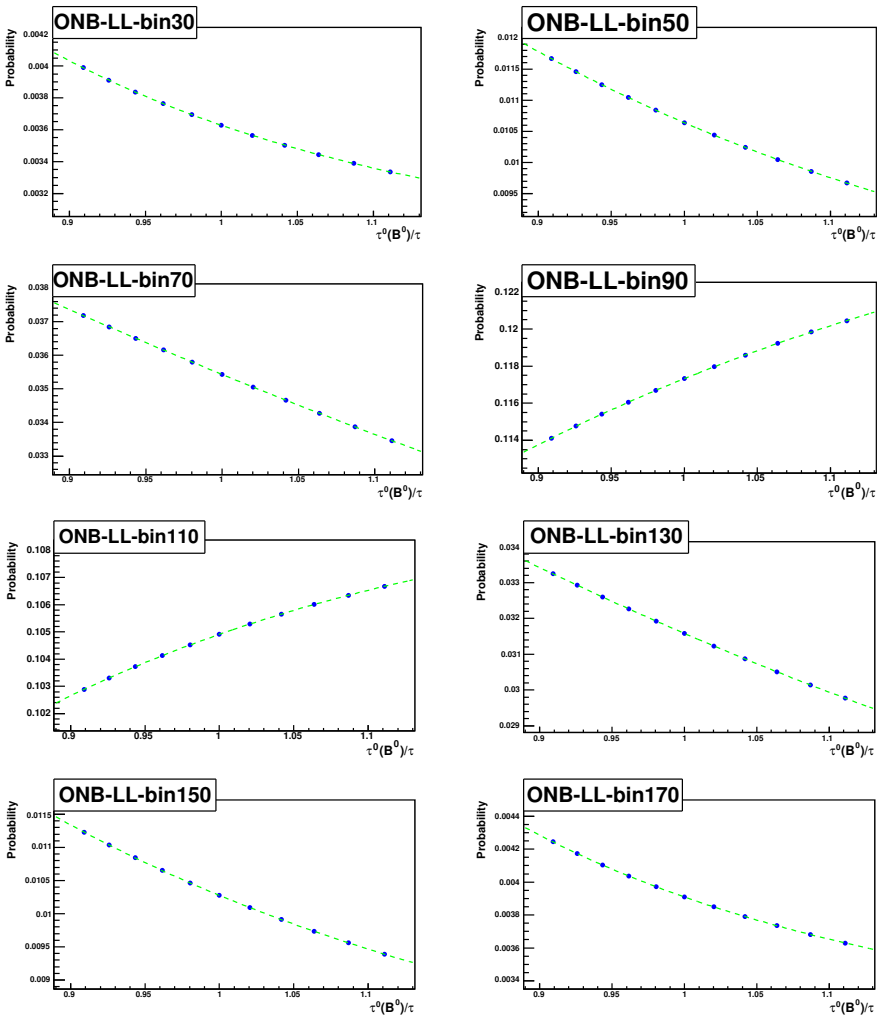

Figure A.7: Examples of $f(\tau)$ fits for the opposite neutral B Low-Low momentum category events (ONB-LL). Here we only show 8 out of 200 fits for the 200 Δt bins. The x axis is the ratio between the default lifetime and the varying lifetime: $\tau^0_{B^0}/\tau$. The y axis is the sum of the same sign and opposite sign (OS+SS) probabilities.

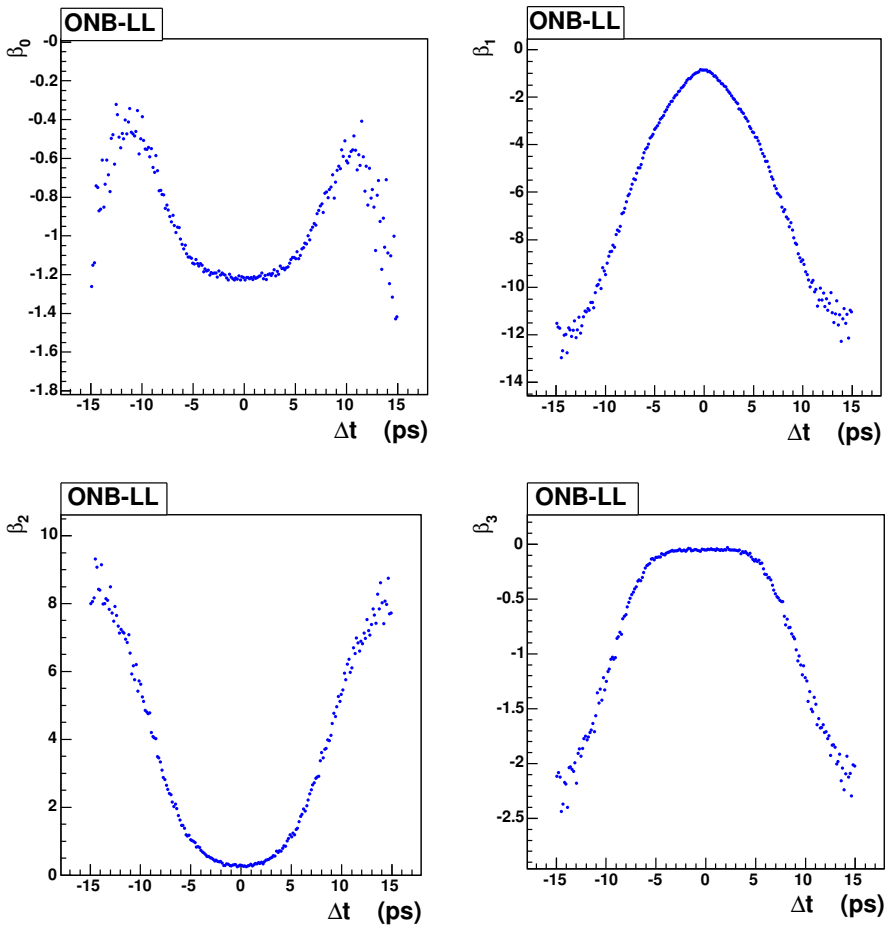

Figure A.8: Fitted parameters ($\beta(\Delta t)$'s) of $f(\tau)$ for the opposite neutral B Low-Low momentum category events (ONB-LL).

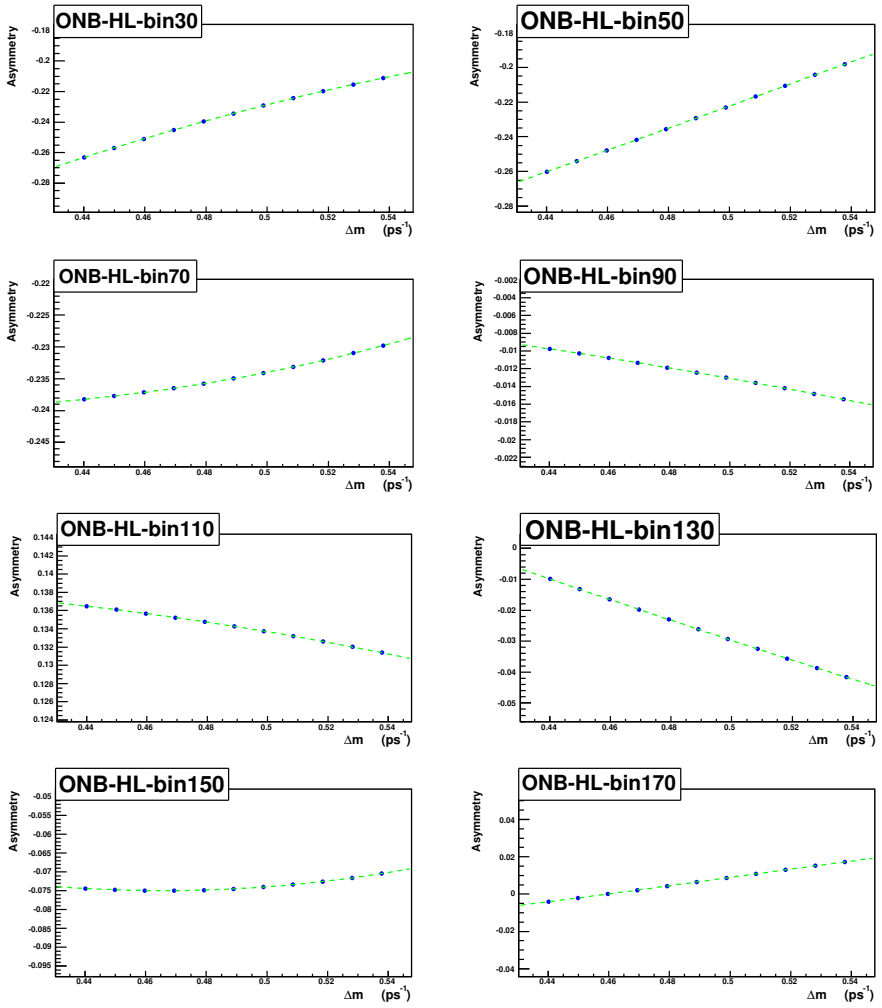

Figure A.9: Examples of $g(\Delta m)$ fits for the opposite neutral B High-Low momentum category events (ONB-HL). Here we only show 8 out of 200 fits for the 200 Δt bins. The x axis is the varying B mixing frequency Δm. The y axis is the asymmetry between the opposite and the same sign probabilities.

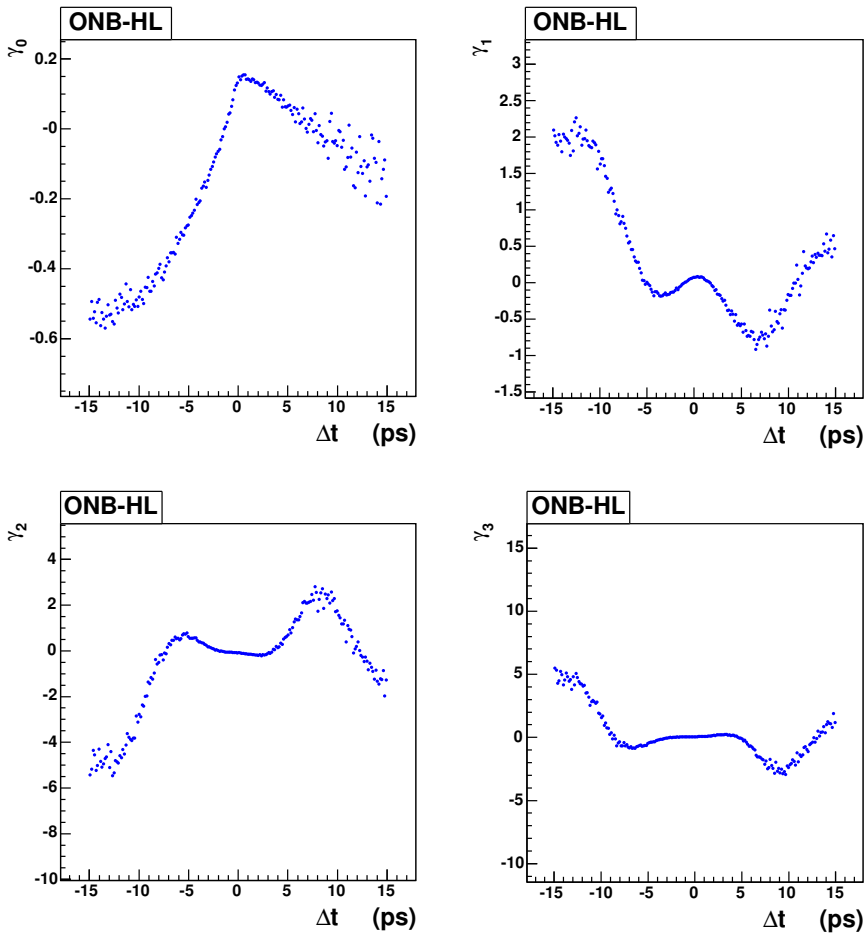

Figure A.10: Fitted parameters ($\gamma(\Delta t)$'s) of $g(\Delta m)$ for the opposite neutral B High-Low momentum category events (ONB-HL).

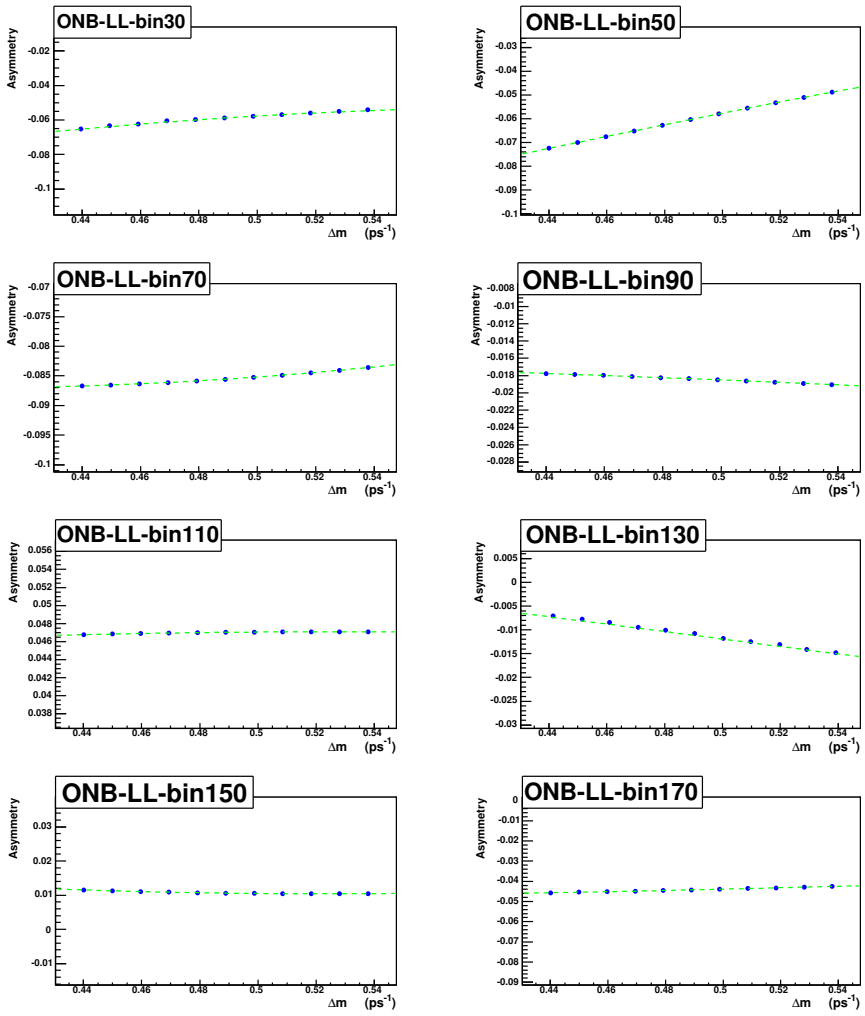

Figure A.11: Examples of $g(\Delta m)$ fits for the opposite neutral B Low-Low momentum category events (ONB-LL). Here we only show 8 out of 200 fits for the 200 Δt bins. The x axis is the varying B mixing frequency Δm. The y axis is the asymmetry between the opposite and the same sign probabilities.

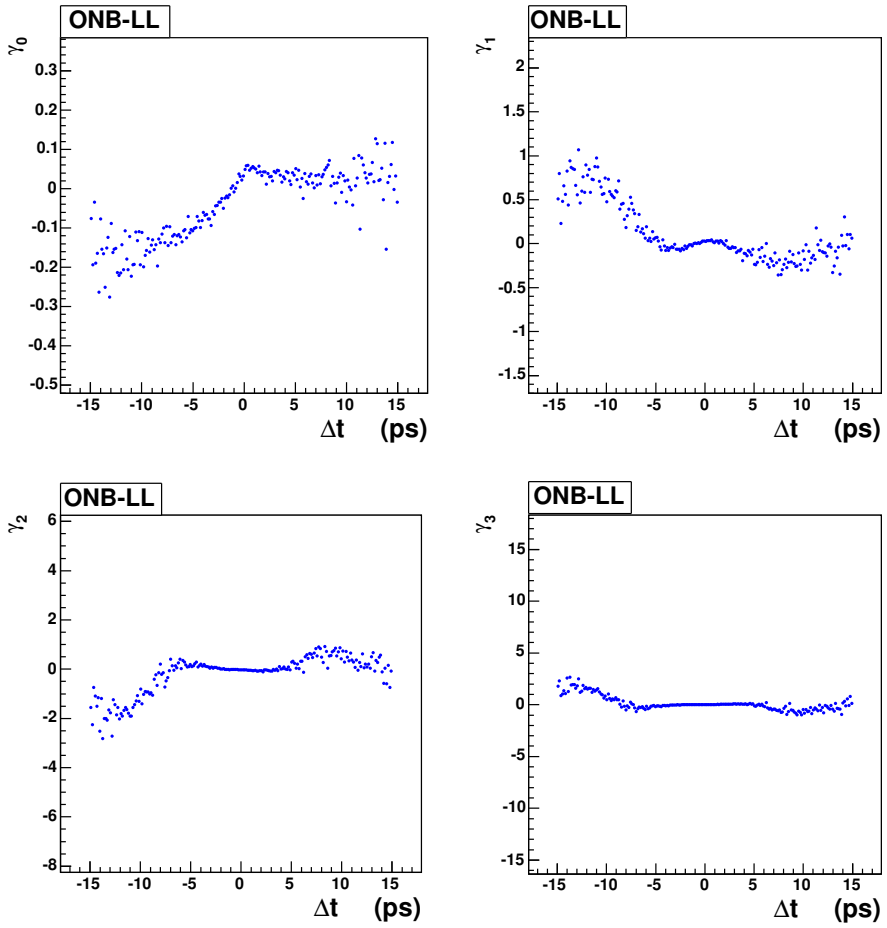

Figure A.12: Fitted parameters ($\gamma(\Delta t)$'s) of $g(\Delta m)$ for the opposite neutral B Low-Low momentum category events (ONB-LL).